INFORMUS   UCL

Evaluation of the Meteosat Surface Albedo Climate Data Record (ALBEDOVAL)

Final Report

Broadband surface DHR
resolution derived by applying the MSA
algorithm to MET-7 MVIRI observations
acquired within the period May 1-10, 2001.

Image by courtesy of EUMETSAT

Commissioned by:

EUMETSAT

Prepared by:

INFORMUS   UCL

Berlin, 22. October 2012

INF⊜RMUS

UCL

Document control sheet

Project	ALBEDOVAL
Customer	EUMETSAT
Document title	Evaluation of the Meteosat Surface Albedo Climate Data Record – Final report
Filename	ALB_Final_Report_2012_10_21.doc
Authors and affiliations	Frank Fell (1), Ralf Bennartz (2), Bronwyn Cahill (1), Alessio Lattanzio (3), Jan-Peter Muller (4) Joerg Schulz (3), Neville Shane (4), Isabel Trigo (5), Gill Watson (4) (1) Informus GmbH, Berlin, Germany (2) University of Wisconsin, Madison, US (3) Eumetsat, Darmstadt, Germany (4) University College London, UK (5) Instituto de Meteorologia, Lisboa, Portugal
Contact	fell@informus.de

Document history

Version	Date	Author(s)	Description
1.0	2012-01-18	All (see above)	Initial version
1.1	2012-10-21	All (see above)	Feedback on initial version included

Table of contents

List of tables

List of panels

Acronym	Explanation
ADC	Atlantic data coverage
AERONET	AErosol RObotic NETwork
AVHRR	Advanced Very High Resolution Radiometer
ASM	Atmospheric scattering module
BHR	Bi-hemispherical reflectance
BRDF	Bi-directional reflectance distribution function
BRF	Bi-directional reflectance factor
BSRN	Baseline Surface Radiation Network
CDR	Climate data record
CORINE	Coordination of Information on the Environment
DCP	Data consistency procedure
DHR	Directional hemispherical reflectance
DIM	Data interpretation module
ECMWF	European Centre for Medium-Range Weather Forecasts
ECV	Essential climate variable
ERA-Interim	ECMWF Re-Analysis Interim
ESA	European Space Agency
EUMETSAT	European Organisation for the Use of Meteorological Satellites
FAPAR	Fraction of absorbed PAR
FCDR	Fundamental climate data record
FUB	Freie Universität Berlin
GCMPs	GCOS climate monitoring principles
GCOS	Global Climate Observing System
GMS	Geostationary Meteorological Satellite (Japan)
GOES	Geostationary Operational Environmental Satellite (US)
GSA	Geostationary Surface Albedo
GSICS	Global Space-based Inter-Calibration System
IGBP	International Geosphere-Biosphere Programme
IODC	Indian Ocean data coverage
ITCZ	Intertropical convergence zone
JMA	Japan Meteorological Agency
LSA SAF	Land Surface Analysis Satellite Applications Facility
LUT	Look-up table
MFG	Meteosat First Generation

Acronym	Explanation
MISR	The Multi-angle Imaging SpectroRadiometer
MODIS	Moderate Resolution Imaging Spectroradiometer
MSA	Meteosat Surface Albedo
MVIRI	Meteosat Visible and Infra-Red Imager
NOAA	National Oceanic and Atmospheric Administration
PFT	Plant functional type
RMSE	Root mean square error
SAF	Satellite Applications Facility
SCOPE-CM	Sustained, Co-Ordinated Processing of Environmental Satellite Data for Climate Monitoring
SEVIRI	Spinning Enhanced Visible Infra-Red Imager
SRB	Surface radiation budget
SSP	Sub-satellite point
SSR	Sensor spectral response
TAM	Time averaging module
TCDR	Thematic climate data record
VIS	Visible part of the spectrum
WMO	World Meteorological Organization
XADC	Extended ADC

Executive Summary

Summary

The MSA data record is a unique data set encompassing up to 25 years of continuous surface albedo coverage for large areas of the Earth. It is therefore of paramount importance to maintain and further improve the existing MSA data record.

The evaluation of the MSA data record has revealed a number of specific strengths and weaknesses as outlined below. While the strengths underlines the already high value of the MSA data record for climate applications, the weaknesses need to be considered for specific applications and should be addressed in the context of a product re-processing. A number of concrete recommendations to improve product quality, usability and sustainability at short, medium and long term have been devised.

In combination with other (EUMETSAT and non-EUMETSAT) geostationary satellites, the MSA method should contribute to creating harmonised surface albedo records of quasi global coverage outside the polar zones serving climate applications and beyond. Going beyond, geostationary and polar-orbiting observations may be fused to provide multi-mission albedo products of higher product quality and full global coverage, capitalizing on the strengths of both approaches.

Thematic context

The surface albedo, i.e. the non-dimensional ratio between the radiation flux reflected by a surface in all directions and the incoming irradiance, is both a direct climate forcing variable and an indicator of environmental degradation. Due to its fundamental role in the climate system, the surface albedo is one of the terrestrial „Essential Climate Variables"(ECV) introduced by the Global Climate Observing System (GCOS). Observing requirements on the surface albedo for use within climate studies have been defined (for example) by GCOS and the World Meteorological Organisation (WMO).

In order to provide the climate user community with a long-term data record on the surface albedo capitalising on more than 30 years of availability of MVIRI (Meteosat Visible and Infrared Imager) and other geostationary satellite data, EUMETSAT has generated the Meteosat Surface Albedo (MSA) Climate Data Record (CDR). In fact, radiometers on geostationary platforms such as MVIRI constitute, together with the polar-orbiting AVHRR (Advanced Very High Resolution Radiometer) instruments, the only available data source to derive multi-decadal surface albedo time series of large-scale coverage needed for change detection.

Evaluation strategy

The strategy to evaluate the MSA data record consisted of the following major activities:

- ➢ *Analysis of MSA method and characteristics of the actual product;*
- ➢ *Assessment of MSA data record in relation to the climate community requirements;*
- ➢ *Evaluation of MSA data record practical utility;*
- ➢ *Provision of recommendations for MSA product improvement.*

Due to the size of an MSA pixel, a direct validation of the MSA product with ground truth measurements is only possible under very specific conditions. The MSA evaluation was therefore based on the following pillars:

- ➢ *Internal consistency checks (i.e. quality checks entirely based on the MSA dataset, partly obtained under different viewing geometries);*
- ➢ *Comparison to other satellite-derived surface albedo products (considering geostationary as well as polar-orbiting instruments);*
- ➢ *Comparison to in-situ data gathered in reference areas believed to be homogeneous over at least one MSA pixel.*

1.1. Thematic context

The surface albedo, i.e. the non-dimensional ratio between the radiation flux reflected by a surface in all directions and the incoming irradiance, is both a direct climate forcing variable and an indicator of environmental degradation. Due to its fundamental role in the climate system, the surface albedo is one of the terrestrial „Essential Climate Variables"(ECV) introduced by the Global Climate Observing System (GCOS). Observing requirements on the surface albedo for use within climate studies have been defined (for example) by GCOS and WMO.

In order to provide the climate user community with a long-term data record on the surface albedo capitalising on more than 30 years of availability of MVIRI (Meteosat Visible and Infrared Imager) and other geostationary satellite data, EUMETSAT has generated the Meteosat Surface Albedo (MSA) Climate Data Record (CDR). In fact, radiometers on geostationary platforms such as MVIRI constitute, together with the polar-orbiting AVHRR (Advanced Very High Resolution Radiometer) instruments, the only available data source to derive multi-decadal surface albedo time series of large-scale coverage needed for change detection.

1.2. Organisational context

Recognizing the importance of global satellite-derived Climate Data Records (CDR) in climate research, WMO has established the "*Sustained, Co-Ordinated Processing of Environmental Satellite Data for Climate Monitoring*" initiative (SCOPE-CM) in 2008. Five pilot projects were started within the framework of SCOPE-CM, of which one, led by EUMETSAT, addresses the generation of a global surface albedo data record derived from geostationary satellite data [SCOPE-CM, 2011].

The ultimate goal of this pilot project is the delivery of a near-global, Level-3 surface albedo dataset covering the years 2001 to 2003 of which EUMETSAT's Meteosat Surface Albedo (MSA) dataset [EUMETSAT, 2010-A,-B] will be an essential contribution The major task of the pilot project was to export the EUMETSAT retrieval software (then called Geostationary Surface Albedo or GSA) to JMA and NOAA in order to demonstrate that a distributed product generation is feasible. As this was successful, further activities in SCOPE-CM are now targeting the product generation for the full set of geostationary satellites available at EUMETSAT, JMA and NOAA.

Prior to the SCOPE-CM project, EUMETSAT has used the MSA algorithm to reprocess almost all MVIRI data utilising images produced by the NRT system. As this was done as a best effort exercise, an extensive validation had not been possible. Enlarging their mandate towards the generation of CDRs in 2010, EUMETSAT has acknowledged the need for more extensive validation activities of its MSA product to comply with international standards and to guide the further development of the SCOPE-CM activity.

In this context, EUMETSAT has commissioned the ALBEDOVAL study to provide an external quality assessment of the existing MSA data record by a group of independent experts to ensure unbiased conclusions and recommendations. ALBEDOVAL is a novel way to assess the quality of a EUMETSAT climate data product which may serve as a baseline for the evaluation of similar products in the future.

1.3. Aims and objectives

The primary aim of ALBEDOVAL was to contribute to the validation of the MSA CDR in support of the product release process. The study should also identify elements leading ultimately to an improved uncertainty assessment of the MSA-CDR. These aims have been addressed through the following objectives:

> ➢ Devise a generic CDR assessment strategy;

➢ Adapt this generic strategy to accommodate the MSA specifics;

➢ Identify suitable reference data sets and surface targets;

➢ Perform actual MSA quality assessment;

➢ Document findings and devise recommendations for product and documentation improvements.

1.4. Evaluation strategy

The strategy to evaluate the MSA data record consisted of the following major activities:

➢ Analysis of MSA method and characteristics of the actual product;

➢ Assessment of MSA data record in relation to requirements from the climate community;

➢ Evaluation of MSA data record practical utility;

➢ Provision of recommendations for MSA product improvement.

Due to the size of an MSA pixel, a direct validation of the MSA product with ground truth measurements is only possible under very specific conditions. The MSA evaluation was therefore based on the following pillars:

➢ Internal consistency checks (i.e. quality checks entirely based on the MSA dataset, partly obtained under different viewing geometries);

➢ Comparison to other satellite-derived surface albedo products (considering geostationary as well as polar-orbiting instruments);

➢ Comparison to in-situ data gathered in reference areas believed to be homogeneous over at least one MSA pixel.

In order to facilitate a potential later re-analysis of a revised MSA product or the evaluation of similar satellite-based data products, an initial version of a hierarchical framework for CDR quality assessment has been established, including suggestions for traceable quality indicators and associated metrics.

To match available resources with the need for a broad understanding of the processes potentially affecting MSA quality, it was decided to identify and characterise as many quality aspects as possible rather than studying individual aspects in much detail. The actual MSA quality assessment was then based on the following approach:

➢ Identify generic challenges to space-borne surface albedo retrievals;

➢ Identify which of these challenges are potentially relevant to MSA;

➢ Devise criteria to measure the impact of a specific challenge on the MSA product quality;

➢ Compile an overall assessment, based on quality assessment of individual aspects;

➢ Devise recommendations for MSA product improvement.

1.5. Terminology

In order to ensure common understanding among those contributing to the study, definitions of terms and concepts relevant to ALBEDOVAL have been compiled in Table 1.

Table 1: Terminology used in the frame of ALBEDOVAL.

Term / concept	Definition	Reference
Accuracy	Closeness of agreement between a quantity value obtained by measurement and the true value of the measurand.	ISO/IEC Guide 99:2007

Term / concept	Definition	Reference
Best practice	Method or technique that has consistently shown results superior to those achieved with other means, and that is used as a benchmark.	Wikipedia
Bias	Systematic error of indication of a measuring system.	ISO/IEC Guide 99:2007
Calibration	The process of quantitatively defining the system response to known controlled signal inputs.	CEOS WGCV
Consistency	Achieving a level of performance which does not vary greatly in quality over time.	Oxford Dictionaries
Error	Difference of quantity value obtained by measurement and true value of the measurand.	ISO/IEC Guide 99:2007
Evaluation	Judgement about the amount, number, or value of something; assessment.	Oxford Dictionaries
Plausibility	Quality of seeming reasonable or probable	Oxford Dictionaries
Quality indicator	Indicator of performance or quality of the result of a process/ activity derived from an uncertainty estimate to allow users to evaluate fitness of purpose. Can be a text descriptor / flag / numeric value.	QA4EO
Stability	Ability of a measuring system to maintain its metrological characteristics constant with time.	ISO/IEC Guide 99:2007
Traceability	Establishment of an unbroken chain of comparisons to stated references each with a stated uncertainty.	NIST
Uncertainty	Dispersion of the quantity values that are being attributed to a measurand, based on the information used.	ISO/IEC Guide 99:2007
Validation	Process of assessing, by independent means, the quality of the data products derived from the system outputs.	CEOS
Verification	Process intended to check that a product, service, or system meets a set of initial design requirements, specifications, and regulations.	Wikipedia

2. The surface albedo

2.1. Definition of the surface albedo

Surface albedo is generally defined as the instantaneous ratio of surface-reflected radiation flux to incident radiation flux (dimensionless) [Schaaf et al., 2009]. In the case of vegetation, a reference surface is typically defined at or near the top of the canopy and must be specified explicitly [GCOS-138, 2010; GCOS-154, 2011]. It can be defined for broad spectral regions (often the full shortwave range from 0.3 to 3.0 µm) or for spectral bands of finite width.

The surface albedo depends on the angular distribution of the incoming radiation. Two simple concepts, corresponding to extreme conditions, have been defined to be able to account for this dependency:

> ➢ The directional hemispherical reflectance factor (DHR) represents the reflectance of a surface when the illumination comes from a single direction. The DHR (or *"black sky albedo"*) corresponds to the albedo in the absence of any atmosphere. It depends on the angular position of the light source and surface properties;

> ➢ The bi-hemispherical reflectance factor under isotropic illumination (BHR_{ISO}) represents the reflectance of a surface when the illumination is isotropic. The surface albedo under an overcast homogeneous cloud deck would be a good approximation of the white sky albedo. BHR_{ISO} (or *"white sky albedo"*) depends on surface properties only.

In practice, the actual instantaneous albedo of a land surface is often approximated by a linear combination of the black and white sky albedos, where the weighing factors are the relative proportions of direct and diffuse radiation. Such a combination is sometimes referred to as the *"blue sky albedo"*.

2.2. Characteristics of the surface albedo

Due to its dependence on both surface properties and illumination conditions, the surface albedo is a complex parameter and may undergo substantial short-term as well as long-term changes that need to be considered in any evaluation approach. This is demonstrated below by a number of field measurements (Figure 1), obtained by the Institute of Meteorology of the Freie Universität Berlin (FUB) in the context of large national or international surface-atmosphere field campaigns carried out in the late eighties and early nineties of the 20th century.
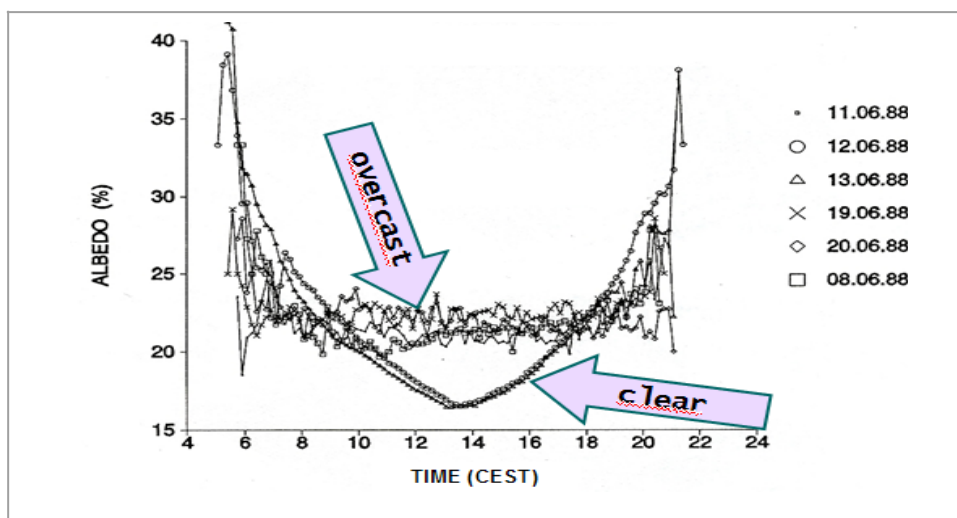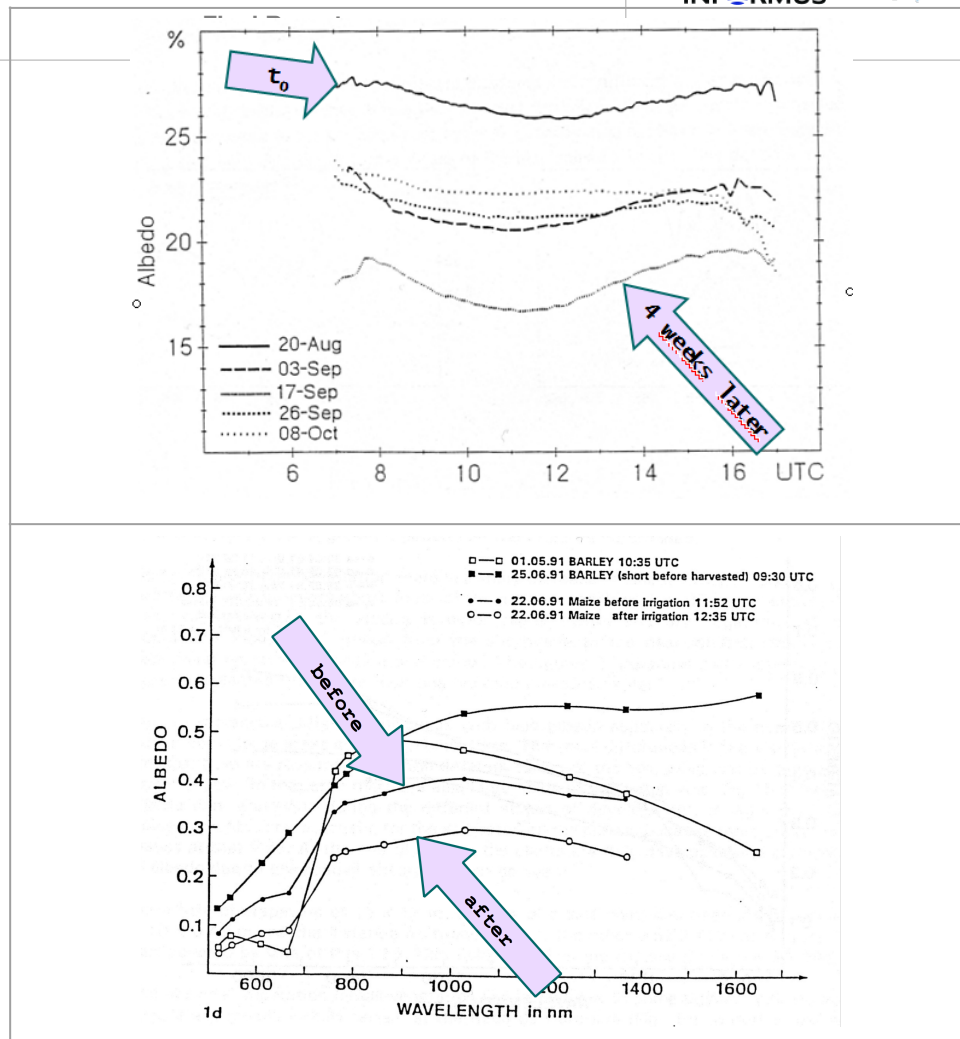
Figure 1: Examples of surface albedo *in situ* measurements Top: Diurnal courses of the broadband albedo over a wheat field in Germany. Middle: Seasonal development of the broadband albedo over fallow ground in Niger triggered by a precipitation event. Bottom: Short-term effect of irrigation on the spectral albedo over a corn field in Spain (all figures by courtesy of H.-J. Bolle).

2.3. How to measure the surface albedo

The surface albedo can be measured *in situ* using pyranometers that integrate the incoming radiation from an entire hemisphere. Coupling two such instruments back-to-back (*"albedometer"*) allows to measure simultaneously the downward irradiance from the sky and the reflected irradiance from the surface. Albedometers are operationally deployed to WMO standards on stationary towers, for example as part of the Baseline Surface Radiation Network (BSRN[1]). Other sustained long-term albedo measurements are available through activities such as FLUXNET[2]. In addition, significant numbers of surface albedo measurements have been made on occasion of national or international measurement campaigns in the context of initiatives such as the *International Satellite Land-Surface Climatology Project (ISLSCP[3]).*

---

[1] http://www.bsrn.awi.de/ (URL verified 2012-07-11)

[2] http://fluxnet.ornl.gov/ (URL verified 2012-06-29)

[3] http://www.gewex.org/islscpdata.htm (URL verified 2012-06-29)

Mostly broadband instruments have been deployed although spectral measurements of the surface albedo do also exist. The characteristic footprint of these sensors depends on their installation height above the surface; the applicability of these on site measurements to satellite derived quantities is therefore governed by the representativeness of their footprint for the (usually) much larger remotely sensed footprint.

2.4. Role of the surface albedo in the climate system

Albedo is both a forcing variable affecting the climate and a sensitive indicator of environmental degradation. Given the amount of energy involved in solar radiation fluxes, a one per cent change in land-surface albedo generates fluctuations on the order of 3.5 W/m² on global and annual averages. Due to its fundamental role in the climate system, the surface albedo has been classified as one of the terrestrial „*Essential Climate Variables*" (ECVs) with the corresponding observation requirements on accuracy, stability, resolution, etc. [GCOS-154, 2011].

2.5. Requirements on satellite-based surface albedo climate data records

Satellite-based methods are indispensable in order to obtain estimates of the surface albedo on a regional and global scale. To this end, the albedo needs to be derived from the directional radiance measurements obtained by space-borne radiometers at the top of the atmosphere. This involves a number of assumptions and approximations inevitably impacting the accuracy of the retrieved product as outlined for the specific case of the Meteosat Surface Albedo (MSA) in this report.

A number of principles have been established for satellite-based climate monitoring systems [GCOS-143, 2010] which are listed in Panel 1 below. More general requirements to be met by any (not only satellite-based) climate monitoring system have also been established by GCOS and are listed in Annex 11.3.

1. Constant sampling within the diurnal cycle (minimizing the effects of orbital decay and orbit drift) should be maintained.

2. A suitable period of overlap for new and old satellite systems should be ensured for a period adequate to determine inter-satellite biases and maintain the homogeneity and consistency of time-series observations.

3. Continuity of satellite measurements (i.e. elimination of gaps in the long-term record) through appropriate launch and orbital strategies should be ensured.

4. Rigorous pre-launch instrument characterization and calibration, including radiance confirmation against an international radiance scale provided by a national metrology institute, should be ensured.

5. On-board calibration adequate for climate system observations should be ensured and associated instrument characteristics monitored.

6. Operational production of priority climate products should be sustained and peer-reviewed new products should be introduced as appropriate.

7. Data systems needed to facilitate user access to climate products, metadata and raw data, including key data for delayed-mode analysis, should be established and maintained.

8. Use of functioning baseline instruments that meet the calibration and stability requirements stated above should be maintained for as long as possible, even when these exist on de-commissioned satellites.

9. Complementary in situ baseline observations for satellite measurements should be maintained through appropriate activities and cooperation.

10. Random errors and time-dependent biases in satellite observations and derived products should be identified.

Panel 1: GCOS Climate Monitoring Principles (GCMPs) for satellite-based climate monitoring systems.

Specific requirements for the surface albedo as ECV are shown in Table 2 [GCOS-154, 2011]. The objective behind these requirements is to detect the change in radiative forcing equivalent to 20 per cent of the expected total change in radiative forcing per decade due to greenhouse gases and other forcing, i.e. ~0.1 W/m^2 per decade. The requirements are global. More accurate observations over ice and snow would be useful for calculating ice and snow melt. The GCOS requirements appear partly difficult to achieve from space-borne measurements, especially regarding product accuracy for dark surfaces.

Table 2: Requirements on the surface albedo as essential climate variable [GCOS-154, 2011].

Parameter	Horizont. Res.	Vertical Resolution	Temporal Resolution	Accuracy	Stability [1/decade]
Black-sky albedo	1km	N/A	Daily to weekly	Max (5%; 0.0025)	Max (1%; 0.0001)
White-sky albedo	1km	N/A	Daily to weekly	Max (5%; 0.0025)	Max (1%; 0.0001)

Another requirements definition process, the *"WMO Rolling Requirement Review",* supports the setting of the priorities to be agreed by WMO Members and their space agencies for enhancing the space-based Global Observing System. In this context, GCOS has provided input for the systematic climate observation elements of the *"WMO Observing Requirements Database"* [4]. The GCOS requirements are only partly consistent with this process in that they provide only target but not *"breakthrough"* or *"threshold"* (i.e. minimum) requirements. GCOS also provides requirements on stability that are not currently included in the WMO requirements database.

Table 3: Requirements on the surface albedo from the WMO Observing Requirements Database.

---

[4] http://www.wmo-sat.info/db/requirements/view/662 (URL verified: 2012-08-20)

WMO Observing Requirements Database

Home | Consult Tables

Values defined for Requirement #662

Variable: Earth surface albedo

	Goal	Breakthrough	Threshold
Uncertainty	5 %	7 %	10 %
Horizontal Resolution	1 km	2 km	10 km
Vertical Resolution	N/A	N/A	N/A
Observing Cycle	24 h	3 d	30 d
Timeliness	30 d	45 d	90 d

Validated:	2007-07-19	Source:	TOPC
Comment:		Confidence:	reasonable

The "*WMO Observing Requirements Database*" specifies requirements on the surface albedo for climatologic applications at three quality levels (see Table 3):

➢ Threshold: Minimum requirement;

➢ Breakthrough: Significant improvement;

➢ Goal: Optimum, no further improvement required (partly equivalent to GCOS requirements). [5]

---

[5] The WMO Observing Requirements Database specifies uncertainties in absolute parameter units. The stated "goal" uncertainty requirement of 5% is thus equivalent to ±0.05 using the unitless albedo definition applied in this report which is considerably less strict than the corresponding GCOS accuracy requirement.

3. Measuring surface albedo from space

3.1. Measurement approaches

The two mostly used orbit types in Earth Observation are the sun-synchronous polar orbit and the geostationary orbit. As regards the retrieval of the surface albedo, both orbit types have characteristic strengths and weaknesses as shown in Table 4 at the example of instruments frequently used for surface albedo retrieval (MVIRI vs. MODIS).

Table 4: Characteristics of geostationary *vs.* polar-orbiting satellite observations.

Parameter	Geostationary	Sun-synchronous
Spatial resolution	Medium, typically 1-10 km (MVIRI: 2.5 km at SSP)	High, typically 1 km or higher (MODIS: 0.25-1.0 km at SSP)
Spatial coverage	Limited to apparent Earth disk, no information in polar areas (MVIRI: Brasil, Africa, Europe up to 60°N, Middle East)	Unlimited, no principle limitation
Global coverage	Limited, fleet of five instruments needed for full global coverage outside polar areas	Unlimited, full global coverage achievable with individual instruments
Temporal resolution	High, diurnal cycles possible. (MVIRI: 48 images per day)	Low, diurnal cycles not possible. (MODIS: 2 images per day, more observations at higher latitudes)
Product availability	High (MVIRI: high repetition rate leading to limited number of product gaps for typical integration periods, e.g. one week)	Medium (MODIS: lower repetition rate leading to higher likelihood of product gaps for typical integration periods)
Spectral resolution	Low (MVIRI: 1 VIS/NIR channel)	Medium (MODIS: 8 VIS/NIR channels at 1.0 km resolution)
Observation geometry	More limited, target always seen under same viewing angle, observation geometries confined to limited subset. Surface anisotropy not fully represented.	Less limited, targets seen under different viewing angles, better potential to cover surface anisotropy
Other	No orbital drift	Local overpass continuously delayed with related effects on product consistency

3.2. Retrieval challenges

Surface albedo retrieval from space is subject to a number of potential error sources. In the following subsections, the relevant processes are classified into "instrumental", "methodological" and "natural" factors. For each factor, its relevance on MSA retrieval is estimated, the potential effects are described, and concrete evaluation strategies are proposed.

3.2.1. Instrumental factors

Instrumental factors				
Process	Relevance	Potential effect on MSA	Evaluation strategy	Remarks
Stability	High	Systematic errors leading to spurious trends.	Investigate surface albedo time series above homogeneous and stable reference surfaces (dark to bright).	Same strategy to investigate stability and cross calibration.
Cross calibration	High	Artefacts in time series between succeeding MVIRIs.	Investigate surface albedo time series above homogeneous and stable reference surfaces (dark to bright).	Same strategy to investigate stability and cross calibration.
Polarisation sensitivity	Low	Under- or overestimation, depending on surface type and atmospheric composition.	Beyond study scope.	
Geostationary orbit	High	Target is always seen under the same viewing angle. Reduced resolution and data availability towards the edges of the Meteosat disk.	Investigate impact of geostationary orbit on MSA product availability.	See also under "BRF model" in "Methodological factors".
Pixel navigation	High	Spurious overestimation of albedo variability at pixel level for heterogeneous surfaces.	Quantify location uncertainty across/along scanlines for individual MVIRIs using suitable reference targets (coastlines).	Verify findings with EUMETSAT experts.

3.2.2. Methodological factors

Methodological factors				
Process	Relevance	Potential effect on MSA	Evaluation strategy	Remarks
Spectral-to-broadband conversion	Low	Potentially significant since MVIRI disposes of only one VIS channel (~0.5-0.9 μm), especially for surfaces with prominent spectral features.	Improvement by new coefficients by Loew & Govaerts (2010), further investigation beyond study scope.	
Temporal compositing	Medium	MSA "best-of-ten" approach may lead to "speckle" or artefacts as neighbouring pixels may have been chosen under different conditions.	Analyse MSA "best-of-ten" probability-based selection process, depict errors potentially resulting from this approach.	The most "probable" value is not necessarily the most accurate or the most plausible value.
BRF model	High	BRF model based on a number of assumptions which do not always represent real conditions. May lead to retrieval errors, especially for strongly non-Lambertian surfaces.	Compare MSA to independent albedo data (sat or in situ) for surfaces with known or expected anisotropic characteristics.	Also compare MSA for reference surfaces seen from different orbits (e.g. 0° vs. 57/63°)
Atmospheric correction, scattering	High	Joint retrieval of surface albedo and AOD (+ 2 anisotropy parameters) by optimal solution approach. Errors in AOD retrieval might be compensated by "counter-errors" in surface albedo.	Compare MSA AOD with AERONET data and MACC-2 re-analysis. Analyse MSA in relation to AOD accuracy. Investigate effect of varying AOD on stable surfaces.	Atm. scattering will make bright surfaces look darker and dark surfaces look brighter.
Atmospheric correction, absorption	Low	Gaseous absorption exists within MVIRI VIS spectral range. Errorneous assumptions on total amount of absorbing gases (mainly water vapour) may lead to errors in MSA.	Impact deemed rather small as compared to other potential error sources. Detailed investigation beyond study scope.	Larger effects may occur for slanted observation geometries.
Cloud screening	high	Undetected clouds lead to albedo overestimation, corresponding cloud shadows to underestimation.	Identify and document cloud screening issues. Analyse MSA cloud screening method and possibly propose improvements (a priori, a posteriori).	Undetected couds lead to many outliers. Cloud screening difficult over high albedo regions/snow.
Sun-sychroneous orbit	Low	Local overpass of polar orbiting instruments continuously delayed due to atmospheric friction with associated changes in solar illumination of a target.	Outside study scope.	

3.2.3. Natural factors Final Report

Natural factors				
Process	Relevance	Potential effect on MSA	Evaluation strategy	Remarks
Sub-pixel/ thin cirrus clouds	Medium	Undetected sub-pixel / thin cirrus clouds lead to albedo overestimation.	Beyond study scope. Possible strategy would be to use high resolution imagery to assess the impact of subpixel clouds on the MSA surface albedo.	Non-negligible impact. Potentially worth being further studied.
Solar intensity, variability	Low	Solar intensity at top of atmosphere varies, e.g. due to elliptic orbit of Earth or sun spot activities.	Impact deemed rather small as compared to other potential error sources. Beyond study scope.	
Surface orientation	Medium	Surface orientation impacts flux on surface, especially at low solar angles. Impact probably mostly limited at MSA pixel size.	Beyond study scope. Possible strategy would be to use DTM (e.g. USGS GMTED2010) to identify and analyze potentially affected areas.	
Hot spot effect	Low	Observer with sun behind looks into the "hot spot" – no shadows, therefore high reflectance. Leads to albedo overestimation.	Impact deemed small for MSA since algorithm excludes hot spot geometries. Possible strategy would be to analyse hot spot geometries for hot-spot prone surface types.	Hot-spot effect potentially signifcant in forests.
Sun glint	Medium	Specular reflection at water surfaces may lead to significant albedo overestimation.	Beyond study scope. Possible strategy would be to study time series of potentially affected areas, e.g. wetlands, rice fields, sub-pixel lakes.	Non-negligible impact. Potentially worth being further studied.
Surface inhomogeneity	High	No direct impact on MSA retrieval, but surface inhomogeneity renders quality assessment difficult.	Use homogeneous surfaces for quality assessment. Identify homogeneous surfaces from land cover information and/or high-resolution imagery.	Surface inhomogeneity combined with geolocation errors leads to "noise" in retrieved surface albedo.
Natural surface variability	High	The albedo of most natural surfaces depends strongly on a number of factors, such as state of vegetation, seasonality, meteorological conditions (wind, snow, ice, …), soil moisture etc.	The natural variability of natural surfaces needs to be considered when analysing MSA.	

3.3. Overview of satellite-derived surface albedo products

Numerous attempts have been made to retrieve the surface albedo from space-borne observations. A non-exhaustive subset of relevant satellite products, not necessarily being climatologies but certainly having value for climate studies, is listed below:

➢ An overview on satellite-derived surface albedo products up to 2007 is given in Schaaf et al. [2008], particularly covering the products from MODIS, MISR and MVIRI (MSA).

➢ BRDF/albedo products from POLDER are described in Leroy et al. [1997];

➢ Information on the BRDF/albedo products derived within the ESA GlobAlbedo project based on MERIS, SPOT-VEGETATION and MODIS data is provided in Muller et al. [2012-B];

➢ Satellite-based surface albedo products are also produced in the context of the Geoland-2 project from SPOT-VEGETATION observations [Camacho et al., 2012];

➢ Surface albedo products from geostationary MSG-SEVIRI observations are for example provided through the EUMETSAT-funded Land Surface Analysis Satellite Application Facility (LSA SAF) [Trigo et al., 2012];

➢ Surface albedo derived from AVHRR observations [Csiszar and Gutman, 1999].

Three different approaches for surface albedo retrieval are employed, all of which require the estimation of bidirectional reflectance factors at the bottom of atmosphere for the instrumental spectral channels using the geometry shown in Figure 2 below.
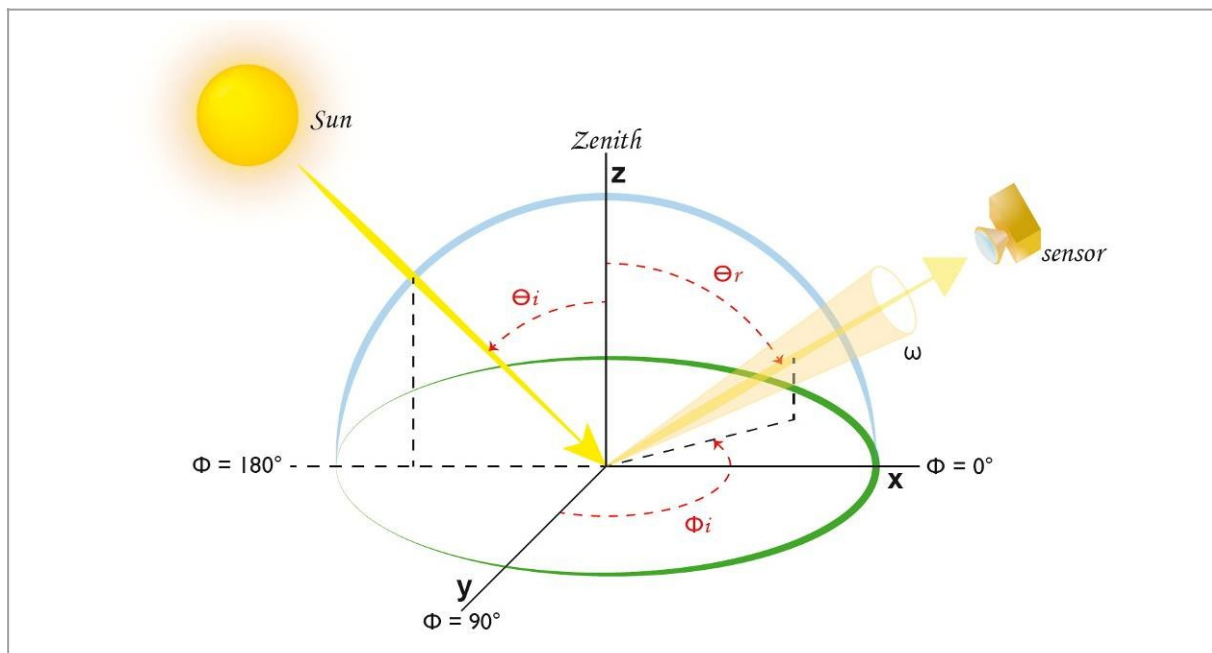
Figure 2. Schematic diagram showing angles used in the definition of BRF, BRDF and albedo (θ: zenith angle; Φ: azimuth angle; i: incident; r: reflected; ω: solid angle).

3.3.1. Near-simultaneous BRF retrieval

A number of polar-orbiting instruments allow observing an area on the Earth under different observation geometries within short time periods. Examples include POLDER [Leroy et al., 1997; Roujean and Lacaze, 2002; Buriez et al., 2005] where up to 40 directional looks at 7 km resolution can be obtained within a few seconds and MISR [Martonchik et al., 1998; Braverman and Girolamo, 2002] where 9 directional looks at 275m resolution are obtained within 7 minutes. Such observations are often referred to as "instantaneous" BRDF/albedo retrievals.

3.3.2. Composite BRF retrieval for polar-orbiting instruments

Most polar orbiting instruments rely on another approach to collect sufficient BRF information to allow for an albedo estimation. The so-called composite retrieval collects observations for a fixed time period, e.g. 16 days for 500 m MODIS [Schaaf et al., 2002] and up to 18 months for 1 km GlobAlbedo [Muller et al., 2012-B]. Albedo values are then typically reported at a shorter interval, e.g. 8 days for GlobAlbedo.

3.3.3. Composite BRF retrieval for geostationary instruments

Geostationary instruments observe a target on the Earth surface always under the same viewing angle. Therefore, the only possibility to collect the BRF information required for albedo estimation is to collect measurements through the course of the day. Due to reciprocity, this is equivalent to multi-directional looks. Geiger et al. [2008] as well as Govaerts et al. [2004, 2008] describe applications of this approach to various geostationary instruments. An example of a near-global map derived from geostationary satellites is shown in Figure 3 below.
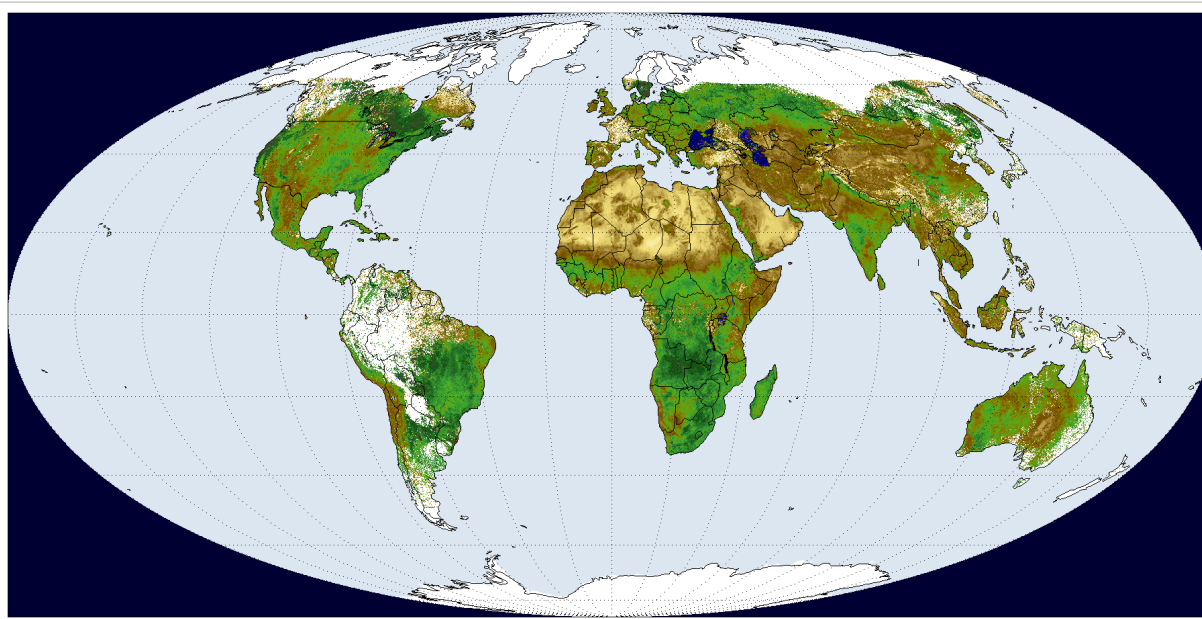
Figure 3. Broadband surface DHR$_{30}$ map at 0.25° resolution derived by applying the GSA algorithm to GMS-5, MET-5, MET-7, GOES-8, and GOES-10 observations acquired on May 1–10, 2001 (figure by courtesy of EUMETSAT).

4. The Meteosat Surface Albedo (MSA)

4.1. The Meteosat Visible and Infrared Imager (MVIRI)

Meteosat's primary instrument is the *Meteosat Visible and InfraRed Imager* (MVIRI), flown on all *Meteosat First Generation*[6] (MFG) satellites since Meteosat-2 launched in 1981. MVIRI acquires radiance data from the full earth disc every half hour. MVIRI operates in three spectral bands, chosen in accordance with Meteosat's primary task of mapping the distribution of clouds and water vapour. The MVIRI Visible (VIS) band extends from 0.45 µm to 1.0 µm with a central wavelength at 0.70 µm. Atmospheric gases are fairly transparent to incoming and outgoing (reflected) solar radiation in this spectral range[7]. The VIS band is used for imaging during daylight and provides the input data to the Meteosat Surface Albedo (MSA) product.
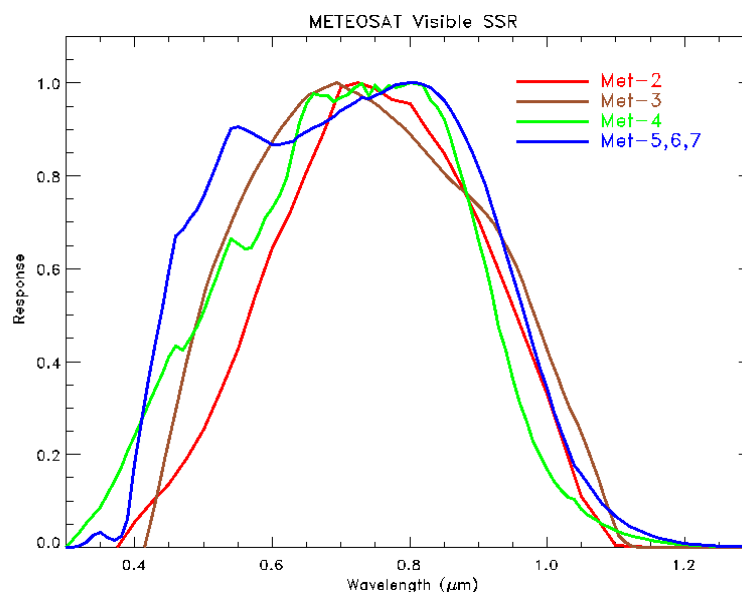
Figure 4: Sensor spectral response of the MVIRI VIS band for all Meteosat First Generation satellites (figure by courtesy of EUMETSAT).

4.2. Nominal coverage areas and periods

The main mission of the MFG satellites was to provide data for the 0 degree (0DEG) service area covering most of Europe, Africa, the Middle East, and the Eastern parts of South America. Consequently, all MFG satellites were first positioned in a geostationary orbit with a nominal sub-satellite point above the equator at 0° longitude.

In order to bridge a gap in the availability of GOES (Geostationary Operational Environmental Satellite, US) data from the western Atlantic Ocean between 1991 and 1995, Meteosat-3 was moved to the west, at first to 50° W and early in 1993 to 75° W. These temporary services, called Atlantic Data Coverage (ADC) and Extended-ADC (XADC) respectively, had the primary purpose of supporting the monitoring of severe weather events such as hurricanes.

In order to increase data availability above the Indian Ocean, Meteosat-5 has been moved in 1997 to a sub-satellite point above the Indian Ocean at 63°E. MVIRI data acquired at this position are

---

[6] http://www.eumetsat.int/Home/Main/Satellites/MeteosatFirstGeneration/index.htm?l=en (verified 2012-08-20)

[7] http://www.eumetsat.int/Home/Main/Satellites/MeteosatFirstGeneration/Instruments/index.htm?l=en (verified 2012-07-12)

available between mid 1998 well into 2007. Meteosat-7 has been positioned at 57.5°E from where it acquires data since November 2006 to date. Meteosat-6 has also been positioned above the Indian Ocean at 67.5° between January 2007 and April 2011 as a back-up satellite but was de-orbited in April 2011. Table 5 provides an overview of the resulting coverage of MVIRI observations in standard operation mode.

Table 5: Overview of MVIRI observations in standard operation mode[8]. The coverage acronyms refer to Indian Ocean Data Coverage (IODC) and [Extended] Atlantic data coverage ([X]ADC). The corresponding sub-satellite points (SSP) are also indicated.

Coverage	SSP	Satellite	Start Date	End Date
0DEG	0° E	M2	16/08/1981	11/08/1988
		M3	11/08/1988	25/01/1991
		M4	19/06/1989	04/02/1994
		M5	02/05/1991	13/02/1997
		M6	21/10/1996	20/01/2000
		M7	03/06/1998	19/07/2006
IODC_63	63° E	M5	01/07/1998	16/04/2007
IODC_57	57° E	M7	01/11/2006	ongoing
ADC	50° W	M3	01/08/1991	27/01/1993
XADC	75° W	M3	21/02/1993	31/05/1995

Figure 5 shows the spatial coverage corresponding to the five different Meteosat orbits. These plots indicate the maximum possible coverage area. Large zenith angles, cloud contamination, and other adverse effects lead to a reduced practical coverage (see section 7.1).
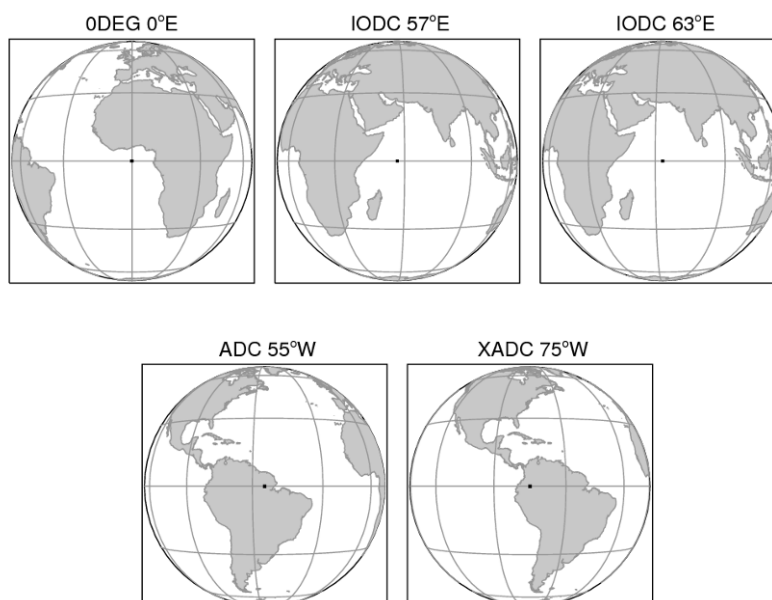
Figure 5: The five different coverage areas in native MSA projection. The respective sub-satellite points are shown as a black dot in the centre of each panel.

---

[8] http://www.eumetsat.int/groups/ops/documents/document/pdf_meteosat_prime_satellites.pdf verified 2012-07-12)

4.3. MSA scientific approach

The Meteosat Surface Albedo (MSA) algorithm has been jointly developed at EUMETSAT and the Joint Research Centre (JRC), based on the method proposed by Pinty et al. [2000-A, 2000-B]. It accumulates MVIRI VIS observations during one day to form a measurement vector for each pixel (see Figure 6). The surface albedo and other parameters are then concomitantly retrieved by inverting a radiative transfer model.

The MSA surface albedo retrieval is based on the following major assumptions:

  ➢ Surface and atmospheric scattering properties are assumed constant along the day;

  ➢ Aerosol scattering can be approximated by a single continental aerosol type;

  ➢ Surface anisotropy can be represented with the simple Bidirectional Reflectance Factor (BRF) model proposed by Rahman et al. [1993] (further on referred to as RPV);

  ➢ The reciprocity principle, i.e. the assumption that the BRDF is unchanged when incident and observation angles are reversed, is valid over terrestrial surfaces at a spatial resolution of a few kilometres [Lattanzio et al., 2006].
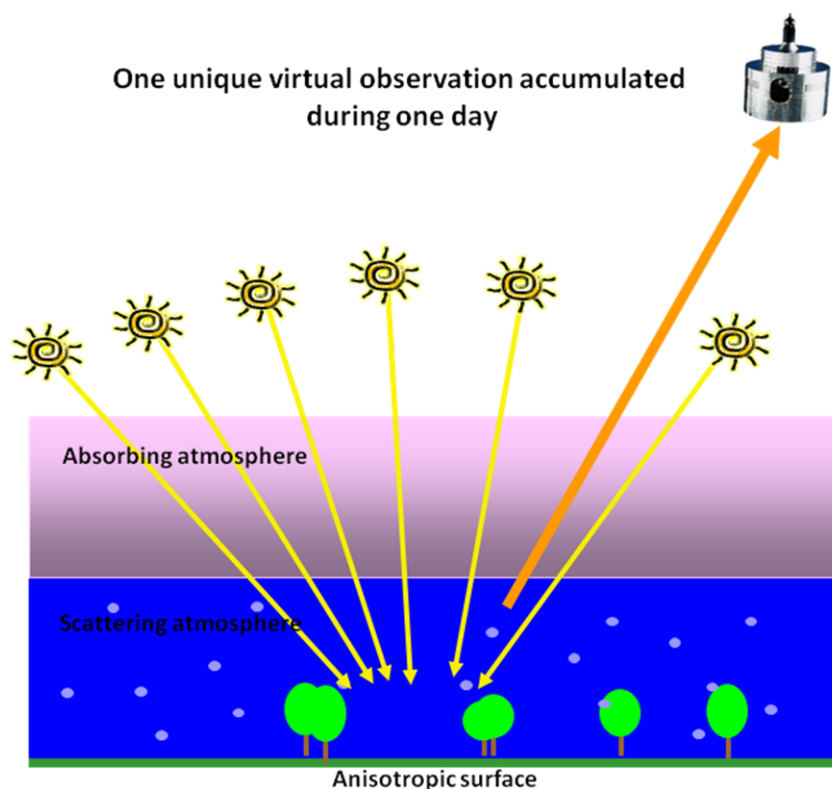
Figure 6: MSA retrieval scheme. Observations accumulated during the day are used as an angular sampling of the surface (Figure by courtesy of EUMETSAT).

The radiative state of the observed medium, i.e., the atmosphere and the underlying surface, is described by a set of six state variables:

  ➢ τ: equivalent aerosol optical thickness (EAOT) at 550 nm;

  ➢ $\rho 0$: amplitude of surface BRF;

  ➢ Θ: asymmetry of surface BRF;

  ➢ k: bowl shape of surface BRF;

  ➢ U_{H2O}: total column water vapour;

➢ U_{O3}: total column ozone.

Due to the limited information content of the measurement in only one channel, it is not possible to retrieve all six variables that characterise the radiative state of the observed medium. In order to reduce the number of free parameters, the total column water vapour is taken from ECMWF re-analyses and the total column ozone from Total Ozone Mapping Spectrometer (TOMS) observations [McPeters, 1996].

The values of the other four state variables (τ, $\rho0$, Θ, k) are concomitantly retrieved through the inversion of (forward) radiative transfer calculations against the measurement vector, minimising the differences between observations and simulations, normalised by the respective observation error [Govaerts and Lattanzio, 2007]. A probability is assigned to each solution that specifically depends upon the number of degrees of freedom and the value of a cost function. The estimation of the retrieved parameter uncertainty relies on a statistical analysis of the solution ensemble. A 10-day temporal compositing technique is applied to maximise the spatial coverage of cloud free pixels. Finally the retrieved surface state variables ($\rho0$, Θ, k) are applied to the RPV model to derive the Directional Hemispherical Reflectance (DHR$_{30}$) for a reference solar zenith angle of 30◦ together with its respective error as well as BHR$_{ISO}$.

The blue sky albedo is not derived within MSA but may be estimated in an additional step as a linear combination of DHR$_{30}$ and BHR$_{ISO}$, using weighting factors representing the estimated ratio between diffuse and direct downwelling atmospheric radiation which itself may be deduced from the aerosol optical depth [Pinty et al., 2005].

4.4. MSA implementation overview

The MSA algorithm is implemented in four sequential steps:

1. Data consistency procedure (DCP)
   This module attempts to screen out cloud affected pixels by identifying measurements that deviate from the course of the diurnal BRF at TOA [Pinty et al., 2000-B];

2. Atmospheric scattering module (ASM)
   This module first corrects for the absorption by atmospheric gases and then inverts a radiative transfer model representing the atmosphere-surface system to provide all possible solutions to a measurement vector;

3. Data interpretation module (DIM)
   This module chooses the most likely solution among all possible solutions retrieved in the previous step;

4. Time averaging[9] module (TAM)
   Steps 1 to 3 are applied on a daily basis. In this last module, the best solution for the 10-day period is selected.

Table 6: Discretisation values used for MSA forward modelling.

Parameters	Values
k	0.4, 0.5, 0.6, 0.7, 0.8, 0.9, 1.0
Θ	-0.30, -0.25, -0.20, -0.15, -0.10, -0.05, 0.00
τ	0.1, 0.2, 0.3, 0.4, 0.6, 0.8, 1.0

---

[9] The (historic) term "averaging" is somewhat misleading here since averaging is not taking place for DHR$_{30}$ and BHR$_{ISO}$ but only for AOD.

In order to speed up model inversion, the 6S radiative transfer code [Vermote et al., 1997] has been used to calculate look-up-tables of an ancillary function for every combination of the discrete values shown in Table 6.

4.5. MSA implementation details

4.5.1. Improving data consistency

Clouds and cloud shadows are screened out in the first processing step (DCP) by analysing the daily cycle of the bi-directional reflectance factor (BRF)[10]. A threshold value of 0.6 is applied on the TOA BRF measurements to reject obviously cloudy conditions[11] [Pinty et al., 2000-B].

In order to further eliminate pixels affected by e.g. undetected clouds, topography shadows, errors in the data geo-rectification process, and/or significant diurnal variations in aerosol load and type, the screened TOA BRF values are additionally checked against a modified version of the RPV model [Engelsen et al. 1996]: An iterative process eliminates the observed BRF value exhibiting the largest absolute deviation with respect to the model prediction (see Figure 7). A pixel is further processed only if it contains at least six valid daily observations. The cloud detection method occasionally fails when the cloud cover remains stable during an entire day.
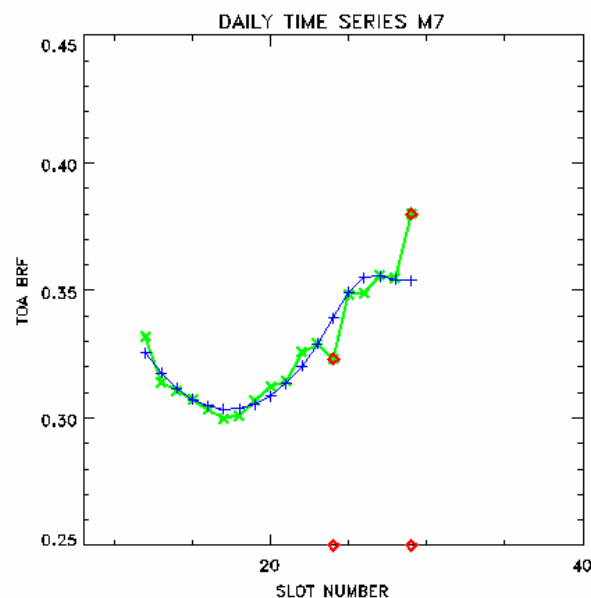
Figure 7: Example of the data consistency procedure (DCP) for MVIRI-7. Green: BRF from MVIRI measurements. Blue: Best-fit. The red squares represent rejected values likely affected by clouds (above fit) or cloud shadows (below fit) (figure by courtesy of EUMETSAT).

The result of the fit between the modelled TOA BRF and the valid observations provides an estimation of the filtering process cost, accounting for an uncertainty σ_{DCP} between data and model.

4.5.2. Atmospheric effects

The MSA algorithm decouples atmospheric gaseous absorption from scattering by subdividing the atmosphere into two distinct layers where the lower layer accounts for the scattering processes and the upper layer for gaseous absorption.

---

[10] In its present version, MSA does neither use the MVIRI IR channels as additional information source for cloud identification nor does it rely on externally generated cloud masks.

[11] This threshold value will also lead to the rejection of cloud-free pixels of snow-covered surfaces.

The atmospheric effects have been calculated for a US-62 standard atmosphere[12], additionally implementing a continental aerosol model, which includes a mixture of dust-like, water-soluble, and soot components (see Vermote et al. [1997]). Two gaseous absorbers are taken into account: The total column water vapour is taken from ECMWF re-analyses and the total column ozone from the Total Ozone Mapping Spectrometer (TOMS) observations [McPeters, 1996].

4.5.3. Directional-effects

As previously mentioned, the MSA retrieval is based on the assumptions that...

> ➤ ... surface anisotropy can be represented with the simple BRF model proposed by Rahman et al. [1993], and

> ➤ ... the reciprocity principle is valid over terrestrial surfaces at a spatial resolution of a few kilometres [Lattanzio et al., 2006].

While the former assumption is drawn from the need to apply a simple BRDF model to account for the limited information content of MVIRI observations, the latter assumptions accounts for the fact that MVIRI, being on a geostationary orbit, always observes a specific pixel under the same viewing angle, meaning that the only variation in the observation geometry comes from the different solar illumination geometries during the course of a day.

The RPV model (see also Pinty et al. [2000-A,-B]), describes the angular distribution of the surface BRF by:

$$\rho_s\left(z_0, \Omega_s, \Omega_v; \rho 0, \Theta, k\right) = \rho_0\, \rho_s'\left(z_0, \Omega_s, \Omega_v; \Theta, k\right)$$

(1)

where Ω_s and Ω_v are the illumination and viewing direction and z_0 denotes the bottom of the atmosphere. The reflective properties of the surface are described by the parameters ρ_0, Θ and k where ρ_0 specifies the amplitude, Θ the asymmetry and k the bowl shape of the surface BRF in the RPV model.

While the reciprocity principle is generally assumed valid, the rather simple BRF model will necessarily lead to an error when attempting to retrieve the albedo from MVIRI measurements. For example, Rahman et al. [1993] observed relative root mean square errors (RMSE) above 20% for optimally fitted asymmetry parameters when comparing modelled to measured bidirectional reflectances, e.g. for soybean, coniferous forest or pasture land.

4.5.4. Temporal compositing

The objective of the temporal compositing is to maximise the number of clear sky processed pixels during a 10-day period. This compositing relies on the selection of the single most representative solution over the accumulation period. The most obvious way is to select the solution with the best fit accounting for the actual number of degrees of freedom. Hence, the most representative solution within a 10-day period is the one with the highest probability.

As clouds tend to increase the signal received at satellite level, selecting the solution with the smallest ρ_0 will tend to minimise the impact of undetected clouds. Thus, if two or more solutions have the same probability, the one with the lowest ρ_0 is selected.

4.5.5. Broadband conversion

A third order polynomial is applied [Govaerts et al., 2006] to transform the directional hemispherical reflectance DHR_{VIS} representing the spectral range 0.45 - 1.0 µm derived from MVIRI VIS measurements into the shortwave broadband albedo DHR_{BB} (0.3 - 3.0 µm:)

---

[12] See for example http://modelweb.gsfc.nasa.gov/atmos/us_standard.html (URL verified: 2012-08-20)

$$DHR_{BB} = a + b \times DHR_{VIS} + c \times \left(DHR_{VIS} \right)^2 + d \times \left(DHR_{VIS} \right)^3 \qquad (2)$$

The coefficients *a* to *d* as well as a measure of uncertainty are specified in the Product User Manual[13] (PUM) for the MVIRI-2 to -7. Use of the original coefficients led to systematic deviations and temporal inconsistencies in the MSA dataset. Recently, Loew and Govaerts [2010] empirically derived correction factors leading to a significantly improved product consistency. Those are reported in the PUM as well and should be used to obtain best results.

---

5. Reference data

Three different types of reference data have been used in the frame of ALBEDOVAL to assess the quality of the MSA dataset:

➢ In situ measurements of the surface albedo;

➢ Satellite-derived values of the surface albedo;

➢ Ancillary information on land cover and atmospheric aerosol.

A list of the reference data used for the MSA assessment can be found in Annex 11.1.

5.1. Surface albedo in situ data

5.1.1. Availability

During the initial stages of ALBEDOVAL, the availability of surface albedo *in situ* data was analysed. Considering …

➢ … the importance of the surface albedo as essential climate variable;

➢ … the availability of relatively inexpensive and robust standard instrumentation, and

➢ … the fact that surface albedo measurements are routinely executed since several decades,

it was expected to find relevant information readily available on the internet. However, this is not the case, especially for the pre-EOS era. On the other hand, a lot of information on surface albedo measurements can be found in the scientific and "grey" literature. However, this information is scattered and not readily available in digital data formats. The published results also do represent only a limited fraction of all measurements made (see section 5.1.3).

Surface reference data optimally suited for validating satellite-based surface albedo retrievals should fulfil the following requirements:

➢ Sites located in areas with homogeneous land cover;

➢ Measurement taken at sufficient height above reference surface to integrate over small-scale heterogeneity;

➢ Sites include a sufficiently broad range of different land cover types [loc. cit.].

Originally, the Base Surface Radiation Network[14], BSRN [Ohmura et al., 1998] was envisaged as such a reference dataset given its frequent use for climate studies [Wild et al., 2001]. However, only a few of the roughly 20 BSRN stations located in the MVIRI field-of-view do actually provide surface albedo measurements and are additionally often located in rather heterogeneous landscapes.

Figure 8 shows an example for the BSRN site in Toravere (Estonia) clearly demonstrating that this site is not suitable for validating satellite-derived surface albedo for pixels at MODIS or even MVIRI size due to highly heterogeneous land cover and the resulting misrepresentation of the surface albedo derived from ground-based instruments.

---
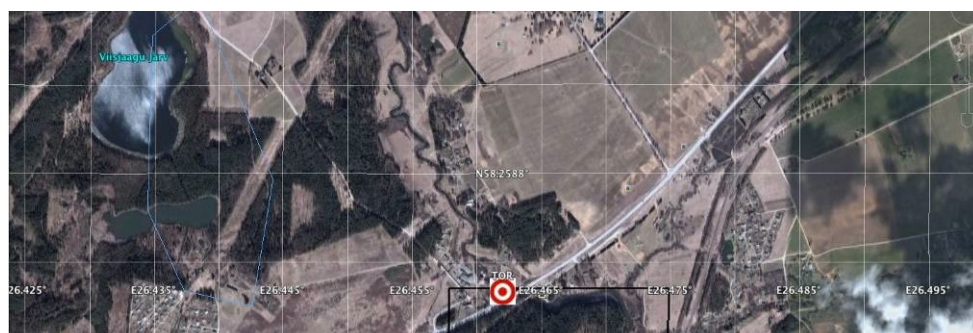
[14] http://www.bsrn.awi.de/en/home/ (URL verified on 2012-07-19)

Figure 8. Aerial image of the area around the BSRN site (red-white symbol) at Toravere, Estonia The typical extension of a MODIS pixel is shown by the black square. An MSA pixel would roughly cover the whole area shown [Image source: Google Earth].

An alternative set of tower albedo measurements have recently become available as a result of a significant effort by the JRC on behalf of the FLUXNET[15] consortium. Cescatti et al. [2012] showed the application of some 53 sites meeting certain surface homogeneity requirements to an assessment of MODIS-derived albedo data for the year 2005 (Figure 9). However, also FLUXNET measurements are not optimally suited for MSA validation purposes as they are concentrated in Europe (and the US) and are limited to vegetated surface types classified into plant functional types (PFTs).

Surface albedo ground truth data finally considered within ALBEDOVAL stem from FLUXNET (19 sites), Safari 2000 (2 sites), and the Baseline Surface Radiation Network (BSRN, 2 sites), as well as from a selection of data originating from individual measurement campaigns in Sudan in 1988 and 1989 (see section 11.1.1 for more details). The comparison of these in situ data with the corresponding MSA values is shown in section 7.8.
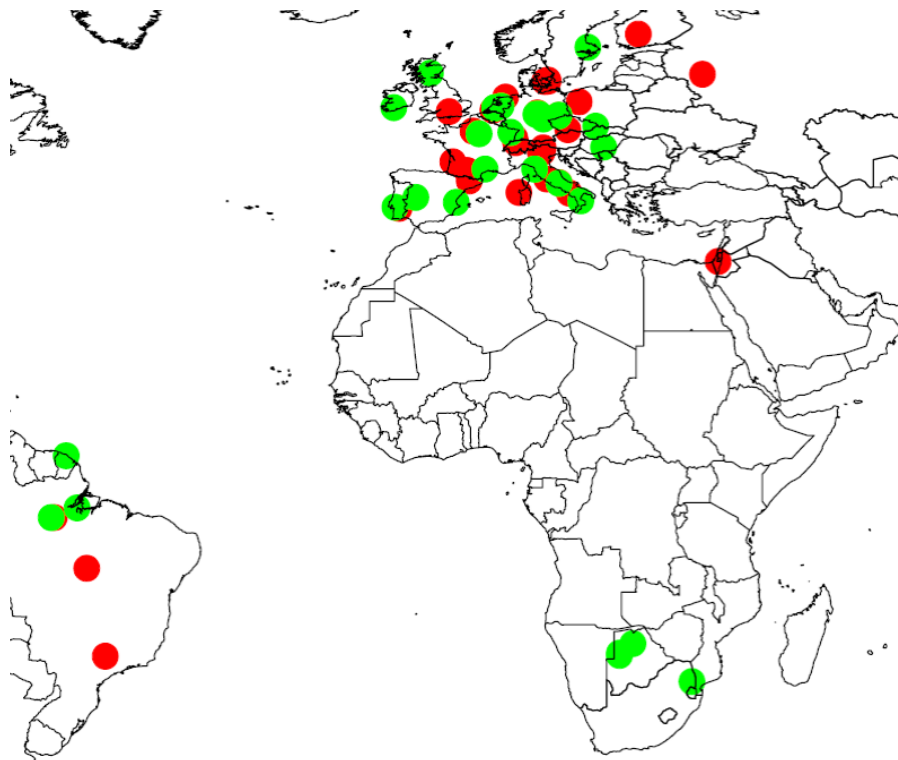
Figure 9. FLUXNET sites within the MVIRI 0DEG field-of-view taking albedo measurements. Green dots represent sites with sufficient plant cover homogeneity at a 1 km² scale. Source: Cescatti et al. [2012].

5.1.2. Scaling up to MSA pixel size

A number of approaches exist to relate ground-based surface albedo measurements (representing areas of typically 100 to 1,000 m²) to the space-based albedo retrievals (representing e.g. ca. 250,000 m² for MODIS at 500m resolution or 6,250,000 m² for MVIRI-VIS).

The direct approach is to only use surface reference data representing the average land cover of the full satellite pixel for validation. In order to quantify the homogeneity of the land cover within the pixel, higher resolution imagery can be applied, either for visual inspection or for deriving

---

[15] http://daac.ornl.gov/FLUXNET/fluxnet.shtml (URL verified on 2012-07-19)

statistical homogeneity metrics. Only pixels above a certain homogeneity threshold would then be used for further analysis. Obviously, the number of suitable reference site reduces with increasing pixel size, especially when considering the geo-location uncertainty (e.g. 1-2 pixels for MVIRI). This is the approach pursued in this study (see section 5.4.2 for more details).

An indirect approach consists in assigning standard BRDFs to the individual classes of a high-resolution land cover dataset (e.g. CORINE[16]) and to then integrate this small-scale information to the required pixel size (see e.g. Fang et al. [2004]). This approach could not be pursued in the frame of this study.

5.1.3. Mechanisms of information loss

Less than expected information on surface albedo in situ measurements is available in online data sources, even though the surface albedo was one of the core measurement parameters measured on occasion of large field experiments targeting surface-atmosphere fluxes. In Panel 2, we try to explain this lack of data availability at the example of albedo measurements taken by a university institute in the 1980s and 1990s-

Between mainly the mid-1980s and the mid-1990s, the Institute of Meteorology of the Free University Berlin (IM-FUB) participated to several large national (e.g. LOTREX-HIBE 87) and international (e.g. HAPEX-Sahel, EFEDA) field experiments to study land surface-atmosphere interactions. During all of these field experiments, broadband albedo measurements in high temporal resolution were routinely taken by tower-mounted albedometers over a variety of surface types for periods extending from days to months. These measurements were complemented by spectral albedo and spectral reflectance measurements carried out with portable instruments in an attempt to better characterise variability and reflective properties of the land surface within the experimental areas.

Further surface albedo and reflectance measurements were taken during smaller dedicated campaigns, e.g. in support of external scientific projects or in the context of MSc or PhD theses.

We assume that surface albedo measurements have been taken at more than 250 different sites by IM-FUB over the years. A subset of these measurements were further processed and published as theses, scientific articles or books [for example Fell, 1991; Bolle et al., 1993; Bolle et al., 2006].

Raw data and processing software were partly stored on paper but mostly digitally on diskettes (5 ¼ or 3 ½ inch), magnetic tapes, magneto-optical disks, hard disks, etc. and remained mainly under the custody of the then responsible scientists. Over the years, scientific interests shifted, relevant personnel retired or took up new responsibilities, offices were moved or cleared out, storage technologies became outdated, etc., all resulting in a situation where only a limited subset of a previously much larger amount of potentially highly relevant ground truth data has remained available until now.

During our search for in situ surface albedo data taken by IM-FUB for the purpose of ALBEDOVAL, a number of processed but unpublished data could be made available. In addition, we could secure further unprocessed raw data in the form of hand-written field protocols (see Panel 3). Attempts should be made towards saving the still available ground truth data before they will forever be lost and to make such data available in a harmonised and quality-controlled manner.

We assume that the situation at IM-FUB is not untypical for other research institutions and that further data of high relevance to the assessment of the surface albedo and other ECVs can be made available, for example from institutions participating to the above mentioned international field experiments.

Panel 2: Mechanisms of losing knowledge about surface albedo in situ measurements.

---

[16] http://sia.eionet.europa.eu/CLC2006/ (URL verified: 2012-08-20)

ALBEDOMETER - PROFIL

1. Standort: 1Km vom Camp in Richtung S / wir hielten auf den rechten Rand des Dj. Ibrahim el Uab- bschi zu

Untergrund: alluvial, Wadi-Vegetation um uns herum (Photo 1)

09:04 kappe: gu 357   t:-10,25   gb:-0,00   gr:-0,01 [mV]

09:06 gu o 1,482 1,72 1,541 1,466 1,478 1,726 1,303 1,372 -1,36 -1,33/Bu -0,39
      t u 0,201 0,201 0,484 0,446 0,579 0,505 0,517 0,580 -0,53 -0,52 -0,41
                                                    » 09:08

09:09 t o 1,636 1,28 1,712 1,250 1,473 1,27 1,294 1,337 -1,20 -1,03 -0,64
      gu u 0,192 0,195 0,452 0,502 0,592 0,529 0,533 0,605 -0,60 -0,67 -0,20
                                                    » 09:12

| | Mittelwert der Bodenalbedo in | | | |
Wellenlänge	Wadi Abu G.	Djebel Fur.	Qoz El Harr	Buweiha/G.
521 nm	0.13 ± 0.01	0.15 ± 0.01	0.14 ± 0.01	0.12 ± 0.01
549 nm	0.16 ± 0.01	0.18 ± 0.02	0.19 ± 0.02	0.14 ± 0.01
615 nm	0.22 ± 0.02	0.31 ± 0.02	0.32 ± 0.02	0.19 ± 0.02
669 nm	0.24 ± 0.02	0.36 ± 0.02	0.37 ± 0.03	0.21 ± 0.02
760 nm	0.28 ± 0.02	0.42 ± 0.03	0.44 ± 0.03	0.23 ± 0.02
782 nm	0.28 ± 0.02	0.43 ± 0.03	0.45 ± 0.03	0.24 ± 0.02
862 nm	0.28 ± 0.02	0.43 ± 0.03	0.46 ± 0.03	0.25 ± 0.02
1024 nm	0.29 ± 0.02	0.46 ± 0.03	0.49 ± 0.03	0.26 ± 0.02
1238 nm	0.36 ± 0.03	0.54 ± 0.03	0.56 ± 0.04	0.29 ± 0.02
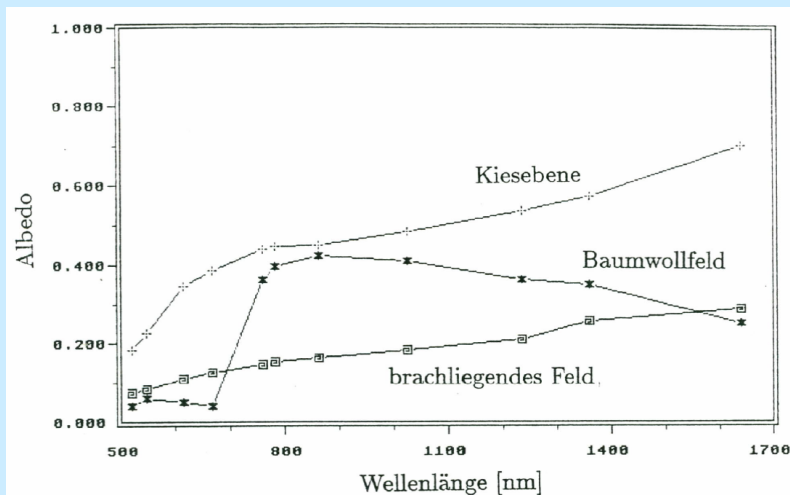
Panel 3. Top: Example of manually recorded spectral surface albedo measurements. Middle: Average spectral surface albedo values along four transects. Bottom: Surface albedo spectra for characteristic surface types ("Kiesebene"=gravel plain, "Baumwollfeld = cotton field, "brachliegendes Feld"=fallow field). All measurements have been taken in Nov. and Dec. 1989 in Central Sudan (see Fell [1991] for further details).

5.2. Satellite-derived surface albedo values

Due to the lack of ground-truth data suitable for a direct validation of satellite-derived surface albedo products, the mostly applied method to assess the quality of such products consists in *"internal"* and *"external"* product plausibility and consistency checks.

The internal plausibility and consistency of a satellite-derived product can be assessed by looking e.g. at time series over stable surface targets, or by looking at a reference surface under different observation geometries but otherwise similar conditions. Such internal quality checks play an important role in the assessment of the MSA and are described in more detail in sections 7.1, 7.3, 7.5, and 7.7.

Table 7: Selected MVIRI characteristics with relevance to MSA retrieval as compared to other space-borne instruments.

Quality aspect	MSA characteristics	Better suited (examples)
Temporal resolution	30 min	SEVIRI (15 min)
Spatial resolution	2.5 km at nadir	MODIS (0.5 km) MISR (0.375 km) MERIS (0.3 km)
Spectral resolution	1 VIS/NIR channel	SEVIRI (3 VIS/NIR channels) MISR (4 VIS/NIR channels) MODIS (5 VIS/NIR channels at 0.5 km) MERIS (15 VIS/NIR channels)
Surface anisotropy	Change in observation geometry only through changing solar position	MODIS, MERIS (single-angle polar orbiting) MISR, POLDER (multi-angle polar orbiting)

In the context of this study, external plausibility relates to the comparison of the MSA with equivalent values from other space-borne sensors. Due to more appropriate measurement approaches, certain space-borne instruments should in principle provide more accurate surface albedo values than does MSA.

For example, an instrument with higher spectral resolution in the VIS/NIR should provide a higher accuracy of the broadband albedo than an instrument that just measures in one spectral channel not fully covering the relevant (0.3 – 3.0 μm) portion of the spectrum. Another example would be polar-orbiting instruments with multi-angular observation capabilities better suited to correct for surface anisotropy effects than single-angle or geostationary instruments.

See section 7.6 to obtain more information on the external MSA quality checks performed in the frame of this study.

5.3. Other relevant datasets

The following auxiliary datasets have been used to assess the impact of the atmospheric aerosol load on the quality of the MSA retrieval:

➢ Aerosol optical depth (AOD) at 550 nm provided by MACC-II[17] (Monitoring Atmospheric Composition and Climate – II) re-analysis project. This dataset provides daily global AOD values and is available for the period 2003 to 2010 with a spatial resolution of 125 km [Benedetti et al., 2011];

---

[17] http://www.gmes-atmosphere.eu/data/

➢ AOD at 550 nm derived from Aerosol RObotic NETwork (AERONET) data. AERONET is a federation of ground-based networks to provide a long-term public domain database of aerosol optical, microphysical and radiative properties.

➢ The International Geosphere-Biosphere Programme (IGBP) ecosystem categories [Belward, 1996] have been used as a reference land cover classification.

As the existence of residual cloud contamination in the MSA product is to some degree detectable by statistical means (see section 7.7), external cloud products were not used in the context of this study. However, cloud masks provided by other sensors (e.g., MODIS) may become important to test the quality of an improved MSA product. In this context, re-analysis datasets such as ERA-Int [Dee et al., 2011] may be useful to identify geographical regions and seasons that are more likely to be affected by cloud contamination.

5.4. Reference sites

5.4.1. Site selection

In order to compare MSA values with other satellite-derived products, a number of suitable reference sites targeting specific potential quality issues have been identified:

➢ Navigational accuracy (coastlines with meridional and zonal orientation);

➢ Cloud contamination (dark surfaces);

➢ Temporal stability (arid surfaces assumed stable over time);

➢ Atmospheric impact (AERONET sites located in both 0DEG and IODC areas);

➢ Angular effects (reference surfaces located in both 0DEG and IODC areas);

➢ Sat-sat comparisons (“*highly homogeneous*” land cover over 5x5 MSA pixels, see section 5.4.2 for a definition of the applied homogeneity measures);

➢ Sat-*in situ* comparisons (“*highly homogeneous*” land cover over 5x5 MSA pixels with concomitant availability of in situ data).

The identification of large homogeneous reference sites was partly done by visual interpretation of Google Earth satellite images, partly by making use of sites suggested in the context other activities e.g. BELMANIP[18]).

In total, a long list of 87 reference surface targets has been established (list provided as separate Excel spreadsheet ALB_Reference_Areas.xls) of which 50 have been used for this study and 17 have been explicitly mentioned in this report (see Table 17).

5.4.2. Surface characterisation

Surface land cover and homogeneity of all potential surface reference targets have been analysed using USGS's Global Land Cover Characteristics (GLCC) Data Base in Version 2.0 in combination with the IGBP land cover legend. The GLCC dataset has been derived from AVHRR data spanning a 12 months period between 04/1992 and 03/1993. Its spatial resolution is 30 arc seconds, equivalent to a meridional resolution of about 1 km. The reason for choosing GLCC and the IGBP land cover legend is due to the fact that this data set is globally available, well tested and documented and frequently used in climatic applications.

The following surface characterisation parameters have been derived for each surface:

➢ Land cover (LC) type at centre of the reference surface (position of in situ measurement if applicable);

➢ Fraction of dominant LC type within a 2.5' x 2.5' area (25 GLCC pixels, ~5x5 km);

➢ Fraction of dominant LC type within 12.5' x 12.5' (625 GLCC pixels, ~25x25 km).

---

[18] http://calvalportal.ceos.org/cvp/web/olive/site-description

The degree of homogeneity of a reference surface target has been assigned according to the following rules:

> *"Average"* if the land cover type at the centre pixel is equivalent to the dominant land cover type within a 2.5' x 2.5' area around the centre covering more than 75% of the area;

> *"High"* if the land cover type at the centre pixel is additionally equivalent to the dominant land cover type within a 12.5' x 12.5' area around the centre covering more than 75% of the area;

> *"Low" (or heterogeneous)* otherwise.

Of the 87 surface reference targets identified for this study, 34 have been classified as being of low, 20 as being of average, and 33 as being of high homogeneity.

While it is not always possible to limit the assessment to homogeneous or very homogeneous surface targets, the homogeneity characterisation of the surface targets may help to explain observed discrepancies.

6. Quality assessment: defining the metrics

In an attempt to achieve the completeness of the MSA quality assessment and to facilitate a later re-analysis of a revised MSA product or the evaluation of similar satellite-based data products, an initial version of a hierarchical framework for CDR quality assessments has been established, including suggestions for traceable quality indicators and associated metrics.

The highest hierarchical level is termed *"[quality] domain"* and covers generic areas that are relevant to satellite products (*"method", "coverage", "accuracy", "sensitivity", "consistency", "usability"*). Each quality domain is represented by one or more specific *"quality aspects"* which, in turn, are represented by one or more concrete *"quality indicators"* to provide quantitative or qualitative traceable *"quality metrics"*.

The hierarchical framework is presented in Table 8, including concrete implementation suggestions. Not all of the presented indicators could be applied in the frame of ALBEDOVAL. It should be reminded that the method has been established on occasion of the MSA evaluation and likely will need to be adapted and further generalised when applied to CDRs other than the surface albedo.

In order to allow users to assess quality and fitness for purpose at a glance, appropriate condensed presentation of the quality related information should be attempted, e.g. in the form of appropriate figures and tables.

Table 8: Initial hierarchical framework for CDR quality assessment.

Quality domain	Quality aspect	Quality indicator	Quality metrics (Examples)
Method	Appropriateness	> Raw data characteristics > Underlying retrieval assumptions > Practical implementation details	> List of potential strengths and weaknesses based on theoretical considerations
Coverage	Spatio-temporal coverage	> Theoretical product availability determined by instrument FOV and operational periods > Practical product availability	> First and last observation per pixel, length of observation period > Average availability per pixel and time period > Duration of longest observation gap
Accuracy	Inherent retrieval accuracy	> Accuracy estimates generated by the retrieval method	> Pixel-wise uncertainty estimates or retrieval probabilities
Accuracy	Pixel navigation	> Deviation of actual from nominal pixel position	> Deviation along/across scan for reference feature points
Accuracy	Bias, i.e. systematic deviations from "true values"	> Comparison with reference data	> Statistical analysis for reference areas and time periods
Accuracy	Random errors	> Frequency of random errors / outliers	> Percentage of values outside corridor around running mean/ median for reference areas
Sensitivity	Sensitivity to individual processes	> Identification of known singular incidents	> Statistical analysis before and after a significant event
Sensitivity	Sensitivity to periodic processes	> Identification of known seasonal effects	> Sinusoidal decomposition of annual course of albedo for reference targets
Consistency, internal	Temporal consistency	> Short-term and long-term temporal stability	> Short-term: standard deviation over stable targets > Long-term: comparison of mean values over predefined periods

Quality domain	Quality aspect	Quality indicator	Quality metrics (Examples)
Consistency, internal	Cross-instrument consistency	> Smooth transition between instruments of the same type	> Statistical analysis pre/after transition for identical observation geometries
Consistency, internal	Cross-observation consistency	> Independence on observation geometry (where applicable)	> Statistical analysis for surface reference targets under different viewing geometries, preferably from the same instrument
Consistency, internal	Long-term stability	> Stability of long-term data series	> Trend analysis for temporally stable reference targets
Consistency, external	Comparison with similar products	> Statistical indicators to identify systematic differences to analogous product from different type of instrument or method	> Test of identical population: Chi-square > Difference statistics over predefined periods and areas
Usability	Product access	> Organisational ease (e.g. need to register, etc.) > Technical ease (e.g. online availability, ordering and retrieval process)	> Availability of support, e.g. through user helpdesk > Comparison with "best practise" product distribution > Number of product downloads
Usability	Product documentation	> Completeness and adequacy of product documentation	> Availability and last revision of PUN and ATBD > Documentation has been externally reviewed > Number of questions to helpdesk
Usability	User confidence	> Transparency on product weaknesses > Unbiased product assessment	> Documentation of product weaknesses available with examples and estimated magnitude > Availability of validation/evaluation report

7. Evaluation of the MSA dataset

7.1. Product availability

Since the beginning of the standard operational mode of Meteosat-3 in August 1988, MVIRI data are continuously available for the 0DEG coverage until July 2006 when Meteosat-7 was replaced by MSG-2. With only a few gaps, availability for the 0DEG coverage dates further back to August 1981. MVIRI data covering the IODC are continuously available between July 1998 and April 2007 for the 63°E SSP and since November 2006 for the 57°E SSP. Figure 10 visualises the temporal coverage of MVIRI-2 to -7 for the 0DEG and IODC areas.
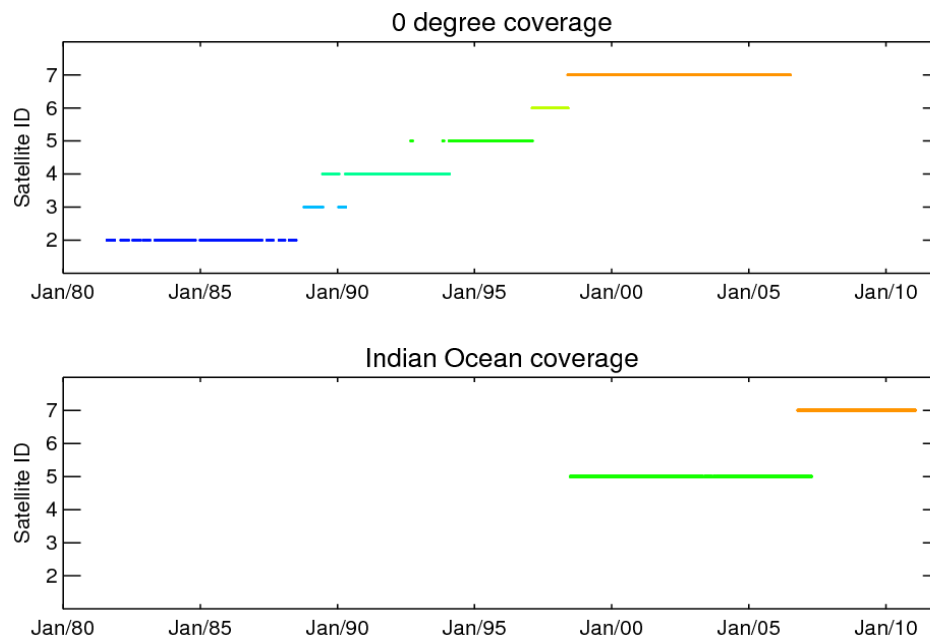
Figure 10: MSA temporal coverage for 0DEG and IODC. Note that Meteosat-5 was positioned at 57°E over the IODC whereas Meteosat-7 is located at 63°E.

Depending on geographical position and season, the number of valid MSA data points will be reduced due to external factors such as cloud cover, low solar elevation, etc. Figure 11 shows the practical MSA availability for the 0DEG, IODC_57 and IODC_63 areas. The availability is given in per cent for each grid cell and indicates the number of valid MSA values relative to all available 10-day periods.

While the MSA availability is near 100% for many desert areas, it significantly reduced for others. For example, availability is on the order of 30 % over northern Europe which is caused by low solar zenith angles in winter and frequent cloud cover throughout the year. Low availability is also observed over the Congo basin due to frequent cloud cover.
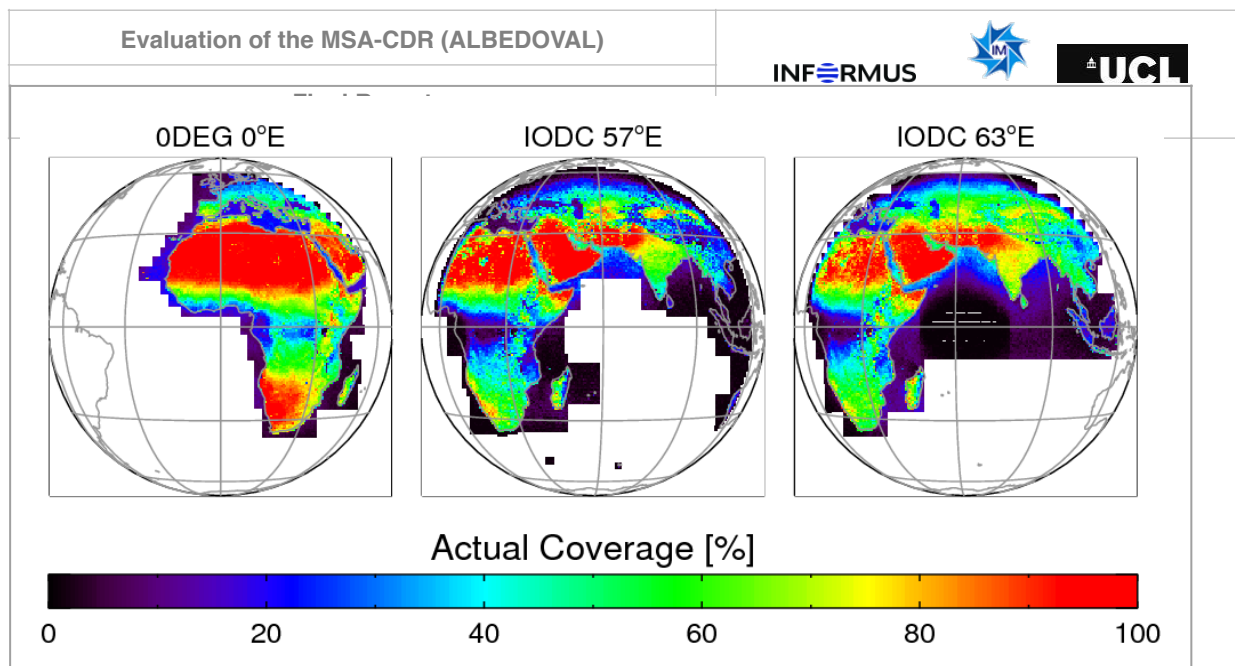
Figure 11: Practical MSA availability for 0DEG, IODC_57 and IODC_63. White areas do not hold any data whereas black areas do occasionally provide MSA data.

7.2. Pixel navigation

7.2.1. Results overview

Little information is found in the literature about MVIRI's spatial resolution and sampling accuracy. The MFG Handbook [EUMETSAT, 2011-A] does not discuss resolution (only sampling). A GSICS MVIRI-IASI inter-calibration study [EUMETSAT, 2011-B] reports a navigation uncertainty of about 1.5 pixels. This is consistent with the findings of this study which can be summarised as follows (see sections 7.2.2 to 7.2.5 for further details):

➢ With the exception of MVIRI-3, the navigation accuracy of the MVIRIs with respect to each other is approximately one pixel vertically and about 1.5 pixels horizontally;

➢ MVIRI-3 appears to be consistently shifted to the top by about 1.5 – 2 lines;

➢ The earlier MVIRIs show additional long-term navigational drifts and oscillations typically within the 1 pixel range;

➢ The scene-to-scene vertical navigation uncertainty is estimated at about 1.5 pixels. The horizontal navigation uncertainty could not be assessed with sufficient accuracy but is probably confined to a similar range.

This analysis has been done in MSA image co-ordinates; we therefore use the terms "horizontal" and "vertical" as well as "top", "bottom", "left" and "right" to describe positional uncertainties.

A more detailed analysis of navigation uncertainties would have to resort back to Level-0 or Level-1 data. This would especially be important in case a reprocessing of MVIRI raw data and derived products is planned.

Studying navigation accuracy was to a certain degree hampered by lacking information on MVIRI pixel resolution as well as on technical details of the geo-location routines. While EUMETSAT User Help Desk proved very responsive and helpful when trying to obtain relevant information, documentation on some of the older geo-referencing routines used in the MVIRI processing could not be made available.

7.2.2. Scene selection

Six coastline scenes consisting of 11x11 MSA pixels were identified in order to study the MVIRI pixel navigation (see Table 17). Reference targets and MVIRI "transects" are shown in Figure 12.
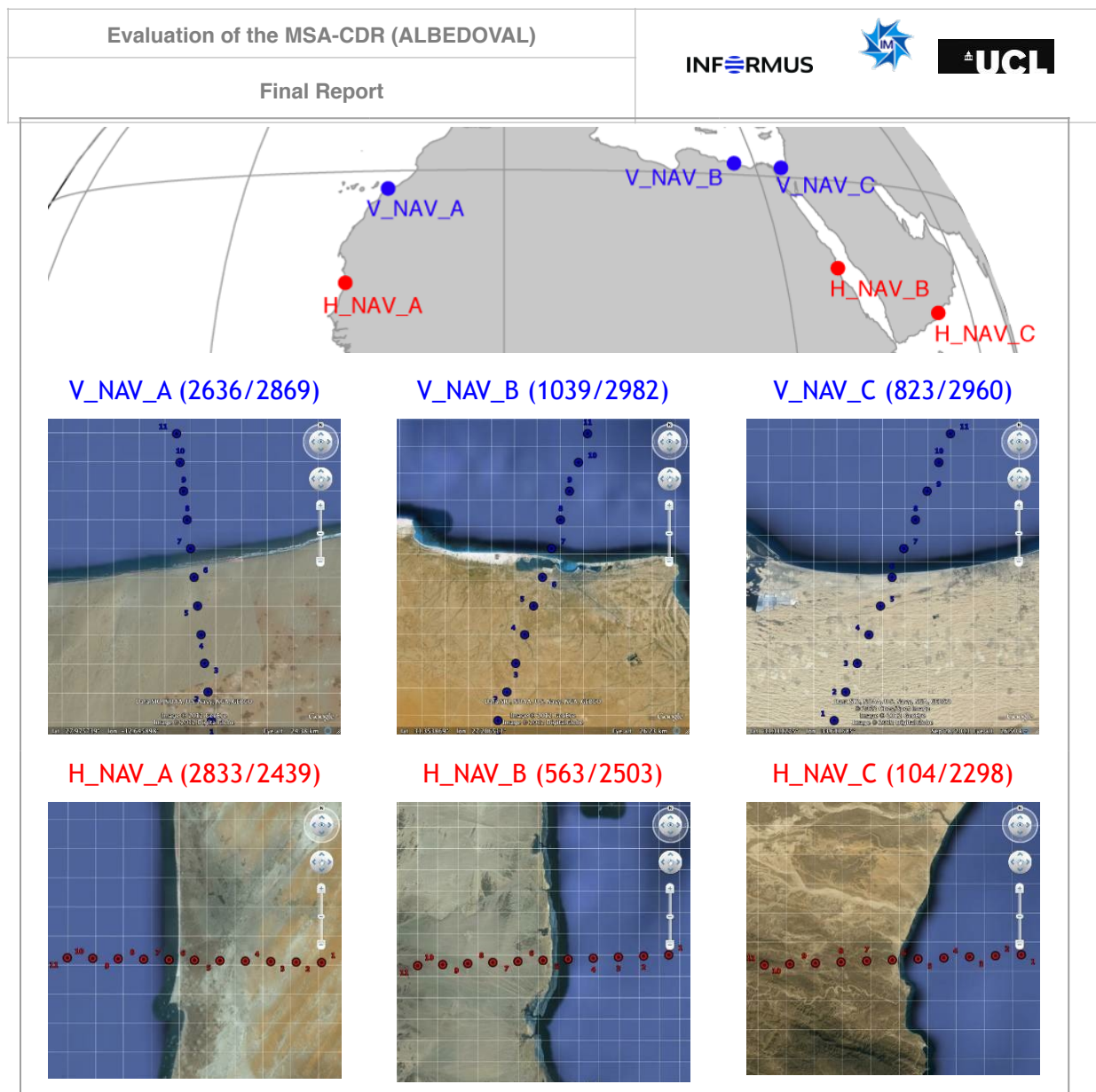
Figure 12: Reference coastlines used for studying MSA geo-location stability and accuracy. The MSA column/row position of the corresponding centre pixels is given in brackets in the header of each image. The blue resp. red dots mark the nominal centre positions of 11 adjacent MSA pixels within a column resp. row crossing the coastline.

The upper panel in Figure 12 shows the location of the 11x11 reference areas on the 0DEG disk. The six images underneath provide a detailed view of each of these areas (high resolution imagery from Google Maps, white grid shown **not** representing the MSA grid). The coastlines have been chosen such that they are approximately parallel in orientation to the rows and columns of the MSA product. In addition, the surface targets are located in desert areas in order to maximise the contrast between bright land surfaces and the dark ocean.

7.2.3. Evaluation methods

Time series of BHR_{ISO} were generated for each pixel of each transect for each satellite. Figure 13 shows an example of such a time series for three selected pixels out of transect V_NAV_C. One can easily identify the "coastal" pixel by its much larger temporal variability as compared to "pure" land and ocean pixels.

INF⬦RMUS
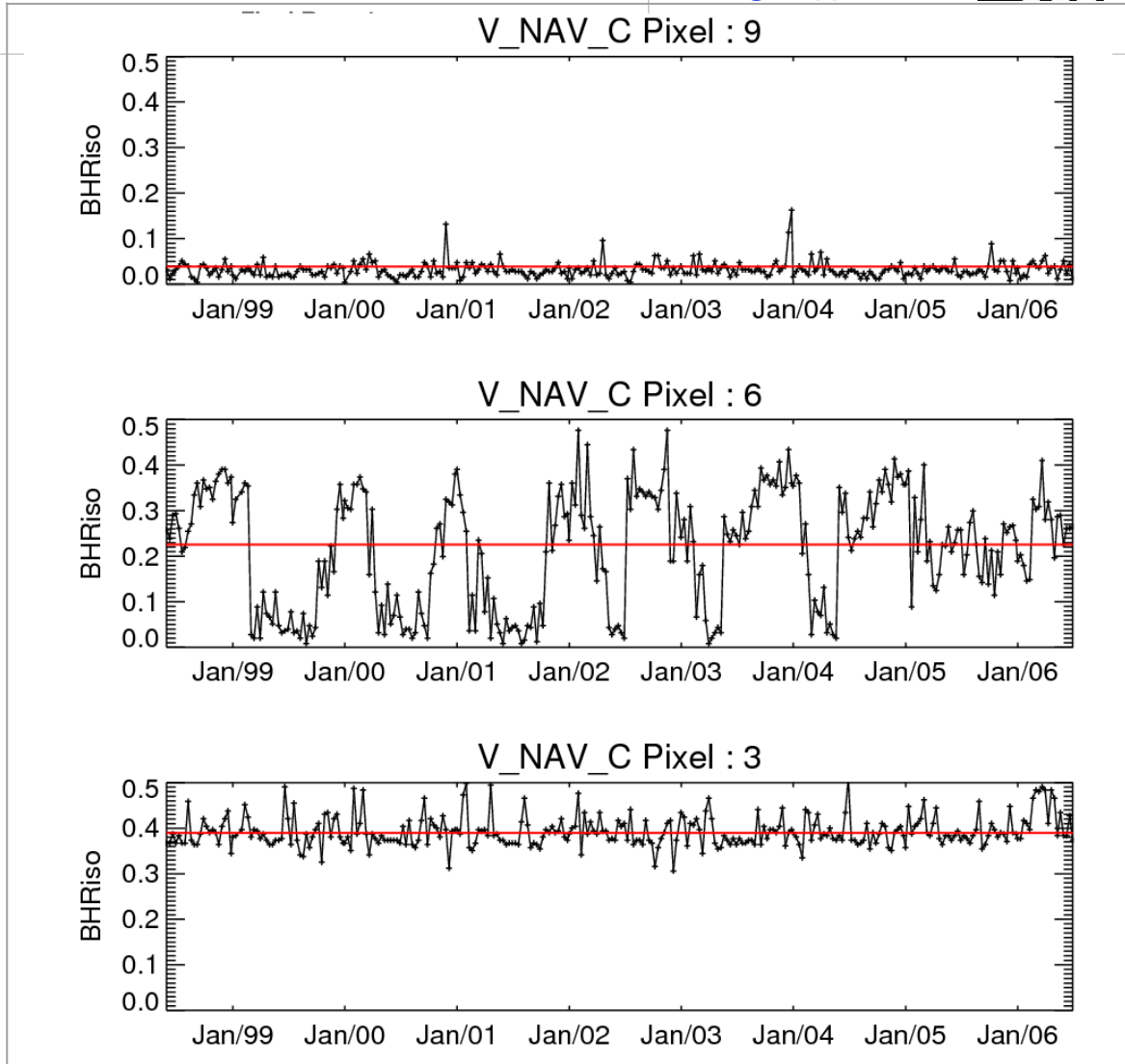
Figure 13: Example of MVIRI-7 time series of BHR$_{ISO}$ for pixel 9 (ocean), 6 (coastline) and 3 (land) for test area V_NAV_C. The red solid line gives the long-term average for each pixel.

In a next step, the data was normalized using the following formula:

$$y(t,i) = \left(BHR(t,i) - BHR(t,1)\right) / \left(\langle BHR(t,11)\rangle - \langle BHR(t,1)\rangle\right),$$

(3)

where $i \in \{1, …, 11\}$ is the respective pixel position and the brackets <…> indicate the temporal average. This will to first order normalize y to the range between 0 and 1, where a value of 1 would represent surface coverage identical to pixel 11 (e.g., entirely water) and a value of 0 would represent surface coverage identical to pixel 1 (e.g., entirely land). Coastal pixels adopt values in between these two extremes. This normalization makes the results of the different locations comparable.

Using long-term averages of y, the navigation of the different satellites relative to each other can be studied (Section 7.2.4). Looking at the variance of y as a function of pixel position allows studying the navigation uncertainty within a satellite's time series (Section 7.2.5).

7.2.4. Average navigation offsets between different satellites

Long-term averages of *y* as a function of the pixel position are shown in Figure 14 for all satellites and transects to show inter-satellite navigation differences. The coloured dots on the x-axis give the best estimate for the location of the coastline in the transects for each satellite.
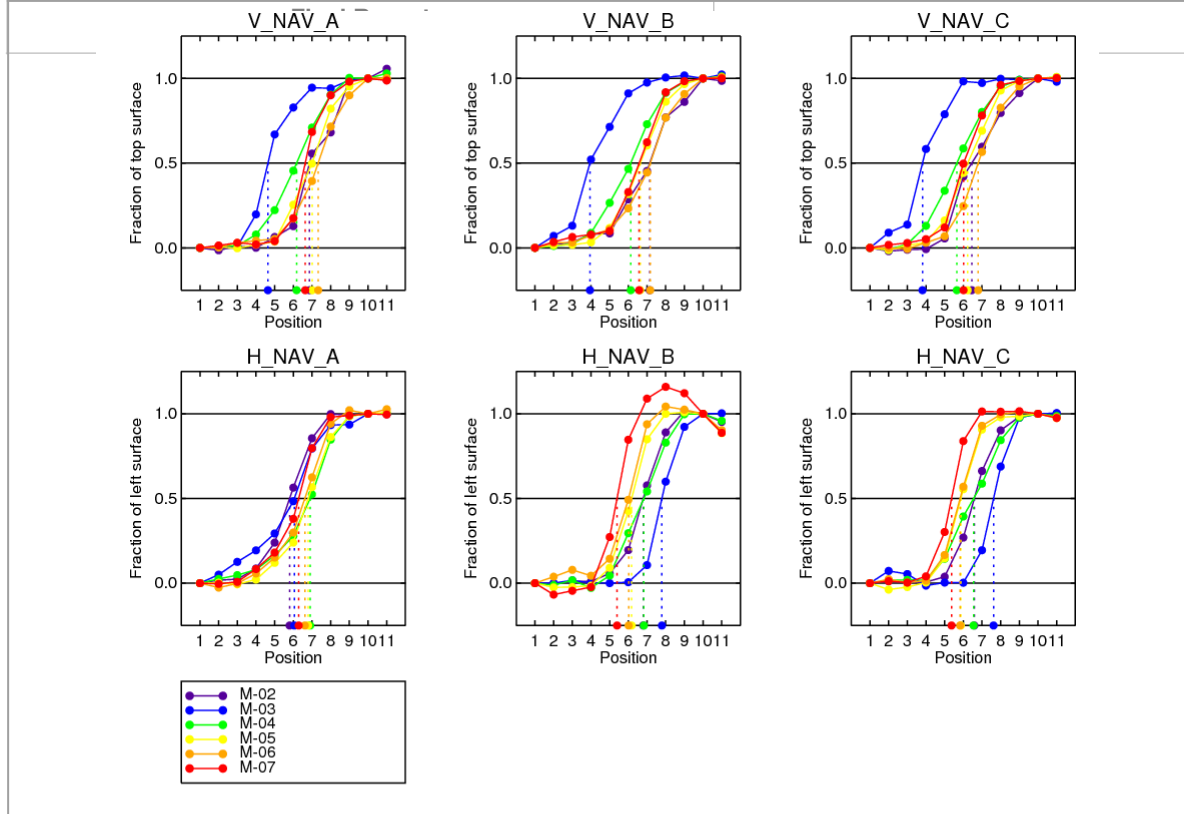
Figure 14: Long-term temporal averages of the function y *(t,i)* as defined in Equation (3) for all transects and satellites. The dots on the x-axis give the position corresponding to a value of <y(t,i)>=0.5, i.e. a pixel position directly on the coastline*.*

The following conclusions about inter-satellite navigation accuracy can be drawn:

➢ With the exception of MVIRI-3, the navigation accuracy of the MVIRIs with respect to each other is approximately one pixel vertically and about 1.5 pixels horizontally;

➢ MVIRI-3 appears to be shifted consistently to the north by about 1.5 – 2 lines (see Figure 14, top row). For example, in the reference area V_NAV_B), pixel 4 would be located directly above the coastline for MVIRI-3 whereas it is nominally located between pixels 6 and 7.

7.2.5. Variations for individual satellites

As can be seen in Figure 13 (middle panel), the pixel nominally positioned above the coastline exhibits a low-frequency (~1/year) variability caused by variations in the actual pixel position relative to the coastline. Superimposed to this systematic variation are random effects dominating the time series of pure ocean or land pixels.

The approach to derive the navigation uncertainty from this variance is outlined below. Assuming linear mixing of water and land surfaces, the variance within each time series caused by geo-location errors can be estimated by solving the following equation for σ_{GEO}:

$$\sigma^2(i) = (1 - f(i))\sigma^2(1) + f(i)\sigma^2(11) + \sigma^2_{GEO}(i)$$

(4)

where $\sigma^2(i)$ represents the total variance in *y (i,t)* observed for the i-th pixel. This simple model assumes a linear mixing of noise caused by the surface of pixel 1 (i.e. the pixel farthest inland in V_NAV_A) and the surface of pixel 11 (i.e. the pixel farthest offshore in V_NAV_A), where *f(i)* is the average fraction of surface 2 within the pixel and the variability of *f* is captured in the additional

term σ_{GEO}. Except for σ_{GEO}, all other quantities can be readily derived from the individual time series, yielding the following expression for σ_{GEO}:

$$\sigma_{GEO}(i) = \sqrt{\sigma^2(i) - (1 - f(i))\sigma^2(1) - f(i)\sigma^2(11)}$$

(5)

Note that by virtue of the definition of the normalized fractions, σ_{GEO} can be interpreted as the standard deviation in pixel navigation in units of fractions of pixels. For theoretical reasons, $0 \leq \sigma_{GEO} \leq 0.5$, because y (i,t) is normalized between 0 and 1.

For a sequence of N equidistant pixels with identical spatial resolution crossing a coastline, σ_{GEO} is a function of y (i,t) only, as all three lengths scales involved can be expressed as function of just the sampling distance between two pixels. The three lengths scales are (1) sampling distance between two pixels, (2) spatial resolution of the pixels, and (3) the navigation uncertainty. If the spatial resolution of the pixels is known, the navigation uncertainty can be derived from the form of the curve σ_{GEO} (i). The general idea is outlined in Figure 15 for a simple numerical experiment. As the navigation uncertainty gets larger, more pixels become affected by the coast (i.e. the curve gets wider) and the variance for the pixels near the coast increases. Note, that for very large navigation uncertainties the variance does not reach zero anymore for pixels 1 and 11 as they also are partially affected by seeing the coastline.
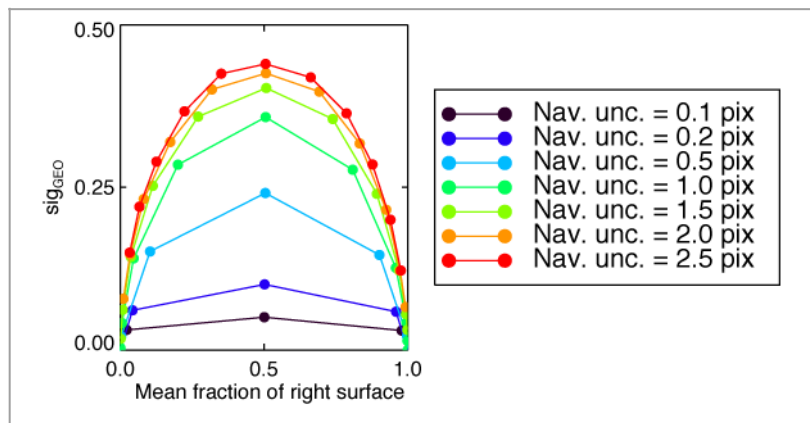
Figure 15: σ_{GEO} as function of the mean fraction of right surface observed in each pixel and as navigation uncertainty derived from a simple numerical experiment over an idealized coastline. The instrument resolution was assumed to be two pixels. The colours indicate different navigation uncertainties.

The same type of plot is shown for the actual MSA observations in Figure 16. Comparing the results obtained for each MVIRI for the vertical cases (V_NAV) to the theoretical curves allows for an estimation of the average navigation uncertainty. The resulting numbers are given in Table 9.
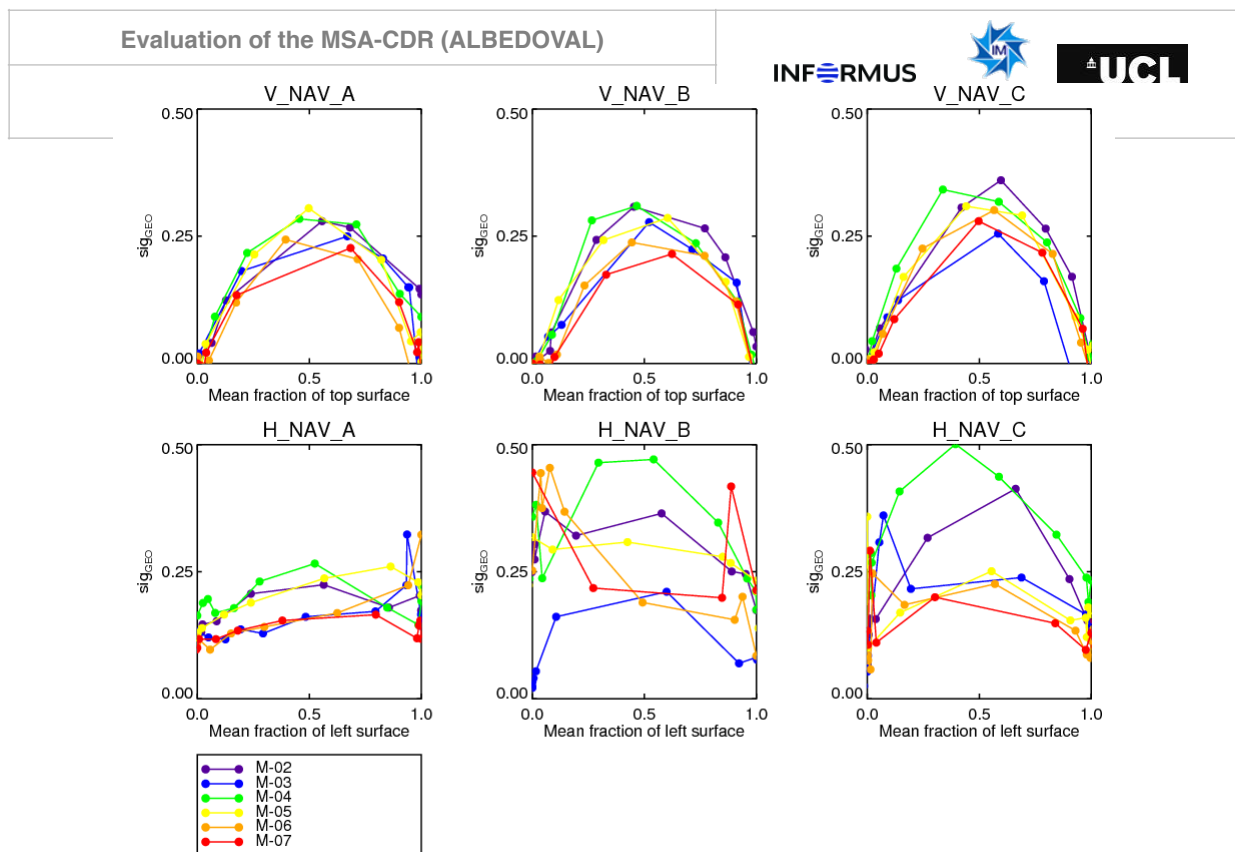
Figure 16: Similar to Figure 15 but for standard deviations from actual MSA observations for all test areas. The colours indicate the different Meteosat satellites.

Due to stronger noise, the same analysis was not possible for the horizontal cases (H_NAV). An in-depth analysis of individual scenes showed that residual cloud contamination is responsible for the encountered difficulties. Considering the scope of the study, it was decided to not further analyse the horizontal navigational uncertainty.

Table 9: Vertical navigation uncertainty in units of MVIRI VIS pixels. The horizontal navigation uncertainty could not be assessed due to residual cloud contamination.

Instrument	V_NAV	H_NAV
MVIRI-2	1.7	-
MVIRI-3	1.6	-
MVIRI-4	1.8	-
MVIRI-5	1.6	-
MVIRI-6	1.4	-
MVIRI-7	1.2	-

7.3. MVIRI stability and consistency

7.3.1. Site selection

Four desert targets were selected in order to assess the long-term stability of the MSA data record (for details on these sites, see Table 17). In addition to constant surface properties, these sites are also characterised by limited residual cloud contamination:

➢ *Murzuq Desert*: Homogeneous and very bright surface;

- ➢ *Libya*: Homogeneous and bright surface previously used for vicarious calibration [Rao et al., 1999];
- ➢ *Egypt One*: Homogeneous and bright surface previously used for vicarious calibration [Knuteson and Revercomb, 2004];
- ➢ *Omani Desert*: Homogeneous and rather bright surface, excellent overlap by both 0DEG and IODC areas.

7.3.2. Time series for selected sites

Time series of DHR_{30} for the four different sites are shown in Figure 17. Time series of BHR_{ISO} and the position of the sites in the 0DEG, IODC_57 and IODC_63 disks are additionally shown in the annex (Figure 40 to Figure 43). Narrow-band to broadband conversion was performed using the empirical coefficients provided by Loew and Govaerts [2010]. The following is apparent from the plots:

- ➢ The individual time series of both 0DEG and IODC are very homogeneous, as already outlined by Loew and Govaerts [2010];
- ➢ Systematic and occasionally significant differences between the 0DEG and IODC areas exist. These differences are analysed in more detail in Section 7.5.
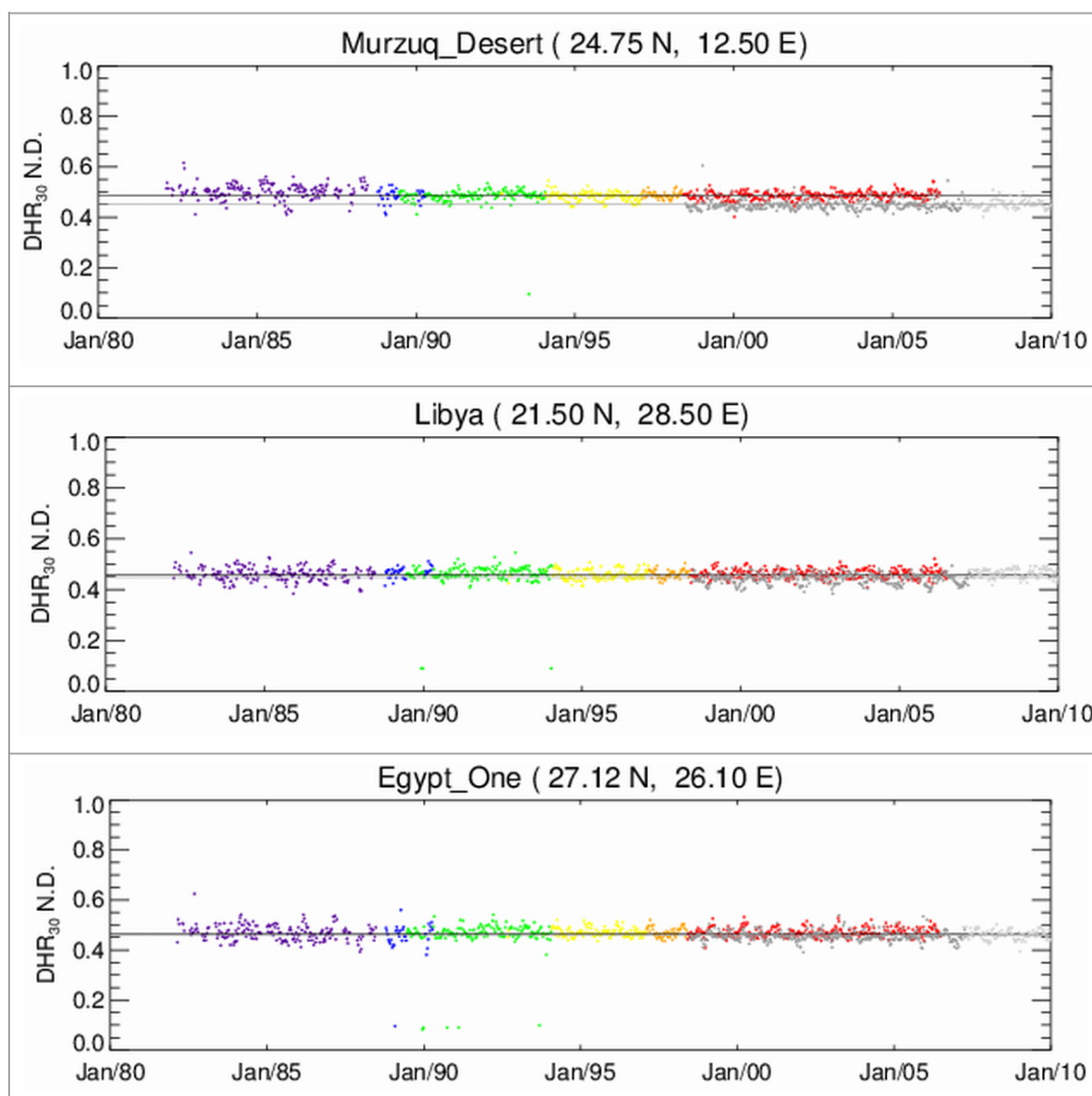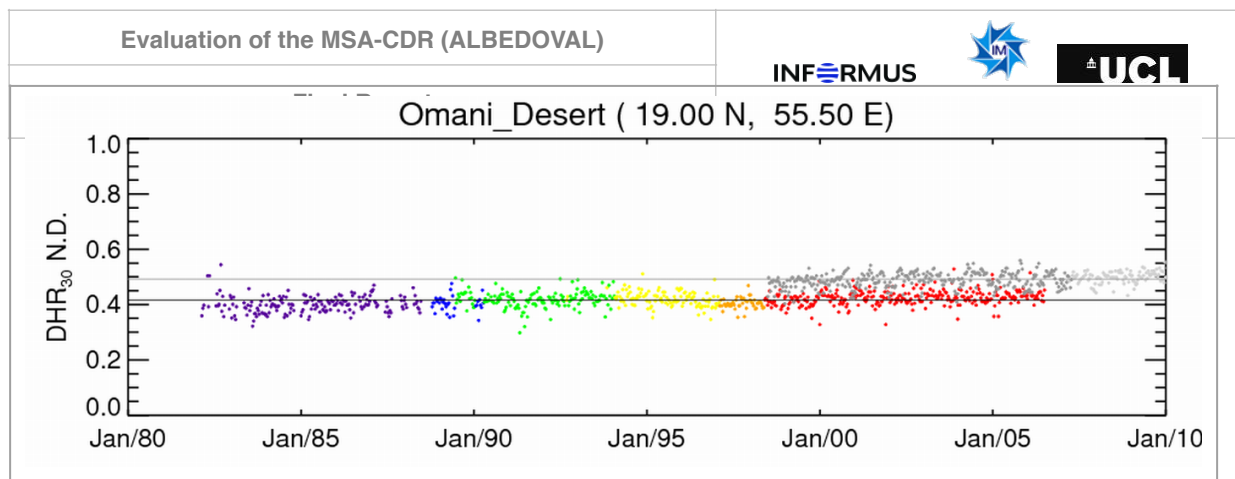
Figure 17: DHR$_{30}$ time series for four desert sites. The colours represent the different MVIRIs on the 0DEG disk from MVIRI-2 (violet) to MVIRI-7 (orange). Dark grey represents MVIRI-5 and light grey MVIRI-7 data covering the IODC.

Especially the central Saharan vicarious calibration sites "Libya" [Rao et al., 1999] and "Egypt One" [Knuteson and Revercomb, 2004] as, to a slightly lesser degree also "Murzuq Desert"[19] appear to be temporally extremely stable (see Table 10). Similar stability is observed for further sites in both arid and non-arid areas (see Annex 11.4, Figure 45 to Figure 48). An exception concerns the "Omani Desert" site, where a trend towards increasing surface albedo is found, especially in IODc observations. It is unclear yet whether these trends are spurious or if they reflect real land cover changes.

Based on the results of the regression analysis presented in Table 10 as well as on the findings of Loew and Govaerts, [2010], the temporal stability of the MSA dataset is assumed to be less than ±0.01 per decade.

Table 10: Regression slopes of the datasets shown in Figure 40 to Figure 43. IODC data are restricted to the 63° coverage (MVIRI-5) to avoid potential effects caused by the different observation angles of IODC_63 and IODC_57. Regression slopes exceeding ±0.01/decade in bold.

Name	0DEG		IODC	
	BHR [1/decade]	DHR [1/decade]	BHR [1/decade]	DHR [1/decade]
Murzuq desert	-0.0084	**-0.0325**	0.0102	0.0099
Libya desert	0.0037	-0.0085	-0.0011	-0.0011
Egypt One	0.0083	0.0071	-0.0006	-0.0006
Omani desert	**0.0170**	**0.0133**	**0.0437**	**0.0421**

7.4. Aerosol effects

This section aims at assessing in how far atmospheric effects are correctly considered in the MSA method:

➢ In a first step, the overall accuracy of the MSA retrieved aerosol optical depth (AOD) was evaluated using the AERONET data as reference;

---

[19] The apparent negative trend for DHR30 under 0DEG at the "Murzuq desert" site is caused by the higher MVIRI-2 values. If these data are removed from the regression analysis, the long term trend is significantly reduced.

➤ In a second step, the MSA-retrieved AOD was spatially analysed against the MACC-II re-analysis.

7.4.1. Aerosol optical thickness against AERONET

In order to perform a homogenized analysis for the 0DEG and IODC disks, only AERONET stations that are part of both coverages were considered. Furthermore, only stations with a temporal coverage of five years or longer were evaluated. 18 AERONET stations[20] were finally retained for further analysis. The location of these sites is plotted in Figure 18.
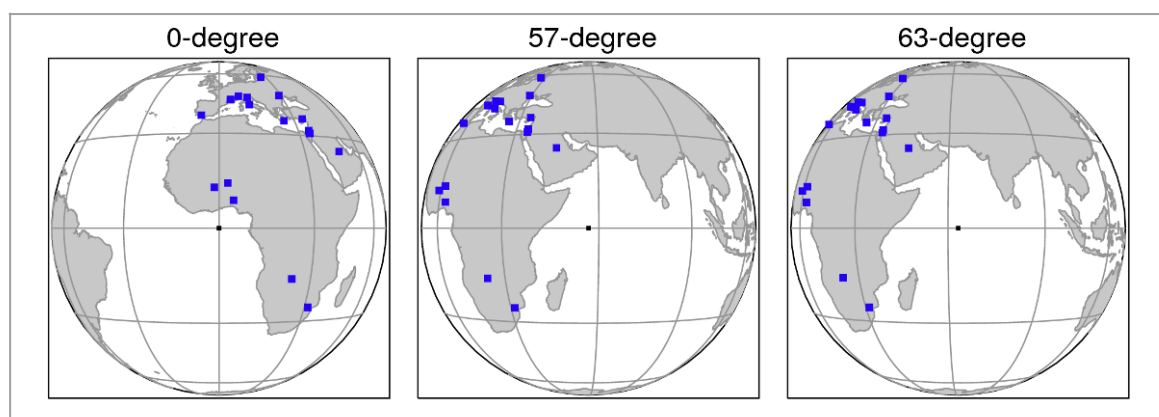
Figure 18: Location of the 18 AERONET sites used in this study.

In order to make the MSA and AERONET products compatible, two pre-processing steps were required:

➤ The AERONET AOD, which is specified for 675 nm, was referenced to 550 nm (reference wavelength of the MSA AOD) by using the Angstrom coefficient derived from concurrent observations at 870 nm;

➤ AERONET data were averaged to match the 10-day MSA periods[21].

A set of 1025 collocated MSA-AERONET AOD data pairs was such derived (see scatter plots in Figure 19), leading to the following observations:

➤ In general, there is a good agreement between MSA and AERONET AOD, even though MSA is based on a continental aerosol model only.

➤ MSA will inevitably overestimate the AOD for values < 0.1. This is due to the fact that the MSA retrieval is bound to discrete AOD values in the range between 0.1 and 1.0 (see Table 6).

➤ MSA seems to slightly underestimate AOD for higher values. However, this statement is based on a limited number of observations as there exist only very few data points with AOD >0.5.

➤ Statistically, the AODs from IODC and 0DEG show a very similar performance against AERONET.

---

[20] AERONET stations used: Avignon, Banizoumbou, Carpentras, El_Arenosillo, FORTH_CRETE, IMS_METU_ERDEMLI, Ilorin, Ispra, Moldova, Mongu, Nes_Ziona, Ouagadougou, Rome_Tor_Vergata, SEDE_BOKER, Skukuza, Solar_Village, Toravere, Venise.

[21] In contrast to DHR_{30} and BHR_{ISO}, the AOD values provided by MSA are averages of the considered 10-day periods.
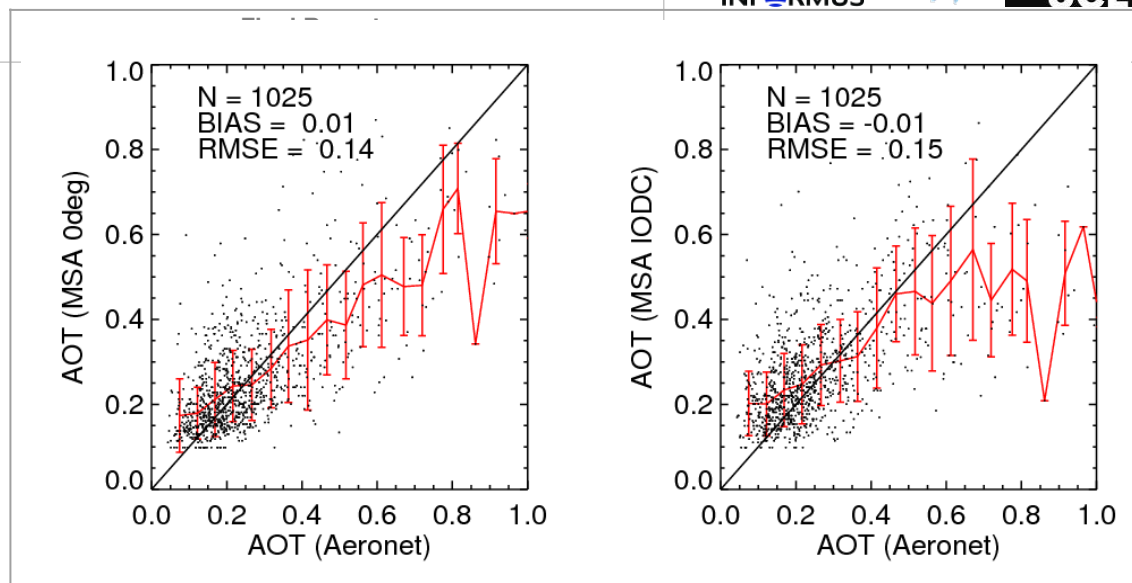
Figure 19: Comparison of AERONET and MSA aerosol optical depth (AOD). Left: 0DEG coverage, right: IODC_57 and IODC_63.

7.4.2. Spatial analysis using MACC-II

The analysis of black-sky (DHR_{30}) and white-sky (BHR_{ISO}) albedo over stable targets obtained under high and low aerosol loads provides an independent indication of the accuracy of the atmospheric correction performed by the MSA. mThe identification of high and low aerosol loads is based on the MACC-II re-analyses (see Section 5.3): MSA observation were sorted into two classes representing high resp. low aerosol loads if the corresponding MACC-II AOD was at least half standard deviation above resp. below the pixel average over the whole MACC-II reanalysis period (2003-2006).

Figure 20 presents composite fields of DHR_{30} obtained from MVIRI-7 for the above defined high and low aerosol cases; only albedo values with a probability of fit of at least 90% were considered for the composite mean. The following analysis concerns the Sahara and the Arabian Peninsula, where albedo values are not expected to change significantly long term. In contrast, the differences observed over the Sahel region correspond to seasonal changes in vegetation cover, i.e., they are associated with a seasonal signal over a non-stable target.

DHR30 M07 2003-2006: DUST AOD > 1/2 StDev

DHR30 M07 2003-2006: COMPOSITE DIFFERENCE (%)

Figure 20: Average of DHR

is higher, (top) resp. lower (middle) than its climatology by at least half a standard deviation;.
Bottom panel shows the relative difference between high and low AOD retrievals with respect
to the low AOD case.
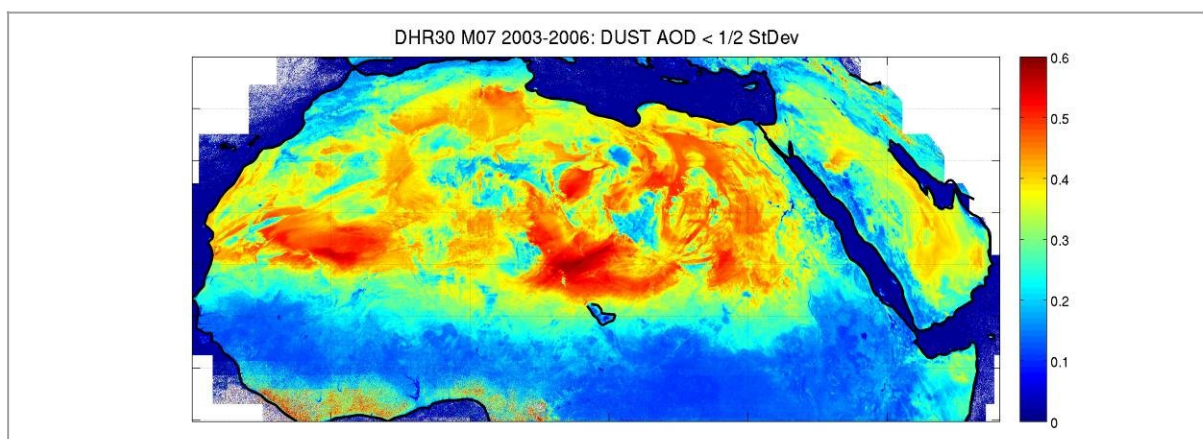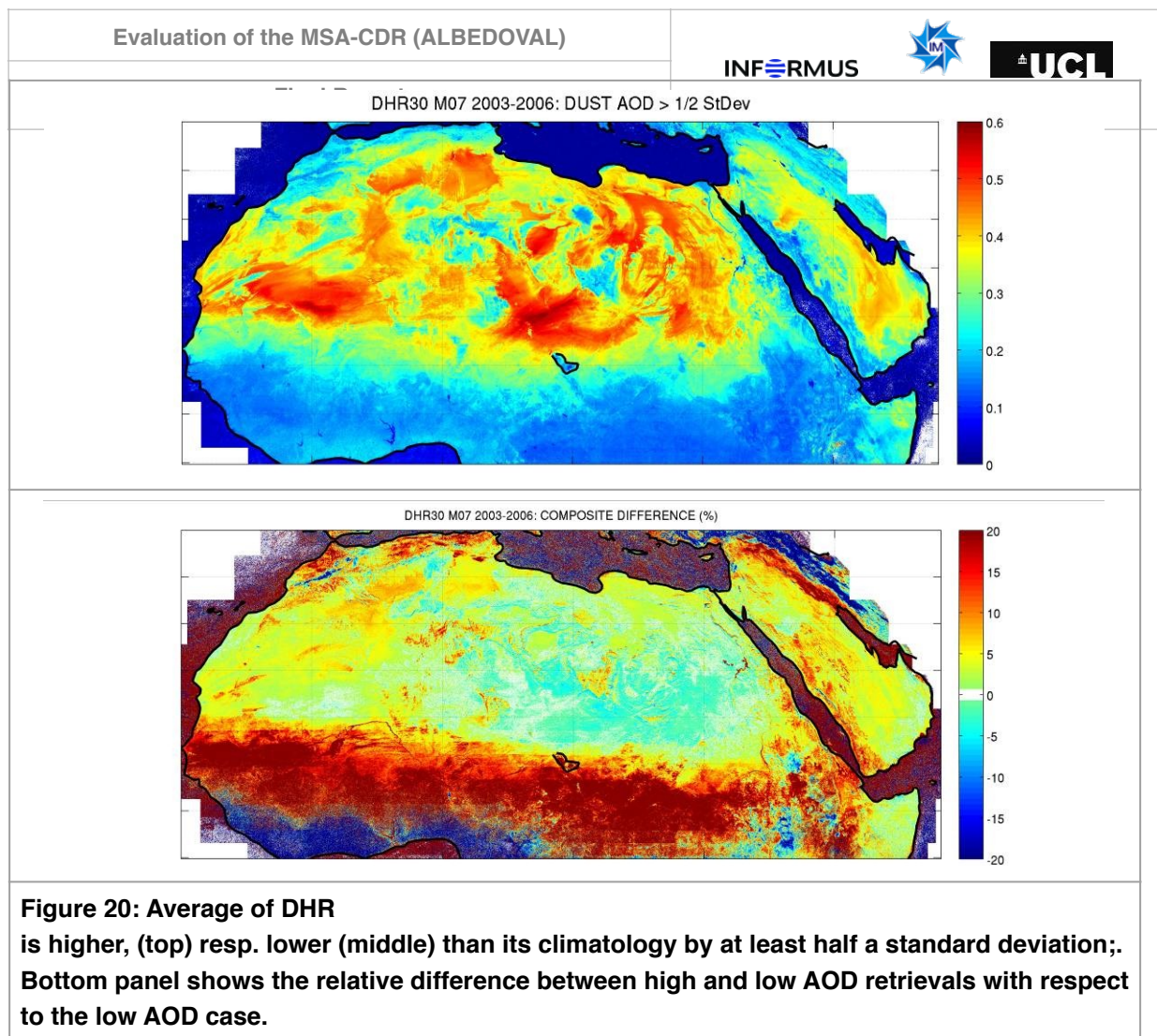
The overall patterns shown in Figure 20 (top) and (middle) as well as the range of observed values appear similar. However, the relative differences between the high and low aerosol load cases reveal DHR_{30} discrepancies between -5% and over +15%. The contrast seems to be particularly pronounced over the Eastern Sahara (Chad, Sudan), where DHR_{30} estimates over dark surfaces tend to be higher for high AOD (positive differences in Figure 20 (c)), while bright surfaces appear to be darker under the same circumstances (negative differences).

As shown in Figure 21, these discrepancies are even more pronounced for BHR_{ISO}. Moreover, the differences seem to be more pronounced towards the eastern part of the domain, i.e. towards larger viewing angles. This suggests that the viewing geometry also plays a role in the performance of MSA (see Section 7.5).

The results indicate the existence of conditional biases in MSA retrievals that depend on the aerosol load. Relative differences between clear and turbid AOD conditions, based on composite averages shown above, may reach values of +10% to –20%. This, in turn, may introduce significant deviations in derived quantities, e.g. the short-wave radiation budget at the surface.

A relative error δA in the surface albedo A leads to a relative error δSRB in the surface radiation budget (SRB) of $\delta SRB = -\delta A \times A/(1-A)$:

➢ Assuming a bright surface of A=0.45 and an albedo retrieval error of δA=+10% (i.e. a retrieved surface albedo of A=0.495), the corresponding relative error of the SRB amounts to δSRB = -8.2%, representing an absolute error of ΔSRB = -0.082 × 550 W/m² = -45 W/m² for an incoming solar radiation of 1,000 W/m².

➢ Assuming a dark surface of A=0.15 and an albedo retrieval error of δA=-20%, the corresponding relative error of the surface radiation budget amounts to δSRB = +3.5%, representing an absolute error of ΔSRB = +0.035 × 850 W/m² = -+30 W/m² for an incoming solar radiation of 1,000 W/m².
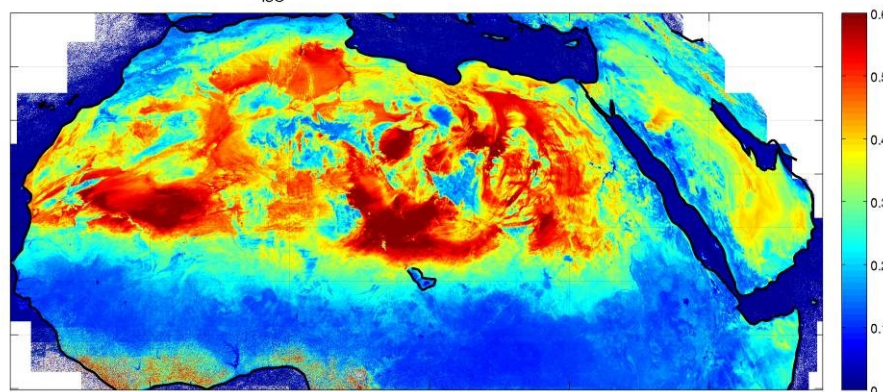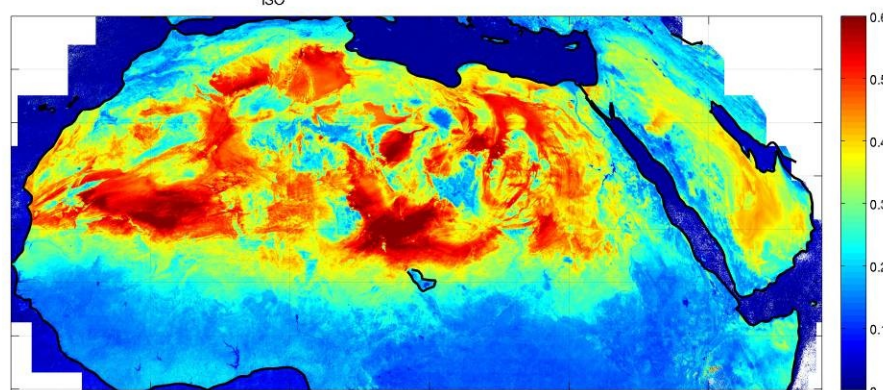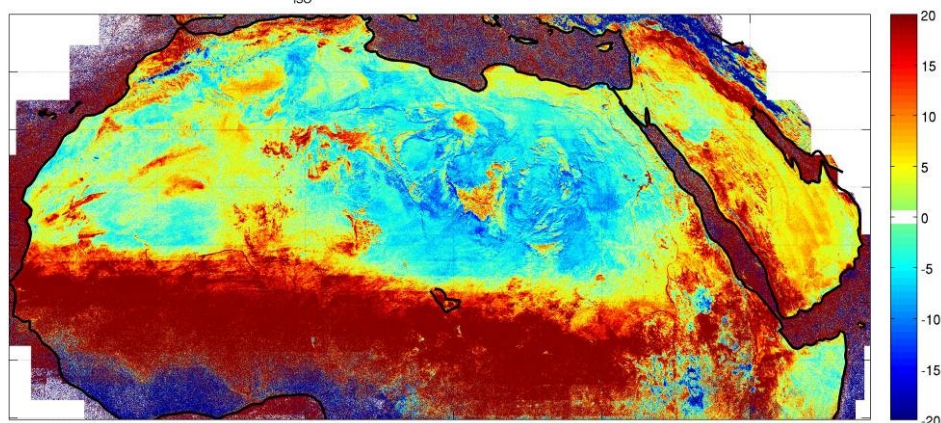
Figure 21: Same as in Figure 20, but for BHR

7.4.3. Analysis using AERONET data

AERONET data of the "Solar Village" site (north-east of Ryad, Saudi Arabia) have been used to perform an analysis similar to the one shown above. Solar Village is the only AERONET site on the Meteosat disk where the surface albedo can be assumed stable over time. Figure 22 shows the results of this analysis: both DHR_{30} and BHR_{ISO} show deviations from their long-term averages correlated with the actual AOD, confirming the existence of biases in MSA surface albedo retrievals depending on aerosol load. The observed deviations for this specific site are mostly confined to a ±10% relative error range and agree thus well with the results from the spatial analysis shown in

section 7.4.2. Following the error estimate presented under 7.4.2 and assuming a surface albedo of A=0.30, this translates into an absolute error of $\Delta SRB = \pm 0.043 \times 700\ W/m^2 = -\pm 30\ W/m^2$ for an incoming solar radiation of 1,000 W/m^2.

The differences between DHR_{30} and BHR_{ISO} as well as between 0DEG and IODC appear small which seems to indicate that angular effects do not play a significant role at this specific site. There also appears to be a positive correlation between AOD and deviation from the average. As "Solar Village" is located in an area characterised by a relatively dark surface (at least for an arid surface), this is in line with previous findings.
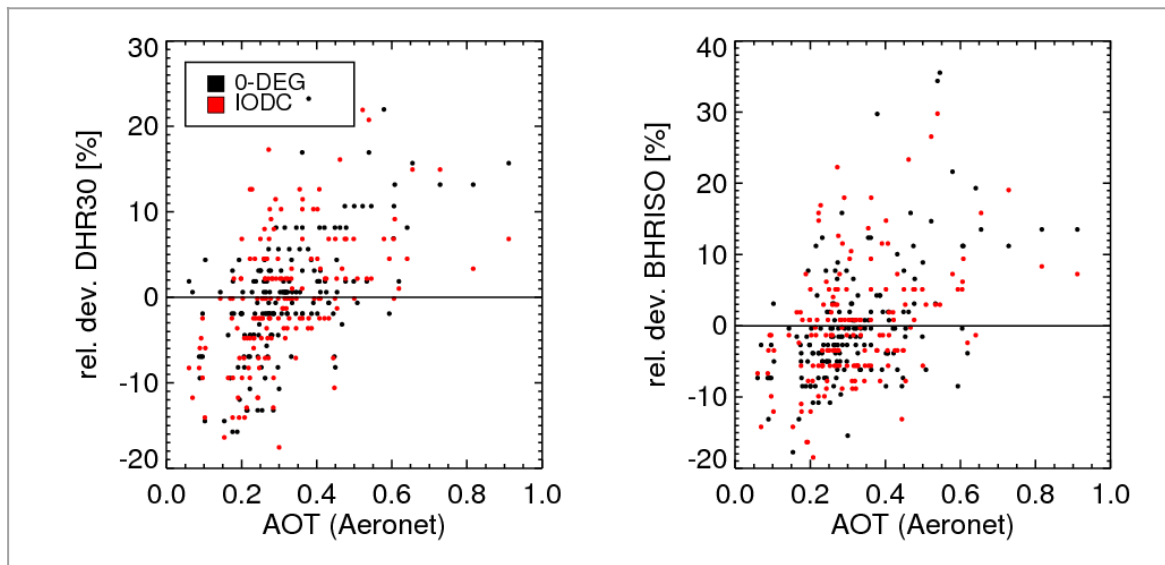
Figure 22: Relative deviation of DHR_{30} (left panel) and BHR_{ISO} (right panel) from their long-term averages as function of the AOD for the AERONET station Solar Village. Relative deviations were calculated as 100.0* (X-⟨X⟩)/⟨X⟩, where X is the time series of either DHR_{30} or BHR_{ISO} and ⟨…⟩ indicates the arithmetic mean.

7.5. Angular effects

Comparisons of the surface albedo of one specific area observed under different geometries are possible for concomitant MVIRI observations under different viewing geometries. The most comprehensive dataset in this respect consists of MVIRI-7 (0DEG) vs. MVIRI_5 (IODC_57) derived MSA values and covers more than five years of concomitant observations. Figure 23 shows the viewing angles of both satellites within the 0DEG-IODC_57 overlap region.
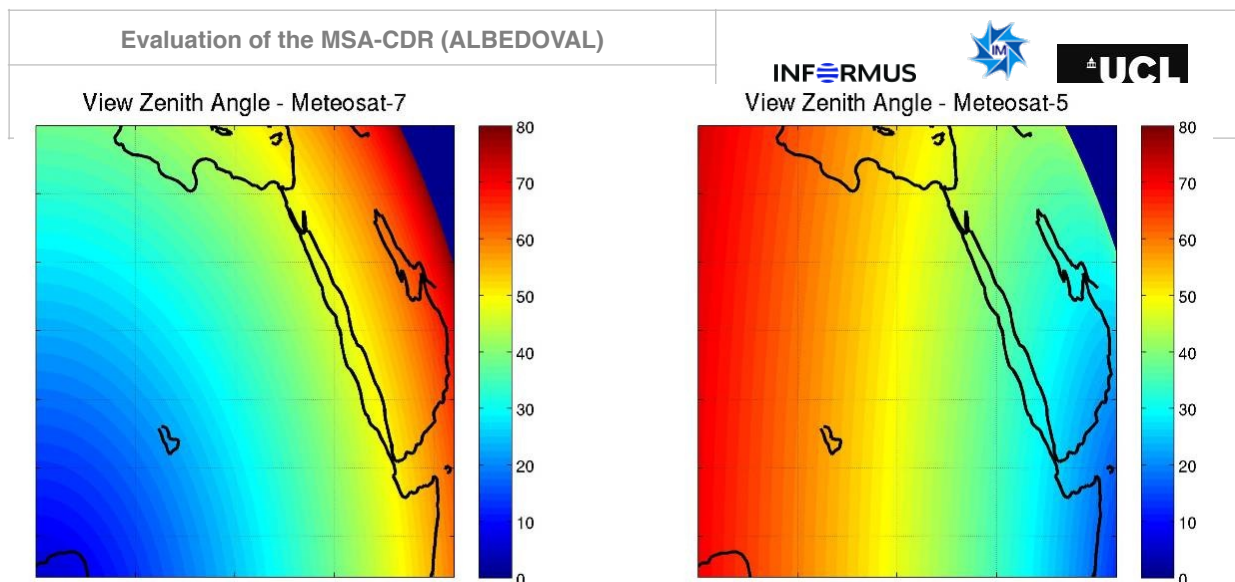
Figure 23: Viewing angle for the MVIRI-7 (0DEG, left) and MVIRI-5 (IODC_57, right) overlapping region in Northern Africa and the Middle East.

A comparison between MSA estimates in the 0DEG and IODC_57 overlapping area suggests the existence of retrieval biases associated with viewing geometry. A striking example is shown in Figure 24 for the Omani desert surface target where DHR_{30} resp. BHR_{ISO} is about 0.08 resp. 0.15 higher for the IODC_57 than it is for the 0DEG observation geometry.
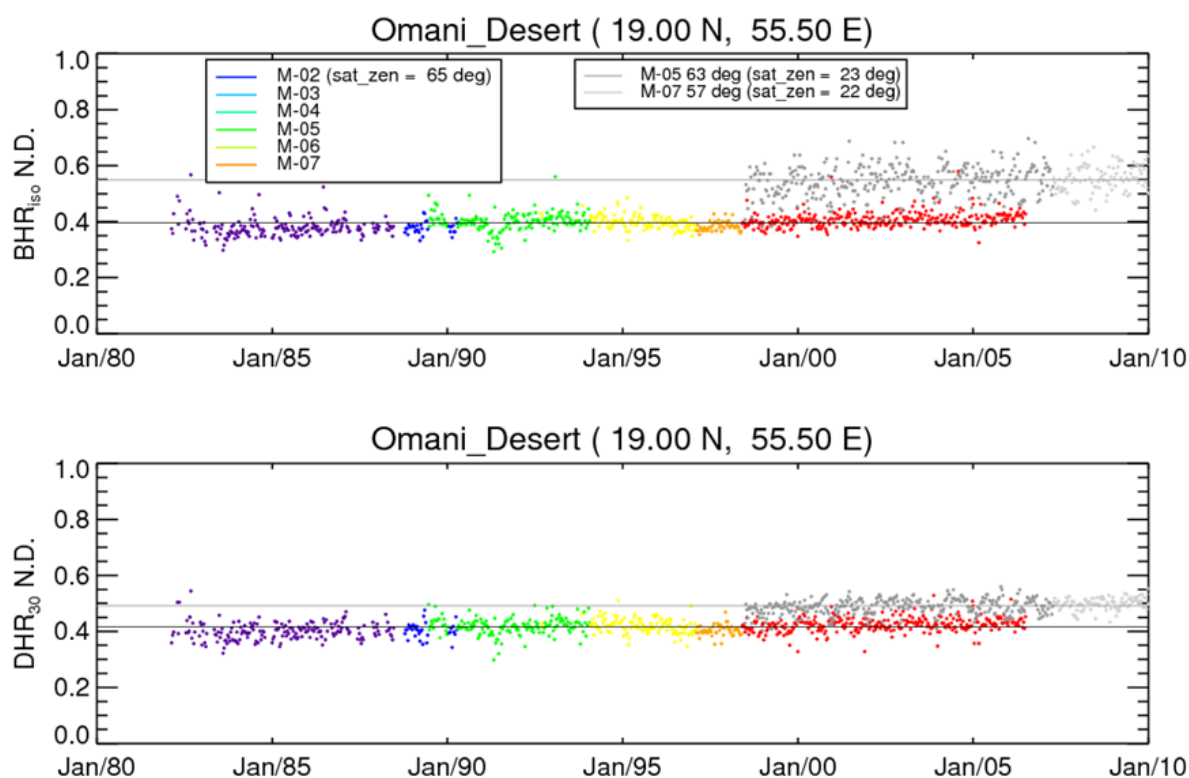
Figure 24: DHR_{30} and BHR_{ISO} time series for a test site in the Omani desert. Large systematic differences are observed for 0DEG (coloured dots) and IODC (grey dots) observations.

7.5.1. Spatial analysis

Figure 25 shows the DHR_{30} differences between the 0DEG (MVIRI-7) and the IODC_57 (MVIRI-5) observation geometries for the 1-10 Jan 2006 compositing period for all pixels classified as "barren"

according to the IGBP land cover classification, grouped by classes of viewing angle difference intervals.
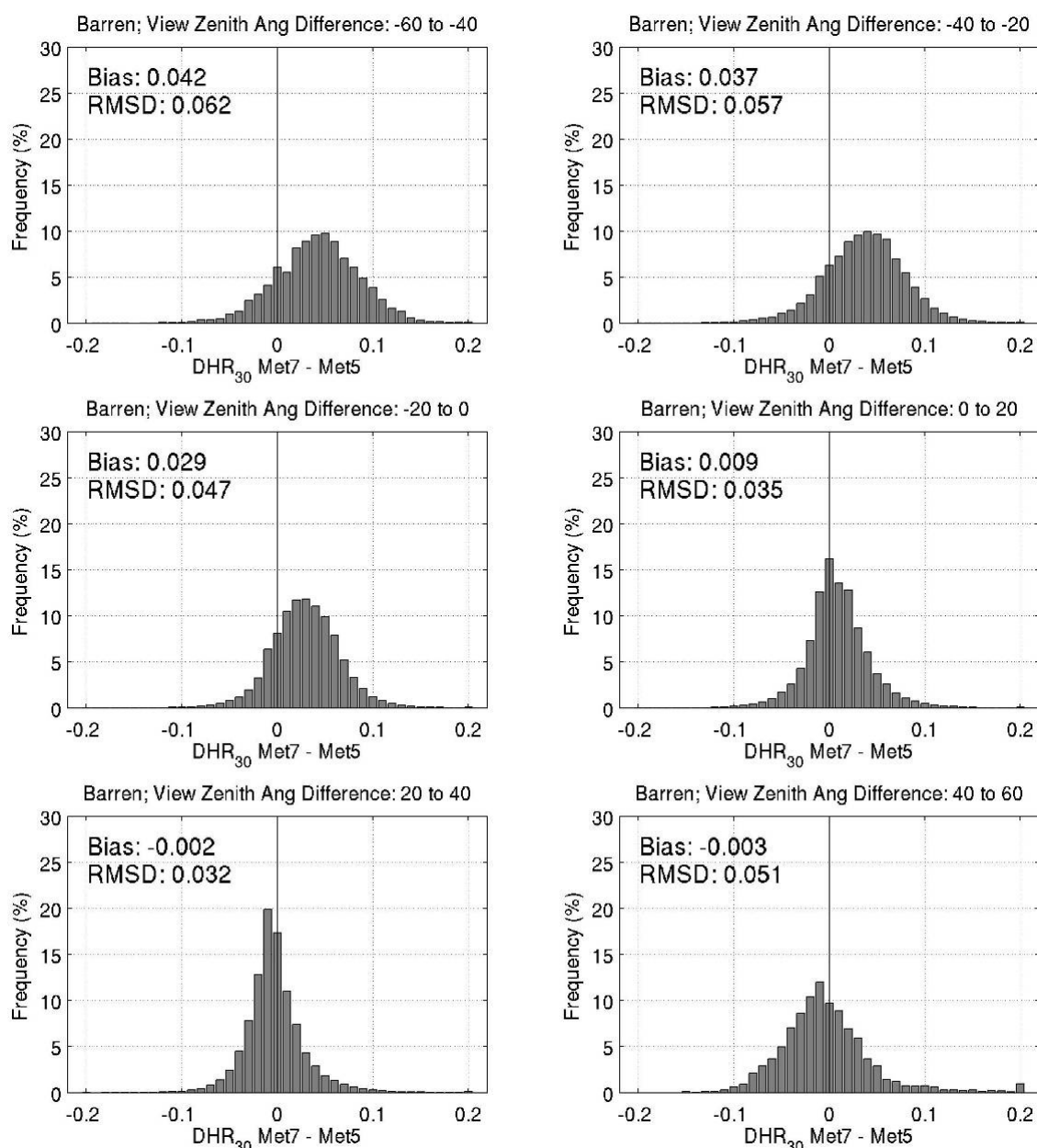
Figure 25: Differences between collocated 0DEG (MVIRI-7) and IODC_57 (MVIRI-5) estimates of DHR$_{30}$ over "barren" pixels within the overlapping region (see Figure 23) for the 1-10 Jan. 2006 compositing period, grouped into viewing angle difference intervals. Average differences (Bias) and root mean square difference (RMSD) are also indicated.

The largest positive differences, i.e. 0DEG larger than IODC_57 values, are observed for the largest negative viewing angle differences. i.e. 0DEG observation angles close to nadir, IODC_57 values highly slanted (Figure 25, top left panel). The DHR$_{30}$ differences then decrease with increasing absolute viewing angles differences (from -60/-40, to -40/-20, -20/0, …), implying that albedo retrievals tend to be lower for larger viewing angles. This pattern is observed for other periods of the year as well (not shown).

The effect is illustrated as function of viewing angle difference for DHR$_{30}$ in Figure 26 (upper panel) over barren (desert) surfaces. Again, it is even more pronounced for BHR$_{ISO}$ (Figure 26, lower panel).

A similar behaviour is observed for other land cover types, such as open shrubs and woody savannah (see also Figure 26). The largest differences between averaged MVIRI-7 and MVIRI-5 MSA retrievals are of the order of 0.04 resp. 0.08 for DHR_{30} resp. BHR_{ISO}, and are obtained for barren surfaces. Such differences are significant and may lead to significant errors when calculating related quantities such as the SRB (see for example the error estimates given at the end Section 7.4.2). In addition to the observed biases, the standard deviation of the differences also tends to be smaller for cases where the viewing angles of the two instruments are close.

Note that the shifts in the distribution are not symmetric, i.e., the number of cases where 0DEG (MVIRI-7) retrievals have larger values than those obtained from IODC_57 (MVIRI-5) is higher for all land cover types considered (see Figure 25). This is likely a consequence of the uneven distribution of viewing angles in the overlapping region, which is closer to the Meteosat-7 sub-satellite point (Figure 17).
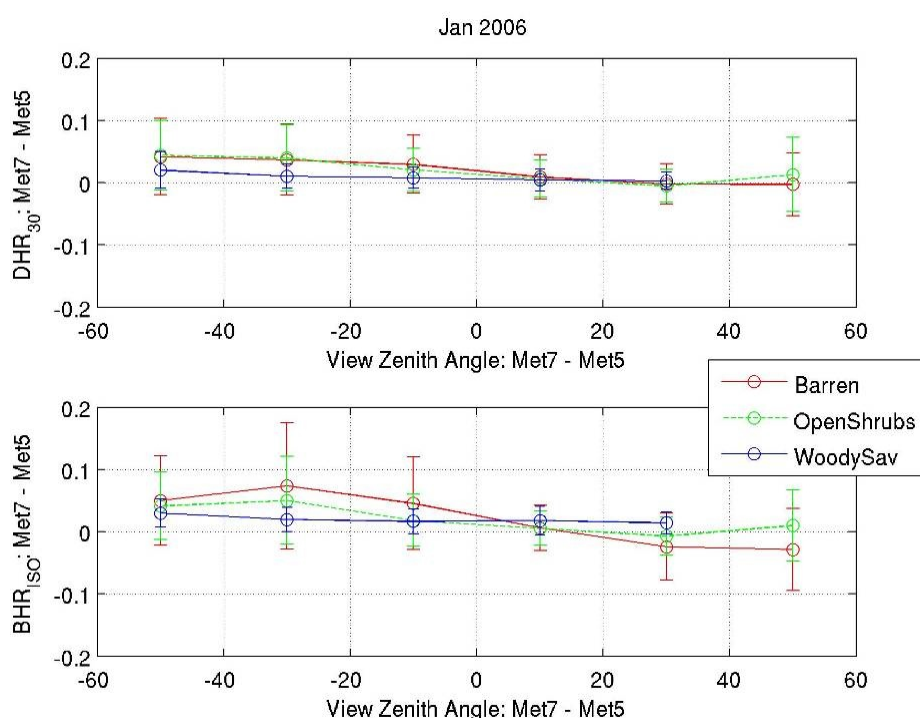
Figure 26: Average (circles) and standard deviation (vertical bars) of the difference between 0DEG (MVIRI-7) and IODC_57 (MVIRI-5) retrievals of DHR_{30} (upper panel) as well as BHR_{ISO} (lower panel) for different land cover types as function of the viewing angle difference.

7.5.2. Temporal analysis

The agreement between concomitantly retrieved MSA values for the 0DEG and IODC areas was additionally studied for the entire overlap period for nine selected sites, including five desert sites, two high latitude sites in Europe, and two savannah sites in Southern Africa. Names and coordinates of the different sites are given in Table 11. The corresponding time series are shown in Annex 11.3 (Figure 40 to Figure 48).

Table 11: Specific sites used to study angular effects on the MSA. Also listed are the corresponding satellite zenith angles for the 0DEG, IODC_57 and IODC_63 areas.

NAME	Final Report	Latitude	Longitude	Zenith Angle		
				0 deg	57 deg	63 deg
Murzuq_Desert		24.75	12.50	32	56	62
Libya		21.50	28.50	40	40	46
Egypt_One		27.12	26.10	42	46	51
Omani_Desert		19.00	55.50	65	22	23
Solar_Village		24.91	46.40	58	31	34
Toravere		58.25	26.46	70	71	73
Moldova		47.00	28.82	60	60	63
Mongu		-15.44	23.25	32	42	48
Skukuza		-25.02	31.48	45	40	45

Long-term mean values for DHR$_{30}$ and BHR$_{ISO}$ for all considered sites are listed in Table 12. The information provided in Table 11 and Table 12 is combined in Figure 27 to show the BHR$_{ISO}$ differences between the 0DEG and IODC areas as function of the corresponding viewing angle difference. Especially for desert sites, systematic deviations are observed: whichever instrument observes the scene at a larger zenith angle will, on average, have a lower surface albedo (see Figure 27, left panel), confirming the results from the spatial analysis shown above.

Table 12: Mean broadband values of BHRISO and DHR30 for all sites listed in Table 11: The spectral-to-broadband conversion was performed using the coefficients of Loew and Govaerts [2010]. A rough indication of the standard deviation is also given for each time series.

NAME	BHRISO [%]			DHR30 [%]		
	0 deg	57 deg	63 deg	0 deg	57 deg	63 deg
Murzuq_Desert	55.5	46.3	44.4	48.8	45.4	45.0
Libya	48.7	50.2	44.6	46.1	46.7	44.1
Egypt_One	51.3	48.7	46.1	46.7	46.1	45.5
Omani_Desert	39.6	56.1	54.4	41.6	50.2	48.7
Solar_Village	29.6	32.4	31.4	31.2	33.6	32.9
Toravere	23.8	20.1	20.9	24.7	20.8	21.6
Moldova	19.2	14.1	16.3	19.2	14.8	17.1
Mongu	16.1	16.7	17.0	17.4	17.8	18.0
Skukuza	15.3	14.8	16.1	16.3	15.8	17.1

For the non-desert sites, such a relation seems not as apparent (see Figure 27, right panel). This does not necessarily mean that vegetated surfaces do not show a similar dependence on the viewing angle. It may just be not visible in the sample data which cover only a comparably small range of viewing angle differences. In addition, residual cloud contamination is more likely for the vegetated sites potentially adding noise which might hide the signal.

A comparison of the two sites "Omani Desert" (Figure 43) and "Solar Village" (Figure 48) points at possible causes for the observed deviations: Both sites are located in relative vicinity to each other; differences in their respective observation geometries are comparably small. In contrast to that, the observed differences in MSA retrieval are large: While "Omani Desert" shows a systematic deviation of ~0.15 between BHR$_{ISO}$ values for 0DEG and IODC, the corresponding difference for "Solar Village" is just ~0.02. This indicates that the correction for anisotropy effects has been inconsistent for the "Omani Desert" surface type and points to the general problem of MSA retrieval errors induced by surface anisotropy.
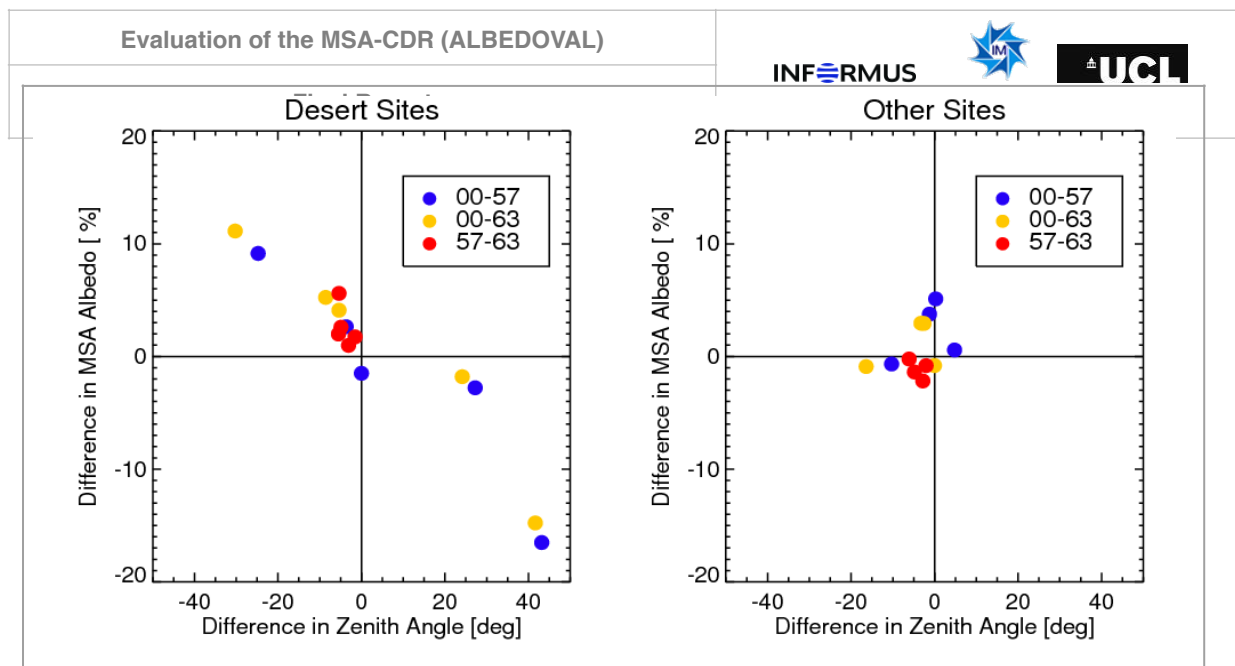
Figure 27: BHR$_{ISO}$ differences as function of satellite viewing angle difference. The left panel shows the five desert sites (rows 1 to 5 in Table 11). The right panel shows the results for the four non-desert sites (rows 6 to 9 in Table 11).

7.5.3. Conclusions on angular effects

As shown above, the observation geometry has a significant impact on the MSA retrieval:

➢ Non-negligible biases exist between surface albedo estimates for the 0DEG and IODC areas in the overlap region;

➢ Differences in the observation geometry may lead to systematic deviations in MSA retrievals that can reach values of up to 0.15 for BHR$_{ISO}$;

➢ Deviations are generally larger for BHR$_{ISO}$ than for DHR$_{30}$, the reason for this being unknown;

➢ The angular effects have been confirmed for arid surfaces and possibly also exist for vegetated surfaces. Further study would be required to confirm this assumption.

In the frame of this study, it was not possible to analyse the causes of the observed angular effects in full detail. We presume that insufficient treatment of the surface anisotropy as one of the main reasons for the observed effects, possibly complemented by aerosol-related effects.

7.6. Satellite-satellite comparisons

7.6.1. Comparing MSA with geostationary products

MSA estimates from MVIRI-7 were compared with LSA SAF surface albedo retrievals from MSG/SEVIRI by Trigo et al. [2011] for the temporal overlapping period in 2006[22]. For this purpose, MSG/SEVIRI albedo retrievals were re-projected to MVIRI-7 pixels using the nearest neighbour approach. The LSA SAF albedo products are based on the inversion of a linear kernel-driven BRF model [Roujean et al., 1992; Geiger et al., 2008], using clear sky surface reflectances for the three SEVIRI short-wave channels centred at 0.6, 0.8 and 1.8 μm.

The LSA SAF provides daily retrievals of black- and white-sky albedo, making use of albedo estimates from previous days as *a priori* information in order to reduce the sensitivity to outliers or

---

[22] After 2006-07-19, Meteosat-7 was moved to an orbital position over the Indian Ocean (IODC_57).

to missing data (e.g., due to cloud cover). The assumed confidence in the *a priori* estimates decreases exponentially with time [Geiger et al., 2008].

The impact of cloud contamination is likely to be significantly lower for the SEVIRI surface albedo retrieval:

➢ The SEVIRI cloud screening takes advantage of the instrument's better spectral resolution;

➢ The SEVIRI 15-minute temporal frequency increases the chances of gathering clear sky observation;

➢ Using *a priori* information will tend to reduce the impact of outliers on the final product.

Figure 28 presents albedo estimates from MVIRI-7 and SEVIRI obtained for the 1-10 Jan 2006 compositing period. Following the recommendations stated in the Product User Manual, only MSA retrievals with a probability of fit higher than 90% were considered in the analysis. The observed differences in surface albedo are uneven distributed: while the bright arid surfaces in the Sahara and Arabian Peninsula mostly present higher values obtained with MSG; the opposite scenario appears over vegetated surfaces in Central and Southern Africa as well as the Iberian Peninsula, but also over dark arid surfaces in the central Sahara. The circular artefacts observed in the BHRISO difference image (bottom right image) likely result from mapping the MSG/SEVIRI albedo on the MVIRI grid.
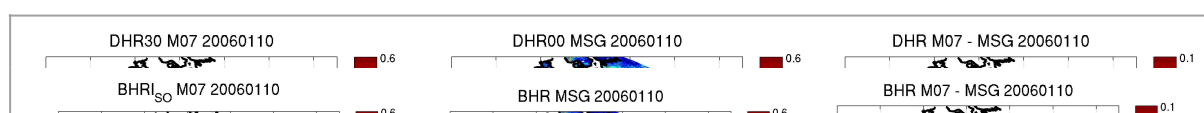
Figure 28. Upper panel: MSA DHR$_{30}$ for the 1-10 Jan 2006 compositing period (left); average of daily values of SEVIRI black sky albedo obtained for the same period (central panel) and the difference [MVIRI-7– SEVIRI] (right). Lower panel: As above, but for white sky albedo (BHR$_{ISO}$).

These findings support the previously stated assumption that the atmospheric correction part of the MSA algorithm seems to cause, on average, underestimation of the retrieved surface albedo above bright surfaces and overestimation above dark surfaces. In addition, the effects of residual cloud contamination are clearly visible, especially along the Gulf of Guinea coastline and large parts of Central Africa.

Figure 29 and Figure 30 provide insight on the joint distribution of MVIRI-7 and SEVIRI estimates for barren surfaces, discriminated by the viewing angle. Several aspects are worth mentioning:

➢ Black-sky albedo (DHR) generally presents better agreement and less scatter than white-sky albedo (BHR), even taking into account that the LSA SAF algorithm estimated DHR using local noon as reference, while MSA refers to the 30° solar zenith angle.

➢ In both cases (DHR and BHR), discrepancies increase with the viewing angle, i.e., MSA estimates appear to become systematically lower with respect to SEVIRI retrievals with increasing angles. Analysing the uncertainty of MSA products for larger viewing angles might provide further insight into the reasons for the observed differences.

➢ MSA BHR values are systematically higher (0.1 and more) than their SEVIRI counterparts above MSG BHR values of ca. 0.45, which might be associated to an inadequate fitting of the narrow-to-broad band conversion due to the limited number of observations for very bright surfaces [see also Govaerts et al., 2006; Loew and Govaerts, 2010].

These results are very similar for the remaining compositing periods of 2006.
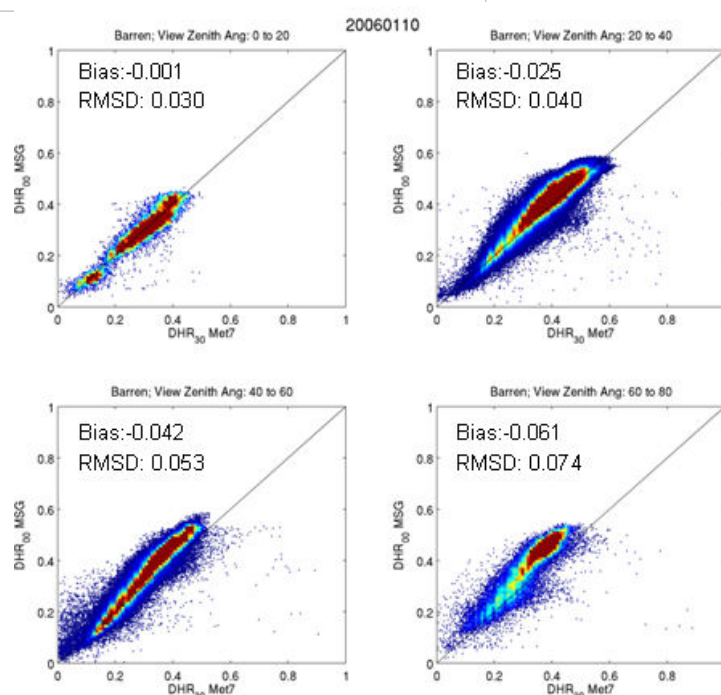
Figure 29 Scatterplots of MSA DHR$_{30}$ (x-axis) vs. SEVIRI black-sky albedo (y-axis) for pixels classified as "Barren" for the 0DEG coverage for the 1-10 Jan. 2006 compositing period. Pixels are grouped according to MSA viewing angle ranges indicated in the top of each panel. Average (bias) and RMS differences within each angular range are also shown.
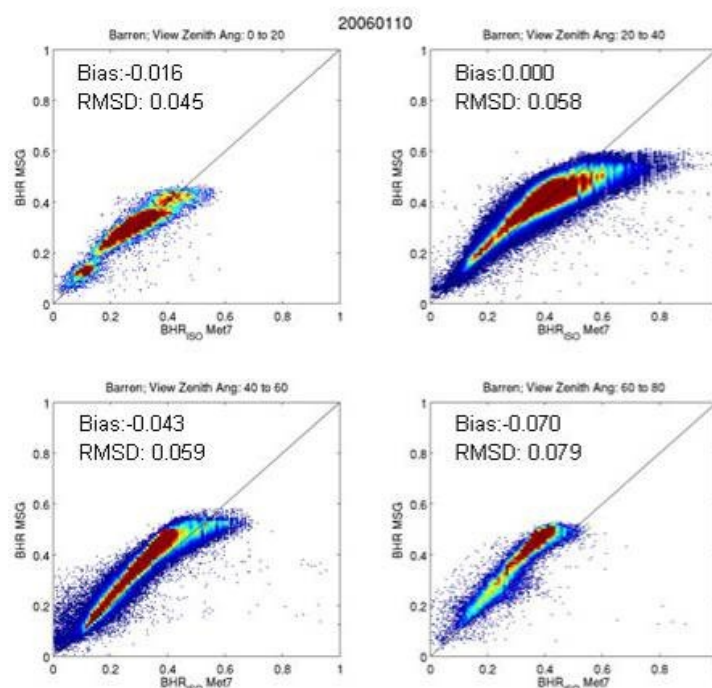
Figure 30 As in Figure 29, but for BHR$_{ISO}$ / white-sky albedo.

The scatter plots in Figure 29 and Figure 30 show a number of MVIRI-7 retrievals with very high values, which is typical of estimates from cloud contaminated observations. Residual MSA cloud

contamination is a much larger problem over dark, vegetated areas due to higher cloud occurrence and larger retrieval errors caused. Figure 31 shows a comparison of MSA vs. LSA SAF albedo retrievals for pixels classified as evergreen broadleaf forest, dominant in tropical Africa. The long horizontal "tails" shown in the scatter plots represent MSA retrievals from observations assumed valid but nevertheless obviously cloud contaminated. As a consequence of the meridional shifting of the intertropical convergence zone (ITCZ), the occurrence of spurious albedo estimations in each view zenith angle range changes throughout the year (not shown here).
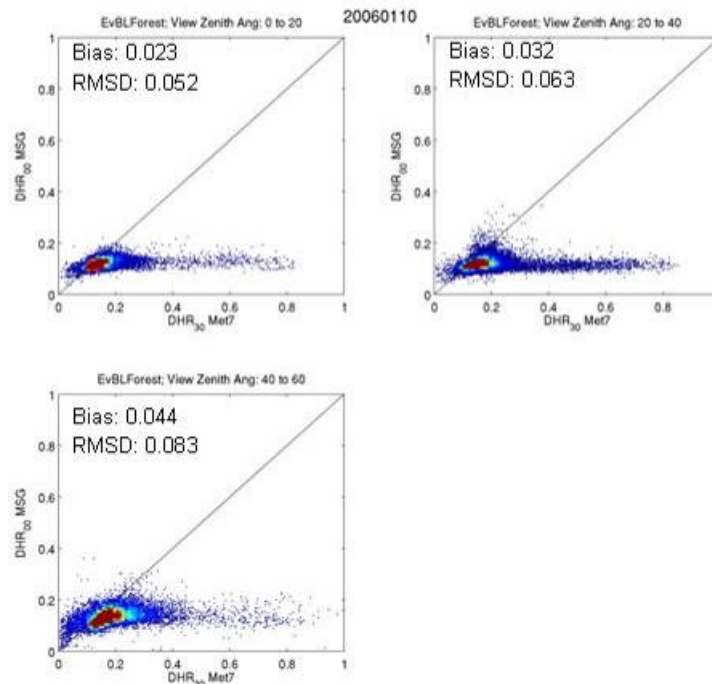
Figure 31 As in Figure 29, but for evergreen broadleaf forest.

7.6.2. MSA with polar-orbiting products

MSA values have also been compared to a number of albedo products derived from polar-orbiting instruments. In a preparatory step, MSA values from MVIRI-5 and -7, as well as the surface albedo products from GlobAlbedo, MODIS Collection 5 and MISR obtained for the year 2005 were projected into a latitude-longitude grid at 0.05° and 0.5° resolution.

Individual comparisons between the MSA and the corresponding MODIS resp. MISR surface albedo products encompassing globally all matches for the year 2005 are shown in Figure 32. There is generally good agreement for albedo values up to about 0.25. For brighter surfaces, MSA estimates are systematically larger than those of the two other products. The lower almost horizontal branch in both panels is likely due to residual cloud contamination in the MSA product (similar to Figure 31). Qualitatively, these results are similar to those obtained when comparing MSA to the SEVIRI albedo product.
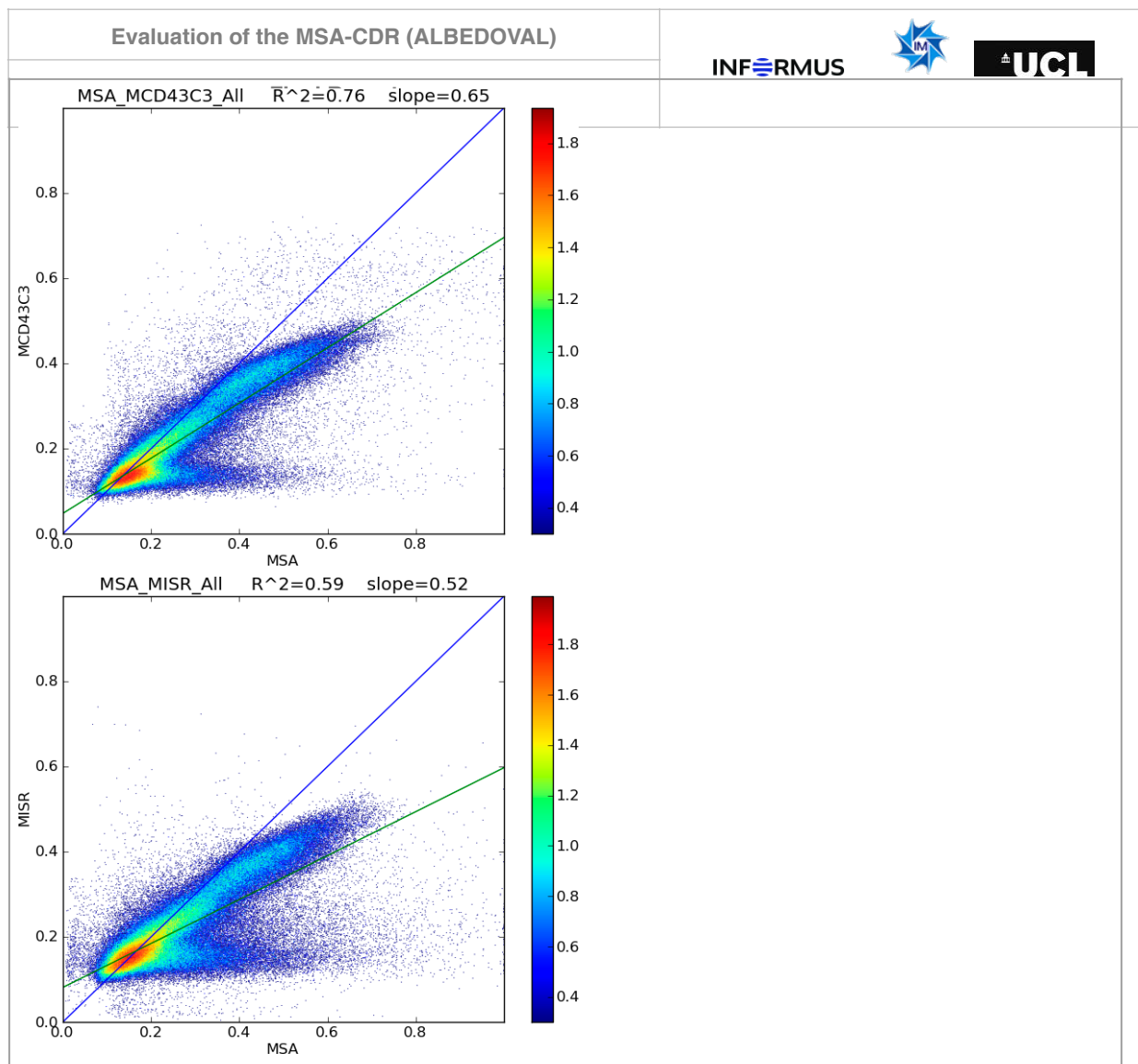
Figure 32: Scatterplots of MSA vs. MODIS Collection 5 (left panel) and MISR (right panel) surface albedo products.

7.7. Cloud screening

In this section, we explore possible criteria to filter out cloud contaminated MSA retrievals by examining quality indicators distributed with the MSA product, i.e., "*probability of fit*" and "*retrieval uncertainty*". As mentioned before, MSA retrievals with a probability of fit lower than 90% were excluded from further analysis. However, this criterion does not seem to be sufficient to eliminate problematic estimates.

Figure 33 shows histograms of estimated MSA retrieval errors for "evergreen broadleaf forest" pixels, exhibiting highly skewed distributions. It is worth noting that the cloudiest amongst the four periods shown (Jan. 2006) is also the one presenting the largest uncertainties. This indicates that the uncertainty values provided as part of the MSA contains information on product quality which may be used for attempts to reduce the amount cloud contaminated pixels.
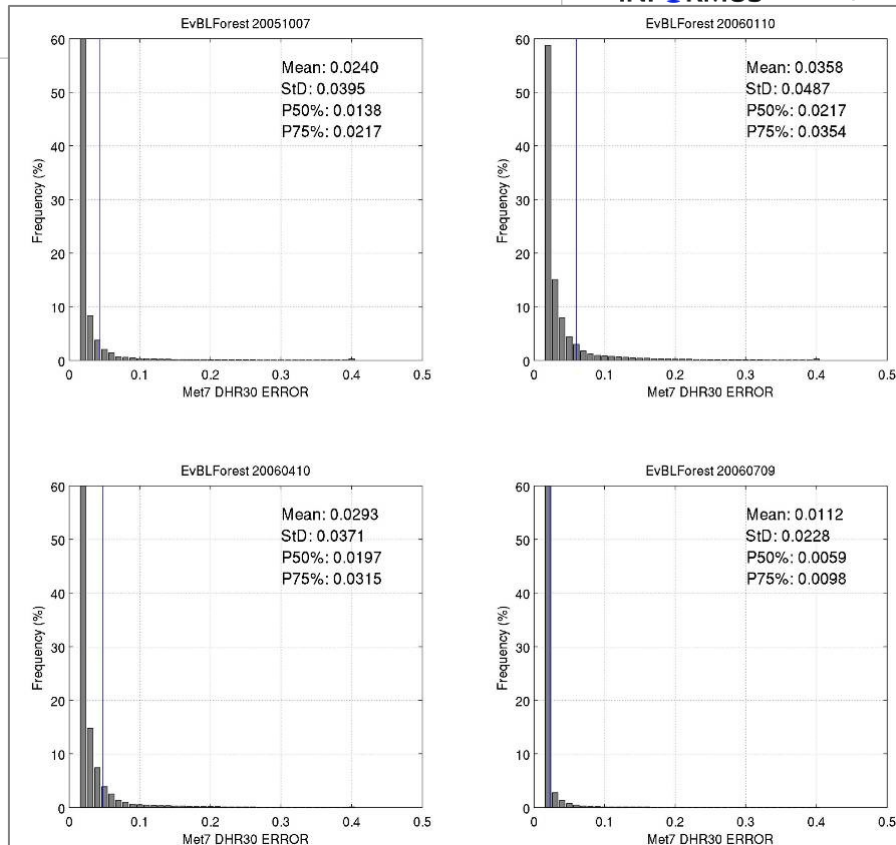
Figure 33: Distribution of MSA estimated retrieval uncertainty for "evergreen broadleaf forest" pixels, for the 4 compositing periods: 28 Sep.-7 Oct. 2005; 1-10 Jan. 2006; 1-10 Apr. 2006 and 30 Jun. -9 Jul. 2006. The blue vertical line indicates the mean uncertainty plus half standard deviation, which is the proposed threshold used to eliminate residual cloud contaminated pixels.

A possible method to eliminate clearly misclassified pixels is to discard (for a given land cover type) all estimates with uncertainty exceeding the average by more than a given threshold. Figure 34 shows the scatter plots from Figure 31 after eliminating cases with errors exceeding the average retrieval error by more than half standard deviation (blue line marked in Figure 33). This seems to be a fairly effective criterion for desert sites. Tropical forests, however, undergo long periods with frequent cloud cover, which makes it very difficult to disentangle "good" from cloud contaminated retrievals. It should be mentioned, that users could also apply a fixed threshold on the retrieval uncertainty (e.g., 0.05) for all land cover types that would allow the elimination of problematic retrievals, with the exception of areas with nearly permanent cloud cover.
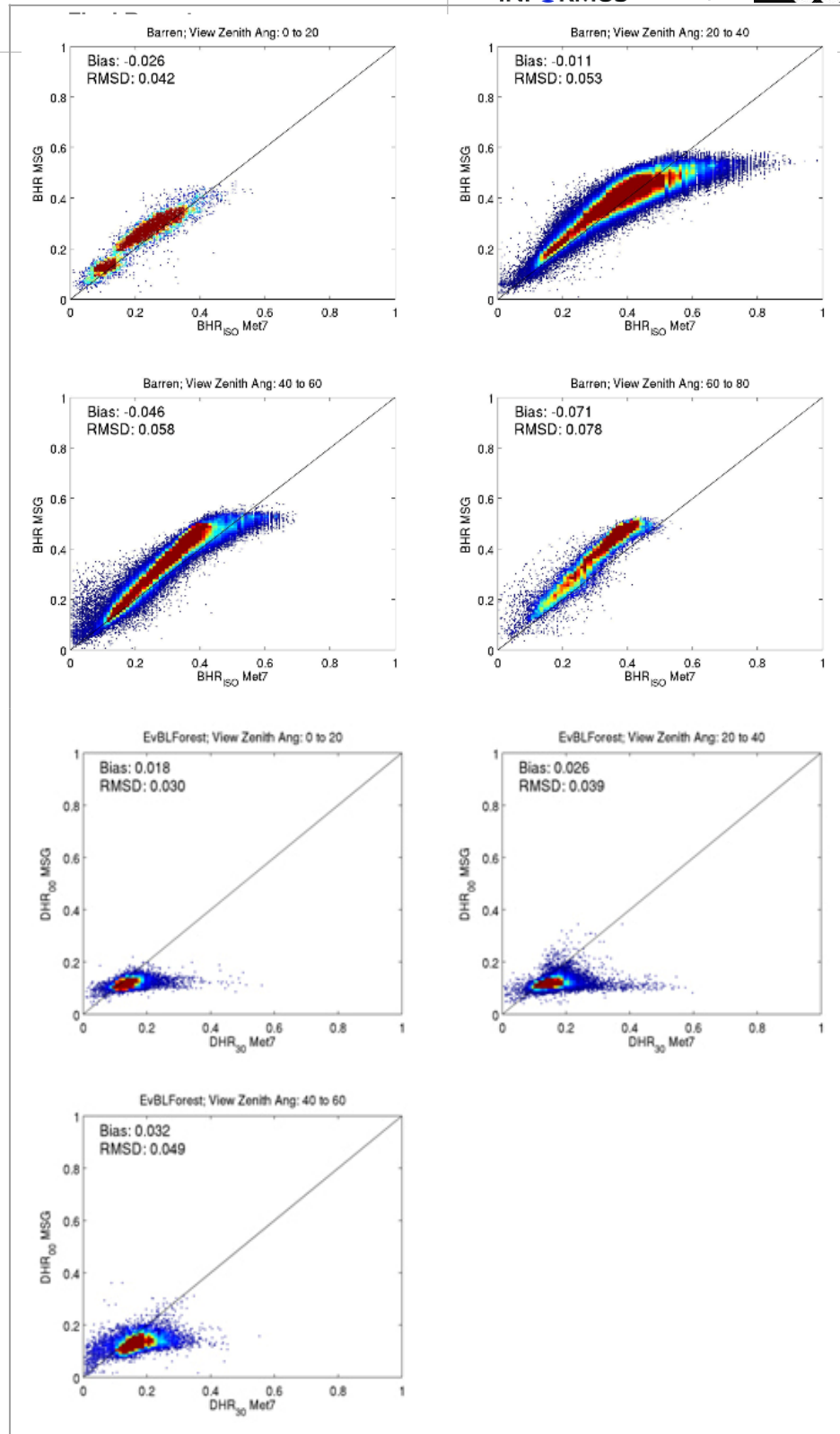
Figure 34 As in Figure 30 and Figure 31, but with retrieval errors additionally fulfilling the condition: retrieval error < mean retrieval error + 0.5* standard deviation for surface types "barren" (upper four left panels) and "evergreen broadleaf forest" (lower three panels).

Other techniques of eliminating outliers within the albedo estimates were also attempted, such as disregarding all DHR_{30} retrievals higher than their average by more than 3 standard deviations.

However, this criterion creates artificial cuts in the distribution of the product, without effectively masking out all cloud contaminated pixels.

7.8. Comparison with surface reference sites: MODIS era

For all FLUXNET reference sites where tower albedometer data was available, Aerosol Optical Depth (AOD) values or direct-to-diffuse irradiation measurements made on-site were used to calculate a blue-sky albedo with each EO-derived DHR/BHR as discussed in Eq. 1 in Liu et al. [2009]. Making the assumption that the tower footprint could be linearly scaled up to the EO pixel size, time series were derived for the investigated FLUXNET sites for the whole of 2005.

Satellite-derived surface albedo values are compared to the corresponding blue-sky albedo gathered at 19 FLUXNET sites in Figure 35. From this figure, it becomes obvious that many FLUXNET sites are likely not well suited for the validation of space-borne surface albedo retrievals, especially for pixels the size of MSA.
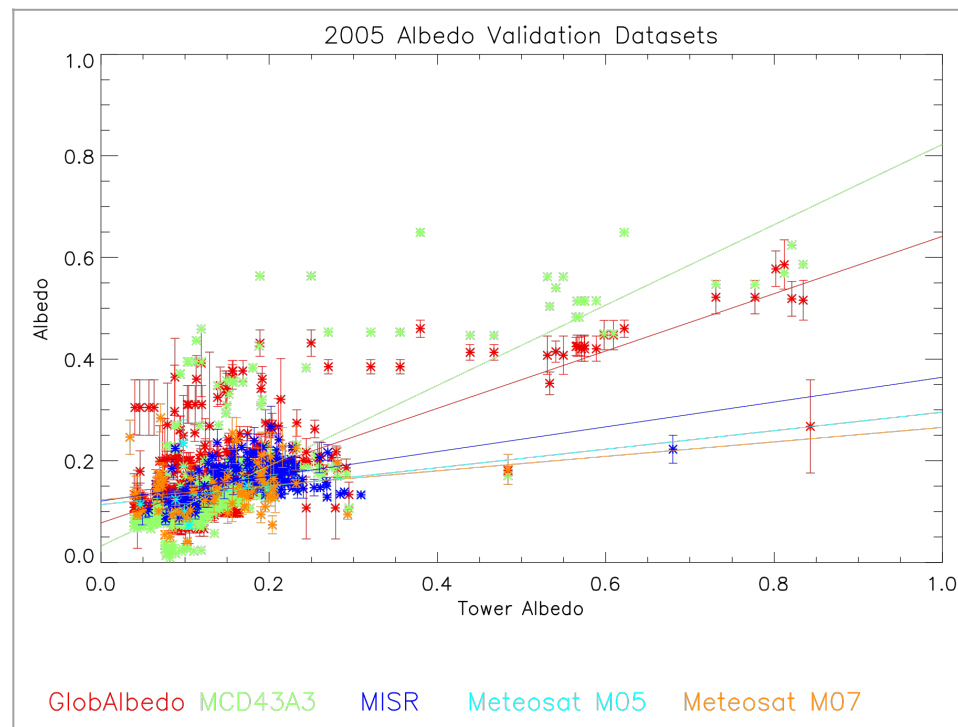
Figure 35: Scatter plot for 19 FLUXNET sites within the MSA geographical coverage.

Looking at individual sites, the reasons for the limited correlation of FLUXNET and satellite-derived surface albedo become clearer: In both cases shown in Figure 36, the satellite-derived albedo products agree quite well among themselves (with the exception of occasional outliers) but partly deviate systematically from the FLUXNET data:

> ➢ For example, the FLUXNET-observed surface albedo increase in DE_HAI between April and June 2005 is not fully represented in the satellite derived data. Later in summer and autumn however, the agreement is very good;

> ➢ Larger systematic differences are observed for the FLUXNET site HU_BUG: Here, the satellite derived albedo values agree well and are rather constant for most of the year with a shallow minimum around DOY 240. Ground truth data at this site are systematically higher with deviations increasing from about 0.03 in March 2005 to about 0.08 (i.e. about 50% above the satellite-derived values) in late October / early November 2005.
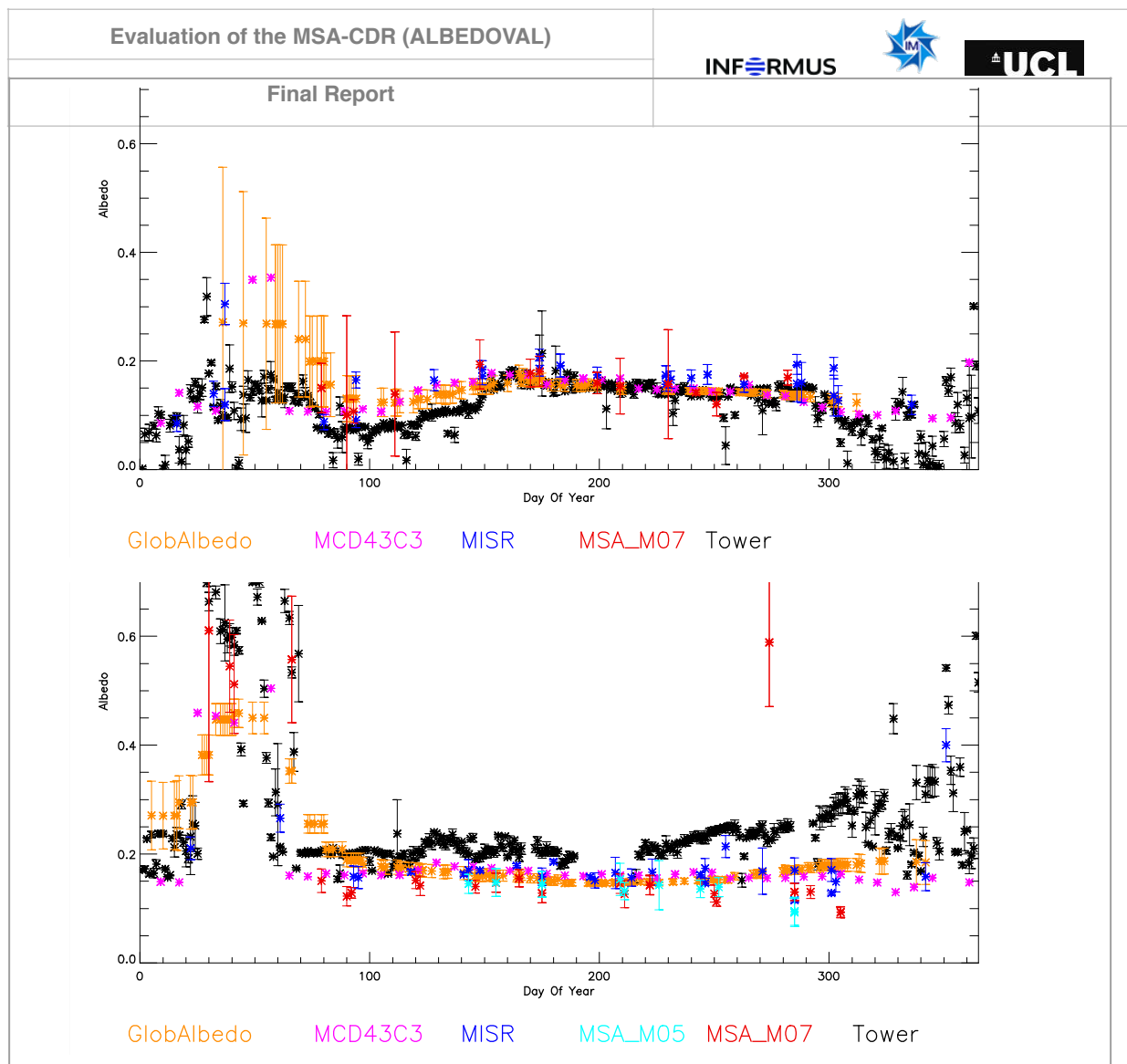
Figure 36: Comparison of FLUXNET ground truth data ("Tower") against surface albedo products from GlobAlbedo, MODIS ("MCD43C3"), MISR, MSA on MVIRI_5 (IODC) and MVIRI_7 (0DEG) for one site in Germany (DE_HAI, IGBP: deciduous broadleaf forest) and one site in Hungary (HU_BUG, IGBP: cropland).

In both cases, it appears that the FLUXNET data is not fully representative of the average land cover within a satellite pixel such that a FLUXNET footprint can generally not be linearly scaled up to MVIRI-size pixels.

Box-and -whiskers plots providing a statistical overview on the albedo retrieval from the different sources are shown in Figure 37 for the two FLUXNET sites DE_HAI and HU_BUG. The horizontal line in the box represents the mean (in some cases, an additional thin line represents the median), the box itself covers the 25-75% percentile range and the whiskers indicate the 12.5 -87.5% percentiles.
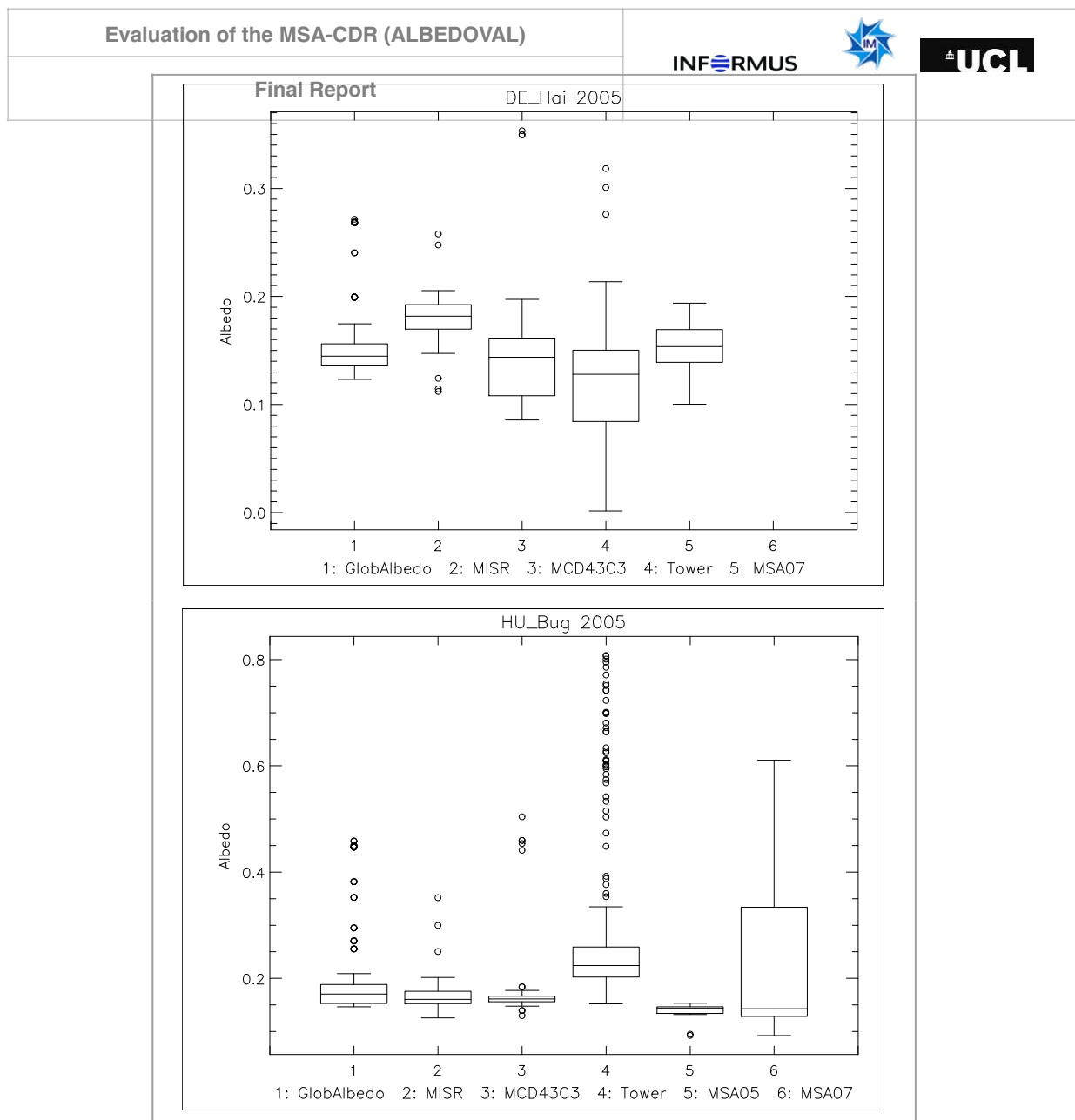
Figure 37: Box-whiskers plots comparing satellite-derived vs. ground-based measurements of the surface albedo at two FLUXNET sites. All satellite retrievals are in their original spatial resolution. The 90% probability criterion has been applied to MSA data. Values outside the 12.5 – 87.5 percentile range are shown as small circles.

These plots indicate that there are surface-dependent systematic biases between some of the EO data-sets, for example between GlobAlbedo and MISR at DE_HAI. On average, the satellite-derived surface albedo values are slightly above the ground truth measurements. MSA fits well into the albedo range provided by the other sensors. A different picture is observed for HU_BUG: Satellite derived values systematically underestimate the values measured on ground with MSA showing the largest deviations. This is a strong indication that the in-situ measurement is only representative in the vicinity of the measurement tower.

7.9. Comparison with surface reference sites: Pre-MODIS era

The following datasets provide in situ albedo observations and were used for validation purposes with a special emphasis on the pre-MODIS era: BSRN, Safari-2000, and a series of albedo

measurements taken during measurement campaigns in Sudan in 1989. The datasets and their characteristics are listed in Annex 11.1.1.

The location of the different observation sites on the Meteosat disks is shown in Figure 38. The datasets were quality controlled and reformatted to facilitate comparing surface albedo estimates with MSA estimates. This format is described in Section 7.9.1. In Section 7.9.2, the datasets are compared to MSA retrieved surface albedo.
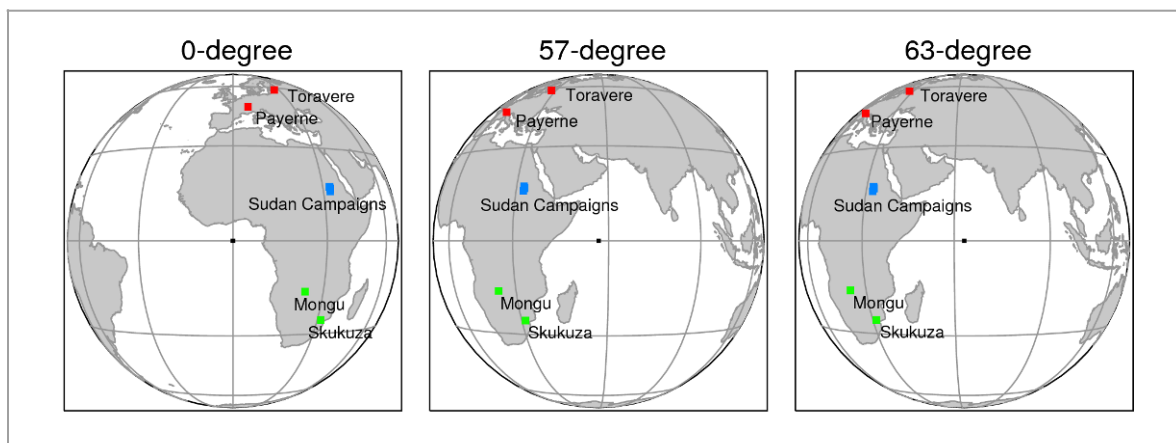
Figure 38: Location of the different validation sites with surface albedo observations predating the MODIS era.

7.9.1. Validation summary files

Validation summary files for subsequent use within the ALBEDOVAL study have been produced from the BSRN, Safari-2000, and the Sudan Campaigns original data. These files hold statistical information on in-situ surface albedo measurements for the 10-day MSA time periods. Table 13 summarizes the information provided. The validation files are available either as NetCDF or IDL ".sav" files.

Table 13: Validation summary file format. Note that time information refers to the first day of each 10-day MSA period.

Name	Type	Description
JUL	Double	Julian Day (IDL JULDAY-Function Format)
DOY	Integer	Day of Year (1 … 361)
MONTH	Integer	Month
DAY	Integer	Day
YEAR	Integer	Year
MEDIAN	Float	Median value of valid in situ albedo observations within 10 day period
MEAN	Float	Mean value of valid in situ albedo observations within 10 day period
MIN	Float	Minimum value of valid in situ albedo observations within 10 day period
MAX	Float	Maximum value of valid in situ albedo observations within 10 day period
Q25	Float	25% Quartile of valid in situ albedo observations within 10 day period
Q75	Float	75% Quartile of valid in situ albedo observations within 10 day period

Name	Type	Description
IQR	Float	Interquartile range of valid in situ albedo observations within 10 day period
SDEV	Float	Standard deviation of valid in situ albedo observations within 10 day period
N	Long	Number valid albedo observations within 10 day period

7.9.2. Comparison with MSA

Data from all stations was compared for individual ten-day periods both for 0DEG and IODC areas. The different combinations of sites, years, and coverage areas led in total to 47 similar annual plots for individual observation geometries and years. Figure 39 compares three consecutive years of MSA observations to surface albedo measurements taken at Mongu (Zambia) during Safari-2000. The equivalent figures for the other 44 annual plots are not shown in this final report but are distributed separately in the form of image files.

The following main conclusions can be drawn by comparing MSA to surface albedo in-situ data:

➢ Residual cloud contamination is clearly identifiable in the MSA data (for example in January 2000 in Figure 39);

➢ The agreement between MSA and the in situ data deteriorates in the winter months at higher latitudes due to variable snow cover and low sun height;

➢ In situations not affected by clouds and/or unfavourable illumination conditions, the agreement between in-situ measurements in large homogeneous surfaces and MSA data is write in almost all cases well within the temporal standard deviation of the ground-based observations;

➢ The in situ albedo is expected to adopt a value between the black-sky (DHR_{30}) and white-sky (BHR_{ISO}) albedos. This is not always the case, but the three albedo values often agree within their ranges of uncertainty for the ten-day periods;

➢ The 10-day variability of the in situ data (in situations not affected clouds, snow, or unfavourable illumination conditions) is typically in the range of 3-5% for the Safari-2000 sites and about 10% for the BSRN stations Payerne and Toravere.
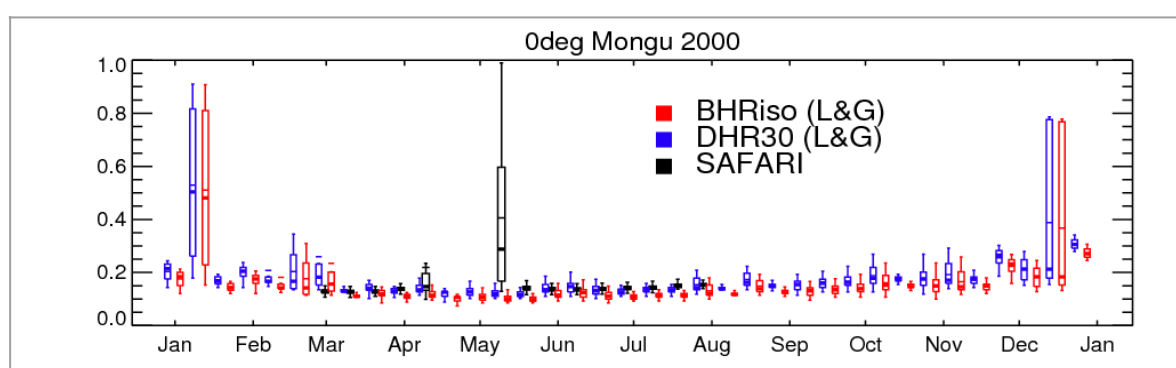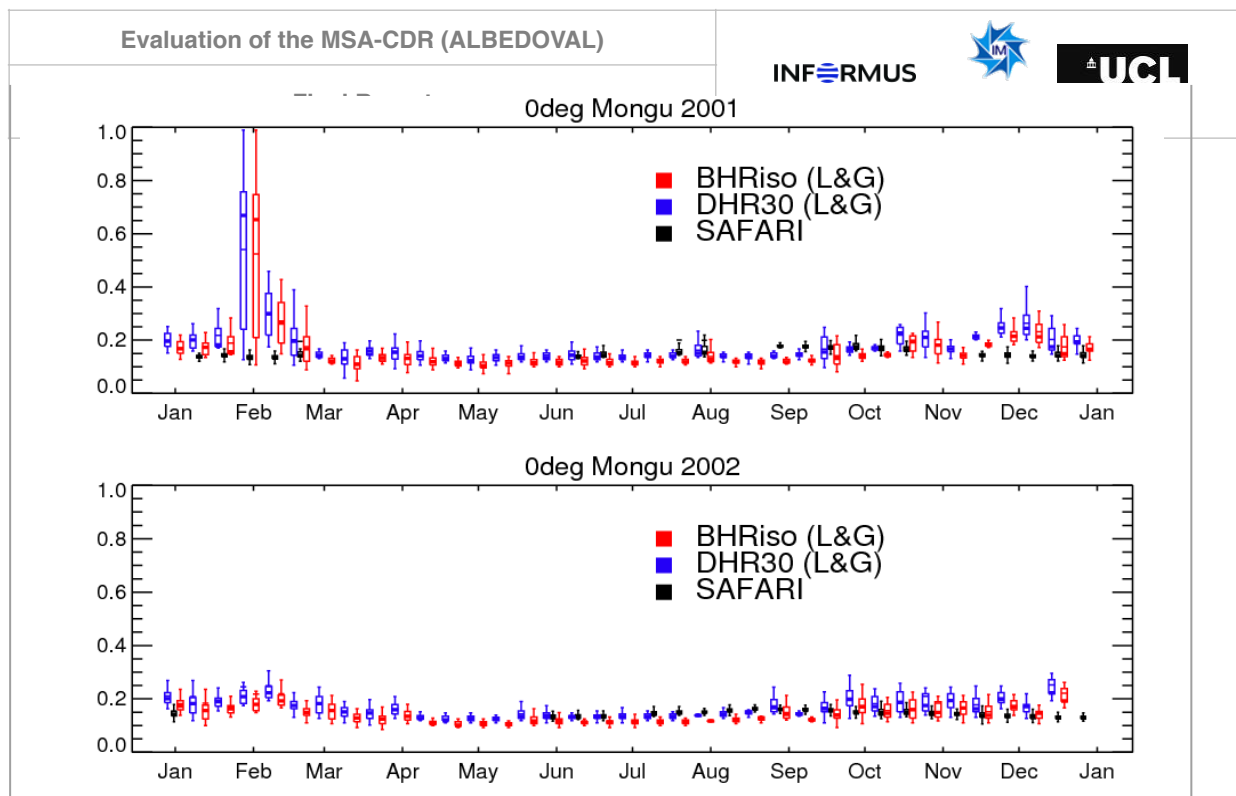
Figure 39: Comparison of MSA vs. in situ albedo observations. The box-and-whisker diagrams represent the spatial variability of the MSA observations (Loew and Govaerts [2010] coefficients applied) within a 3x3 window centred at Mongu (Zambia). For the in situ observations (black), the diagrams represent the temporal variability within a ten-day observation period.

8. Practical experience

8.1. Availability and accessibility

When trying to obtain the full MSA data set from EUMETSAT's online archive[23] it was found that MSA was offered in HDF-5 format on the EUMETSAT product navigator although the product is not delivered in this format. The EUMETSAT Product Navigator has meanwhile been corrected and does no longer offer HDF-5 as a possible delivery format for MSA.

Product documentation as well as static geo-location files can be found at: http://navigator.eumetsat.int/discovery/Start/DirectSearch/Extended.do? freeTextValue(resourceidentifier)=EO:EUM:DAT:MFG:MSA1

This link can be reached from the top-level EUMETSAT website (http://www.eumetsat.int) by navigating as follows:

→ Data & Products

    → Land

        → Meteosat Surface Albedo MFG 0 deg (new window opens)

           → Meteosat Surface Albedo MFG 0 deg

Currently there is no apparent link to access this important auxiliary information directly from the data archive.

8.2. User documentation

Documentation of the dataset is available via the MSA Surface Albedo Factsheet [EUMETSAT, 2010-A] and the more detailed 'Meteosat Surface Albedo Product User Manual and Format Guide'. [EUMETSAT, 2010-B]. The two documents provide accurate and comprehensive documentation of the technical aspects of the dataset. The scientific description provided in the Product User Manual has not been fully assessed at this point.

A few minor inconsistencies in the Product User Manual are listed below. In addition a number of recommendations for improving the user documentation are provided:

➢ The meaning of "broad-band" is not clear. In should be specified in section 4.3 that "broad-band" corresponds to albedo within the 0.3 – 3.0 µm spectral range;

➢ Detailed information on the navigation of the MSA data should be included:

    o   (i) conversion of line/column into to latitude/longitude;

    o   (ii) vice-versa;

➢ In Section 1.4, it is stated "*in the list of products, the MSA product is identified as the MTP Mean Surface Albedo 0100*". This information appears to be wrong. Instead, the product appears to be listed as "*Meteosat Mean Surface Albedo*";

➢ In Section 1.4, a reference should be added pointing the reader to the data documentation website at: http://navigator.eumetsat.int/discovery/Start/DirectSearch/ Extended.do?freeTextValue(resourceidentifier)=EO:EUM:DAT:MFG:MSA1.

8.3. Working with the MSA-CDR

The MSA data product in HDF-4 format could be ingested easily with standard HDF tools. The dataset appears complete and the attributes added to the HDF-4 files provide all relevant information. In the following subsections, we briefly discuss the science datasets, the attributes, and the geo-location.

---

[23] http://archive.eumetsat.int (URL verified 2012-08-20, login required)

8.3.1. Science Datasets Final Report

The albedo files for the 0DEG coverage hold four science datasets:

- ➢ BHR_{ISO} Array[3261, 3842];
- ➢ DHR_{30} Array[3261, 3842];
- ➢ DHR_{30}_ERROR Array[3261, 3842];
- ➢ PROBABILITY   Array[3261, 3842].

In order to convert the values of BHR_{ISO} and DHR_{30} from narrow-band to broad-band albedo, a formula provided in Eq. (33) of [EUMETSAT, 2010-A] needs to be applied. The values of corresponding satellite-dependent constants are given in tables provided on pages 12 and 13 of the PUM [EUMETSAT, 2010-A].

8.3.2. Attributes in dataset

The HDF-4 files of the MSA provide 45 global attributes as shown in Table 14 below. The ancillary files provide exactly the same set of attributes.

Table 14: List of the 45 global attributes in MSA Albedo files.

Number	Name	Example value
1	NOMINAL_SSP	0
2	START_LINE	919
3	HEIGHT	3842
4	START_PIXEL	400
5	WIDTH	3261
6	HDF_CONVERSION_TIME	24/10/2011 08:02
7	SATELLITE_NUMBER	4
8	START_YEAR	1994
9	START_JULIAN_DAY	1
10	END_YEAR	1994
11	END_JULIAN_DAY	10
12	NUMBER_OF_PRODUCTS	6268972
13	ACTUAL_NBR_DAY	10
14	MSA_MAJOR_VERSION	2
15	MSA_MINOR_VERSION	1
16	CALIBRATION_VERSION	07.07.01
17	WATER_REFLECTANCE_THRESHOLD	0.05
18	CLOUD_FOR_SURE_THRESHOLD	0.6
19	CLOUD_SCREENING_SMOOTH	0.1
20	PROBABILITY_ALPHA	0.95
21	AUTOCORRELATION_COEFFICIENT	0.9
22	PERCENT_GOOD_PIXELS	85

Number	Name	Example value
23	MEAN_RELATIVE_RADIOMETRIC_ERRO	9.81
24	MEAN_NUMBER_SLOTS	15.7
25	MEAN_NUMBER_PROCESSED_SLOTS	11.9
26	MEAN_VALID_PIXELS	78.51
27	MEAN_WEAK_SOLUTIONS	6.73
28	MEAN_PERCENT_DUBIOUS	2.75
29	MEAN_PERCENT_NO_SOLUTIONS	19.57
30	MEAN_OPTICAL_THICKNESS	0.355
31	ACTUAL_SSP_LATITUDE	-0.11233
32	ACTUAL_SSP_LONGITUDE	-0.75787
33	MEAN_PROBABILITY_THRESHOLD	85.69
34	MEAN_DHR30	0.218
35	MEAN_DHR30_RELATIVE_ERROR	0.037
36	MSA_VERSION_STRING	2.1
37	START_DAY	1
38	START_MONTH	1
39	END_DAY	10
40	END_MONTH	1
41	START_DATE_STRING	01/01/1994J001
42	END_DATE_STRING	10/01/1994J010
43	PERIOD_INDEX	1
44	PROCESSING_TIME	1072850117
45	SATELLITE_GENERATION	MET

8.3.3. Data dimensions

The dimensions of any MSA field are 3261 columns x 3842 rows for 0DEG, 4485 columns x 3794 rows for IODC_63 and 4662 columns x 4358 rows for IODC_57.

The static geo-location fields (latitude, longitude) have the same dimension as the corresponding MSA data fields. These fields are subsets of the full MVIRI disk, which comprises 5000 x 5000 pixels (see Table 15).

Table 15: Image dimensions of the different MSG coverage areas as well as the position of the lower left corner on the full MVIRI disk. These values are given as attributes in the static HDF navigation files.

Coverage	Rows	Columns	Startline (Row)	Startpixel (Column)
0DEG	3842	3261	919	400

	Final Report				
IODC_57	4358	4662	470		167
IODC_63	3794	4485	941		278

8.4. Geo-referencing routines

Geo-referencing routines for the MSA product were provided by EUMETSAT. A simple IDL wrapper routine was provided as well. These routines were evaluated with the following results (see Annex 11.5 for further details):

➢ The routines provided are consistent with the static geo-location files disseminated as part of the MSA product;

➢ Consistent with the IDL programming language, counting starts at zero (rather than 1);

➢ The first pixel is in the lower left corner of the image, i.e. the lower left pixel is (0/0);

➢ The routines reference to the center of each MVIRI pixel;

➢ The routines are not vectorized, i.e. they can only be applied to individual pixels. This may be critical in terms of computation time, if larger sets of pixels need to be geolocated;

➢ The terms "row" and "line" are used interchangeably for the vertical coordinate (e.g. "startline" refers to the first row);

➢ Similarly, the terms "column" and "pixel" are used interchangeably for the horizontal coordinate (e.g. "startpixel" refers to the first column);

➢ The geo-location files do not provide any land/sea classification.

9. Summary and conclusions

9.1. Summary of findings

9.1.1. General findings

➢ Depending on surface type and a number of external parameters, the albedo of a specific surface target may undergo significant short-term, daily and seasonal variations;

➢ Surface albedo retrievals from directional space-borne observations are further complicated by the need to account for atmospheric effects and surface anisotropy;

➢ The ability for satellite-based surface albedo retrieval is generally reduced due to insufficient illumination at higher latitudes in the winter months and, more importantly, due to frequent cloud cover in several parts of the world, such as the mid-latitudes in winter and tropical areas in the ITCZ;

➢ Systematic surface albedo retrieval errors occur for complex surface types. For example, the albedo of a snowy coniferous forest is underestimated at off-nadir geometries with the instrumental field-of-view being over-proportionally filled by dark snow-free trees;

➢ A validation of the MSA product in the strictest sense was not possible since the effective reflective properties of potential reference areas sufficiently large for direct pixel-wise MSA validation are unknown;

➢ The MSA data record was produced using MVIRI data produced during near real time operations. As a consequence, the MSA product encompasses a range of different image navigation and rectification procedures. These have shown to have only a minor impact on product quality.

➢ Different sets of product requirements on the surface albedo for climate applications have been established by GCOS and WMO:

o The GCOS requirements on the surface albedo aim at detecting a change in radiative forcing with an accuracy of 0.1 Wm^{-2}. The resulting accuracy requirement on the surface albedo (MAX (5%; 0.0025)) appears difficult to achieve from space-borne observations. In contrast to that, the stability requirement (MAX (1%; 0.0001))[24] is within the reach of space-borne surface albedo retrievals;

o The WMO observing requirements database distinguishes between the three requirement levels "threshold", "breakthrough" and "goal". All levels are within the reach of space-borne surface albedo retrievals or have already been met;

9.1.2. MSA strengths

➢ The chosen scientific approach is simple, robust and well documented in the scientific literature;

➢ With only a few short gaps, MSA data are available between August 1981 and July 2006 for the 0° coverage (0DEG) and since July 1998 for the Indian Ocean data coverage (IODC);

➢ A wealth of additional information is provided through the MSA ancillary files allowing user-specific in-depth analysis or post-processing of the MSA product;

---

[24] The stability requirement appears to make little sense: The (relative) 1% criterion gives higher values than the (absolute) 0.0001 criterion for surfaces with albedo values >0.01 (1% of 0.01 equals to 0.0001). Even the darkest surfaces on Earth are characterised by albedo values >0.01 which makes that the 0.0001 stability criterion in practice never applies. To make it equivalent to the accuracy requirement, the GCOS stability requirement should read "MAX(1%, 0.0005)".

➢ Scene-to-scene as well as MVIRI-to-MVIRI geo-location accuracy is on the order of ±1-1.5 pixels both horizontally and vertically. Only Meteosat-3 images appear systematically shifted by 1.5-2 scan lines to the top of the image.

➢ No significant artefacts are observed at satellite to satellite transitions when applying the new spectral-to-broadband conversion factors provided by Loew and Govaerts [2010];

➢ The MSA data record agrees well with corresponding values from both satellite-derived and ground-based observing systems under many observation conditions;

➢ MSA long-term observations are very consistent and have been shown to match the GCOS stability requirement of 1% per decade for a number of desert reference surfaces.

➢ WMO observing requirements:

  o In its current version, MSA already meets the "threshold" requirements of the WMO observing requirements database on spatial (10km) and temporal (30d) resolution;

  o Based on plausibility requirements, we assume the "threshold" uncertainty requirement (±0.1 ΔA) is also being met;

  o MSA has the potential to reach the "breakthrough" level for temporal resolution (3d) and probably also uncertainty (±0.07 ΔA) if the relevant suggested improvements (see below) are implemented.

9.1.3. MSA weaknesses

➢ The most obvious quality issue concerns undetected clouds visible as spikes in MSA time series and also as regions of high albedo in time animated visualisations. Undetected clouds usually result in an overestimation of the surface albedo and may thus create a systematic bias;

➢ Likely due to the cloud contamination issue highlighted above, MSA shows a greater spatial and temporal variance than other EO-derived albedo products (e.g. MODIS, GlobAlbedo). This underlines the necessity for an optimised cloud screening;

➢ When using the recommended threshold of TOA BRF = 0.6 to eliminate potentially cloud contaminated pixels, snow covered surfaces are also often filtered out. This affects MSA availability and representativeness for concerned areas, e.g. Siberia (IODC);

➢ The 90% probability threshold criterion recommended in the MSA Product User Manual to identify high quality values removes good values while letting invalid (mostly cloud-contaminated) values pass. An additional filtering step has been recommended for a better removal of invalid pixels;

➢ Surface desert targets shown to be temporally stable in long-term time series show short-term deviations in the MSA product between +10 and -20%, depending on aerosol load, surface brightness, and observation geometry. The observed pattern seems to indicate that the aerosol path radiance is, on average, insufficiently removed;

➢ Some surfaces show large MSA differences between 0DEG and IODC observation geometries. Aside aerosol related effects, we infer insufficiently characterised surface anisotropy as the main reason for the observed behaviour;

➢ Due to the size of the MSA pixels, reference targets of precisely known surface albedo are not available, limiting the ability to evaluate MSA absolute accuracy. Based on plausibility considerations, we assume that the GCOS accuracy requirement is not met by MSA;

➢ BHR_{ISO} values show a higher temporal variability and also a larger dependence on the observation geometry than do DHR_{30} values. The reasons for this unexpected behaviour are still unclear.

9.2. Does MSA match the requirements?

Table 17 lists a selection of important requirements on satellite-based climate monitoring systems in general and on the surface albedo in particular. The last column states in how far these requirements are met by the MSA data record.

Table 16: Selection of important requirements to be met by the MSA data record. WMO_ORDB indicates the WMO Observing Requirements Database.

ID	Requirement	Source	Match?
GCMP-SAT_01	Consistent sampling within diurnal cycle	GCOS-154	Y
GCMP-SAT_02	Overlap period for old and new satellite systems	GCOS-154	Y
GCMP-SAT_03	Continuity of satellite measurements	GCOS-154	Y
GCMP-SAT_04	Rigorous pre-launch instrument calibration and characterization	GCOS-154	Depending on satellite
GCMP-SAT_05	On-board calibration adequate for climate system observations	GCOS-154	N, vicarious calibr.
GCMP-SAT_06	Sustained operational production of priority climate products	GCOS-154	Does not apply
GCMP-SAT_07	Data systems to facilitate user access	GCOS-154	Y
GCMP-SAT_08	Use of functioning baseline instrument meeting calibration and stability requirements	GCOS-154	Does not apply
GCMP-SAT_09	Complementary in situ baseline observations	GCOS-154	Do not exist
GCMP-SAT_10	Identification of random errors and time dependent biases	GCOS-154	Y, e.g. in ALBEDOVAL
GCOS-HRES	Horizontal resolution (1 km)	GCOS-154	N
GCOS-TRES	Temporal resolution (1-7 days)	GCOS-154	N, but can be achieved
GCOS-ACCU	Accuracy (MAX (5%, 0.0025))	GCOS-154	N (plausib.. consideration)
GCOS-STAB	Stability (MAX (1%, 0.0001))	GCOS-154	Y (for bright surfaces)
WMO_TH_UCRT	Threshold: Uncertainty (10%)	WMO_ORDB	Y (for bright surfaces)
WMO_TH_HRES	Threshold: Horiz. resolution (10 km)	WMO_ORDB	Y
WMO_TH_OBCY	Threshold: Observing cycle (30 d)	WMO_ORDB	Y
WMO_TH_TIME	Threshold: Timeliness (90 d)	WMO_ORDB	N, but can be achieved

9.3. Other related findings

Only very few in situ measurements are available that meet the specific needs for evaluating the accuracy of satellite-retrieved global surface albedo products:

➢ Measurements taken at sufficient height above ground (≥50m);

➢ Reference surfaces homogeneous at the 0.5 to 5km level;

➢ Reference sites covering a variety of different land cover types, especially for dark targets.

This lack of information severely limits the ability to evaluate the absolute accuracy of most space-borne surface albedo products. A network of dedicated reference sites providing the required information in a harmonised form online would greatly facilitate this (and other) important task(s).

FLUXNET covers a limited number of such reference sites with observations dating back to 1995. Unfortunately, the Baseline Surface Radiation Network (BSRN) which is an activity of the World Climate Research Programme (WCRP) does not provide the data required for evaluating space-based surface albedo retrievals, as most stations are located in heterogeneous terrain and albedo measurements are being taken close to the surface.

9.4. Issues not covered by this study

A number of relevant issues could not (or not in sufficient detail) be studied in the frame of ALBEDOVAL due to the limited resources. Studying these issues will lead to a further improved understanding of the MSA product quality. The analysis of those issues classified below as "*highly relevant"* will significantly contribute to an enhanced understanding of MSA product quality and might thus lead to further recommendations to be considered for an eventual MSA re-processing.

➢ Provide a better assessment of anisotropy effects on product accuracy, e.g. by analysing anisotropy effects individually for different land cover types [HIGHLY RELEVANT];

➢ Assess the performance of methods for residual cloud cover screening other than the suggested 90% probability approach [HIGHLY RELEVANT];

➢ Analyse why BHR_{ISO} shows larger variability and larger errors than does DHR_{30} [HIGHLY RELEVANT];

➢ Provide a better assessment of the MSA performance over snow covered surfaces [HIGHLY RELEVANT]:

  o How much valid information over snow is lost due to cloud screening?

  o How is the algorithm performance for various land cover types in the presence of snow (e.g. forest vs. grassland)?

➢ Analyse of the MSA product uncertainty in more detail [HIGHLY RELEVANT]:

  o Assess whether it really reflects retrieval conditions, including cloud cover during retrieval period, aerosol load, and viewing angle.

  o Analyse the MSA product uncertainty information in order to obtain further insight into the observed differences as compared to the corresponding SEVIRI-derived albedo products;

➢ Obtain a statistically improved estimate of the MSA temporal stability by enlarging the range of stable surface reference sites;

➢ Use AVHRR time series for a better estimation of algorithm performance in the pre-EOS era;

➢ Assess the impact of the various MSA retrieval errors on regional or global albedo estimates;

➢ Investigate the potential of high resolution land cover datasets for MSA validation;

➢ Obtain and integrate feedback from the real users:

  o Who are they?

  o Are their requirements met?

➢ Perform a SWOT (Strengths/Weaknesses/Opportunities/Threats) analysis to better understand the aspects relating to MSA sustainability.

9.5. Recommendations

A number of concrete measures should be considered to further improve quality and usability of the MSA dataset and to ensure its sustained availability to the climate community. To indicate a time horizon for the implementation of the recommendations, we distinguish between "*short term*", "*medium term*" and "*long term*":

➢ Short term measures do not require significant changes to the MSA processing chain and should be implemented as soon as possible.

➢ Medium term measures require more substantial changes to the MSA processing chain or involve a careful scientific evaluation of possible options. These should be implemented over the next 1-1.5 years.

➢ Long term measures require fundamental changes of the MSA processing chain or a full re-processing of the underlying MVIRI raw data. These should be implemented over the next 2-3 years.

9.5.1. Usability

➢ Instruct users on how to reduce the number of cloud-contaminated pixels in the MSA product by applying the additional retrieval error based cloud screening criterion described in this report [SHORT TERM];

➢ Improve the user documentation [SHORT TERM]:

o Include information on product projection and geo-location in the Product User Manual;

o Provide a validation report (which could be based on this evaluation) to give users a better understanding of strengths and weaknesses of the MSA product;

o MSA is given for a solar zenith angle of 30°. Explain in the Product User Manual how this relates to surface albedo products (e.g. from MODIS) given at local solar noon;

➢ Enhance user friendliness and enlarge range of applications by allowing spatial and temporal subsetting during the MSA ordering process [MEDIUM TERM];

➢ Provide online animated visualisations through the ordering tool to allow an efficient pre-screening of the MSA product and enhanced transparency for users [MEDIUM TERM].

9.5.2. Product quality

➢ Provide a static land-water mask stating the percentage area of water surfaces within each MSA pixel to avoid erroneous use of the MSA product over water surfaces. Explain the characteristics of the land-water mask in the MSA Product User Manual [SHORT TERM];

➢ Integrate the Loew and Govaerts [2010] spectral-to-broadband conversion coefficients into the MSA product (e.g. into the ancillary files) and explain the importance of these coefficients in the Product User Manual [SHORT TERM];

➢ Alternatively (or additionally), provide a ready-to-use broadband albedo product based on the Loew and Govaerts [2010] coefficients to the MSA product suite [MEDIUM TERM];

➢ Revise the narrow-to-broad band conversion for very bright surfaces to potentially reduce the differences between MSA and SEVIRI-derived surface albedo for albedo values above ca. 0.45 [MEDIUM TERM].

➢ Produce daily MSA estimates to enable user-specific temporal compositing (and other analyses) and to comply with GCOS requirements on (daily) temporal resolution [MEDIUM TERM];

➢ Introduce a dedicated cloud-masking step (e.g. consideration of IR channels or time series analysis) into the MSA processing chain. This will inherently contribute to a better consideration of snow-covered areas [MEDIUM TERM];

➢ Utilisation of redundant observations in identical coverage areas to enable better cross-calibration between subsequent MVIRIs [MEDIUM TERM];

➢ Explore temporal compositing strategies potentially allowing for a higher quality product. For example, by using all values of the compositing period to create an observation vector with a sufficient amount of cloud-free observations instead of doing so on a day-by-day basis [MEDIUM TERM].

➢ Re-process all MVIRI raw data using a single rectification algorithm and following commonly accepted file naming (e.g. WMO) and metadata (e.g. WMO, INSPIRE) conventions and standards to create a homogeneous image dataset [LONG TERM].

9.5.3. Product sustainability

➢ Secure long-term availability of all information, namely from the early Meteosats, required for MVIRI re-processing by assuming responsibility for relevant data archaeology stewardship [MEDIUM TERM];

➢ Explore the best way to ensure the sustained utility of the MSA dataset after the end of the MVIRI operations [MEDIUM TERM].
Two options appear feasible:

   o Coupling new surface albedo products from recent instruments (namely SEVIRI) to the existing MSA product;

   o Generating "pseudo-MVIRI" observations from recent instruments (namely SEVIRI) for subsequent injection into the MSA processing chain.

9.5.4. Further activities

➢ Inquire at GCOS whether their MAX (1%, 0.0001) stability requirement makes sense [SHORT TERM];

➢ Additionally create a Fraction of Absorbed PAR (FAPAR) product to enlarge the potential user base and to further add value to the MVIRI time series [MEDIUM TERM].

➢ MSA is based on a number of assumptions and trade-offs that were made more than ten years ago. Considering recent scientific and technological progress, it is worthwhile to consider introducing available external knowledge into the retrieval process [LONG TERM]:

   o A-priori knowledge on the surface albedo to identify and exclude unlikely results;

   o Information on the surface BRDF to better account for surface anisotropy;

   o Global aerosol re-analyses or climatologies to reduce aerosol related retrieval uncertainties.

9.6. Conclusions

The MSA data record is a unique data set encompassing up to 25 years of continuous surface albedo coverage for large areas of the Earth. It is therefore of paramount importance to maintain and further improve the existing MSA data record.

The evaluation of the MSA data record has revealed a number of specific strengths and weaknesses as outlined above. While the strengths underlines the already high value of the MSA data record for

climate applications, the weaknesses need to be considered for specific applications and should be addressed in the context of a product re-processing. A number of concrete recommendations to improve product quality, usability and sustainability at short, medium and long term have been devised.

In combination with other (EUMETSAT and non-EUMETSAT) geostationary satellites, the MSA method should contribute to creating harmonised surface albedo records of quasi global coverage outside the polar zones serving climate applications and beyond. Going beyond, geostationary and polar-orbiting observations may be fused to provide multi-mission albedo products of higher product quality and full global coverage, capitalizing on the strengths of both approaches.

Belward, A. S. (1996). The IGBP-DIS global 1km land cover data set (DISCover) – proposal and implementation plans. IGBP-DIS working paper No. 13. IGBP-DIS Office, Météo-France, Toulouse, France, 61 pp.

Benedetti, A., J.W. Kaiser and J.-J. Morcrette (2011): [Global Climate] Aerosols [in "State of the Climate in 2010"]. BAMS, 92(6) pp. 65-67.

Bolle, H. J., et al. (1993). EFEDA: European Field Experiment in a desertification-threatened area, Ann. Geophys., 11, 173-189.

Bolle, H.-J.; Eckardt, M; Koslowsky, D.; Maselli, F.; Menenti, M. ; Meliá-Miralles, J.; Olesen, F.-S.; Petkov, L.; Rasool, I.; Van de Griend, A.; Editors (2006). Mediterranean Land-surface Processes Assessed from Space, Springer-Verlag Berlin Heidelberg, ISBN 9783540401513; 9783540453109.

Braverman, A., and L. Di Girolamo (2002). MISR global data products: a new approach. IEEE Trans. Geosci. Remote Sens. 40, 1626-1636.

Buriez, J.C., Parol, F., Cornet, C., Doutriaux-Boucher, M. (2005). An improved derivation of the top-of-atmosphere albedo from POLDER/ADEOS-2 narrow-band albedos. JGR-Atmos., 110, D05202, doi: 10.1029/2004JD005243.

Camacho, F., Sanchez, J., Lacaze, R., Schaaf, C., Cescatti, A. (2012). Validation of GEOLAND-2 global albedo products based on SPOT/VEGETATION observations. Geophysical Research Abstracts 14, EGU2012-3474.

Cescatti, A., Marcolla, B., Vannan, S.K.S., Pan, J.Y., Roman, M.O., Yang, X., Ciais, P., Cook, R.B., Law, B.E., Matteucci, G., Migliavacca, M., Moors, E., Richardson, A.D., Seufert, G., Schaaf, C.B. (2012). Intercomparison of MODIS albedo retrievals and in situ measurements across the global FLUXNET network. Remote Sens. Environ. 121, 323-334.

Csiszar, I., and G. Gutman (1999). Mapping global land surface albedo from NOAA AVHRR. *J. Geophys. Res.*, 104(D6), 6215–6228, doi:10.1029/1998JD200090.

Dee et al., 2011: The ERA-Interim reanalysis: configuration and performance of the data assimilation system. Quart. J. Roy. Meteorol. Soc., 137, 553-597, DOI:10.1002/qj.828.

Engelsen, O., Pinty, B., Verstraete, M. M., and Martonchik, J. V., 1996, Parametric bidirectional reflectance factor models: Evaluation, improvements and applications. Report of the Joint Research Centre of the European Commission, EU 16426, Ispra, Italy.

EUMETSAT, 2010-A. Meteosat Surface Albedo Fact Sheet: Version 1, EUMETSAT, Darmstadt, Germany.

EUMETSAT, 2010-B. Meteosat Surface Albedo (MSA) Product User's Manual and Format Guide, 24 pp, EUMETSAT, Darmstadt, Germany.

EUMETSAT, 2011-A. Meteosat First Generation User Handbook. Report, 40 pp, EUMETSAT, Darmstadt, Germany.

EUMETSAT, 2011-B. GSICS MVIRI-IASI Inter-calibration Uncertainty Evaluation. Report, EUMETSAT, Darmstadt, Germany.

Fell, F. (1991). Ein Test der aus Satellitendaten in den Spektralbereichen der AVHRR-Kanäle eins und zwei bestimmten Bodenalbedo durch vergleichende Bodenmessungen im Sudan. Diploma thesis, 91 pp., Inst. f. Meteorologie, Freie Universität Berlin, Germany.

GCOS-138 (2010). Implementation Plan for the Global Observing System for Climate in Support of the UNFCCC (2010 Update), WMO, Geneva, Switzerland.

GCOS-143 (2010). Guideline for the Generation of Datasets and Products Meeting GCOS Requirements, WMO, Geneva, Switzerland.

GCOS-154 (2011). Systematic Observation Requirements for Satellite-based Products for Climate Supplemental details to the satellite-based component of the Implementation Plan for the Global Observing System for Climate in Support of the UNFCCC - 2011 Update, WMO, Geneva, Switzerland.

Geiger, B., Carrer, D., Franchisteguy, L., Roujean, J.-L., Meurey, C. (2008). Land Surface Albedo Derived on a Daily Basis From Meteosat Second Generation Observations. IEEE Trans. Geosci. Remote Sensing 46, 3841-3856.

Govaerts, Y.M., Lattanzio, A., Pinty, B., Schmetz, J. (2004). Consistent surface albedo retrieval from two adjacent geostationary satellites. Geophys. Res. Lett. 31.

Govaerts, Y.M., Pinty, B., Taberner, M., Lattanzio, A. (2006). Spectral conversion of surface albedo derived from meteosat first generation observations. IEEE Geoscience and Remote Sensing Letters, 3(1), 23-27.doi : 10.1109/LGRS.2005.854202.

Govaerts, Y., and Lattanzio, A. (2007). Retrieval Error Estimation of Surface Albedo Derived from Geostationary Large Band Satellite Observations: Application to Meteosat-2 and -7 Data. Journal of Geophysical Research 112, doi:10.1029/2006JD007313.

Govaerts, Y.M., Lattanzio, A., Taberner, M., Pinty, B. (2008). Generating global surface albedo products from multiple geostationary satellites. Remote Sens. Environ. 112, 2804-2816.

Knuteson, R. O., and H. E. Revercomb (2004). Land surface temperature and emissivity from advanced sounders. 2004 EUMETSAT Meteorological Satellite Conference, Prague, Czech Republic. Proceedings. EUMETSAT, Darmstadt, Germany, 2004, pp.241-247. Reprint #4269.

Lattanzio, A., Y. Govaerts, et al. (2006). Consistency of surface anisotropy characterization with Meteosat observations. Advanced Space Research, doi:10.1016/j.asr.2006.02.049.

Leroy, M., Deuze, J., Breon, F., Hautecoeur, O., Herman, M., Buriez, J., Tanre, D., Bouffies, S., Chazette, P., Roujean, J. (1997). Retrieval of atmospheric properties and surface bidirectional reflectances over land from POLDER/ADEOS. JGR-Atmos. 102, 17023-17037.

Loew, A., and Y. Govaerts (2010). Towards multidecadal consistent Meteosat surface albedo time series, Remote Sensing, 2(4), 957-967.

Martonchik, J., Diner, D., Pinty, B., Verstraete, M., Myneni, R., Knyazikhin, Y., Gordon, H. (1998). Determination of land and ocean reflective, radiative, and biophysical properties using multiangle imaging. IEEE Trans. Geosci. Remote Sensing 36, 1266-1281.

McPeters, R. D., S. M. Hollandsworth, L. E. Flynn, J. R. Herman, and C. J. Seftor (1996). Long-term ozone trends derived from the 16-year combined Nimbus 7/Meteor 3 TOMS Version 7 record, Geophys. Res. Lett., 23(25), 3699–3702, doi:10.1029/96GL03540.

Muller, J.-P., López, G., Watson, G., Shane, N.S., Tom Kennedy, T.E., Lewis, P., Fischer, J., Guanter, L., Domench, C., Preusker, R., North, P.R., Heckel, A., Danne, O., Krämer, U., Zühlke, Z., Brockmann, C. (2012-B). The ESA GlobAlbedo Project for mapping the Earth's land surface albedo for 15 Years from European Sensors., IEEE Geoscience and Remote Sensing Symposium (IGARSS) 2012. IEEE, Munich, Germany, 22-27.7.12.

Ohmura, A., Dutton, E.G., Forgan, B., Frohlich, C., Gilgen, H., Hegner, H., Heimo, A., Konig-Langlo, G., McArthur, B., Muller, G., Philipona, R., Pinker, R., Whitlock, C.H., Dehne, K., Wild, M. (1998). Baseline Surface Radiation Network (BSRN/WCRP): New precision radiometry for climate research. Bull. Amer. Meteorol. Soc. 79, 2115-2136.

Pinty, B., Roveda, F., Verstraete, M.M., Gobron, N., Govaerts, Y., Martonchik, J.V., Diner, D.J., and Kahn, R.A. (2000-A): Surface albedo retrieval from Meteosat: Part 1: Theory, Journal of Geophysical Research, 105, 18099-18112.

Pinty, B., Roveda, F., Verstraete, M.M., Gobron, N., Govaerts, Y., Martonchik, J.V., Diner, D.J., and Kahn, R.A. (2000-B): Surface albedo retrieval from Meteosat: Part 2: Applications, Journal of Geophysical Research, 105, 18113-18134.

Pinty, B., A. Lattanzio, J. V. Martonchik, M. M. Verstraete, N. Gobron, M. Taberner, J.-L. Widlowski, R. E. Dickinson, and Y. Govaerts (2005): Coupling Diffuse Sky Radiation and Surface Albedo. J. Atmos. Sci., 62, 2580-2591. doi: http://dx.doi.org/10.1175/JAS3479.1

Rahman, H., B. Pinty, and M. M. Verstraete (1993). Coupled surface-atmosphere reflectance (CSAR) model. 2. Semi-empirical surface model usable with NOAA Advanced Very High Resolution Radiometer data', Journal of Geophysical Research, 98, 20,791-20,801.

Rao, C. R. N., J. Chen, J. T. Sullivan, and N. Zhang (1999). Post-launch Calibration of Meteorological Satellite Sensors, Advances in Space Research, 23(8), 1357-1365.

Roujean, J.L., and Lacaze, R. (2002). Global mapping of vegetation parameters from POLDER multiangular measurements for studies of surface-atmosphere interactions: A pragmatic method and its validation. JGR-Atmos, 107, 4150, doi:10.1029/2001JD000751.

Schaaf, C.B., Gao, F., Strahler, A.H., Lucht, W., Li, X.W., Tsang, T., Strugnell, N.C., Zhang, X.Y., Jin, Y.F., Muller, J.P., Lewis, P., Barnsley, M., Hobson, P., Disney, M., Roberts, G., Dunderdale, M., Doll, C., d'Entremont, R.P., Hu, B.X., Liang, S.L., Privette, J.L., Roy, D. (2002). First operational BRDF, albedo nadir reflectance products from MODIS. Remote Sens. Environ. 83, 135-148.

Schaaf, C., Martonchik, J., Pinty, B., Govaerts, Y., Gao, F., Lattanzio, A., Liu, J., Strahler, A.H., Taberner, M. (2008). Retrieval of Surface Albedo from Satellite Sensors. Advances in Land Remote Sensing: System, Modelling, Inversion and Algorithms, Ed. S. Liang, 219-243.

Schaaf, C.B., J. Cihlar, A. Belward, E. Dutton, and M. Verstraete, 2009. Albedo and Reflectance Anisotropy, ECV-T8: GTOS Assessment of the status of the development of standards for the Terrestrial Essential Climate Variables, ed., R. Sessa, FAO, Rome.

SCOPE-CM (2011). SCOPE-CM statement of needs to GSICS, Version 1.0

Trigo, I., Freitas, S., Barroso, C., Macedo, J., Perdigão, R., Silva, R., Viterbo, P. (2012). Radiation Products based on a constellation of Geostationary Satellites. Geophysical Research Abstracts 14, EGU2012-7883.

Vermote, E., D. Tanré, J. L. Deuzé, M. Herman, and J. J. Morcrette, 1997: Second simulation of the satellite signal in the solar spectrum: An overview. IEEE Trans. Geosci. Remote Sens., 35-3, 675-686.

Wild, M., Ohmura, A., Gilgen, H., Morcrette, J.J., Slingo, A. (2001). Evaluation of downward longwave radiation in general circulation models. J. Clim. 14, 3227-3239.

WMO (2006). World Meteorological Organization Commission for Instruments and Methods of Observation (WMO/CIMO) Guide to Meteorological Instruments and Methods of Observation. Preliminary seventh edition. Report WMO-No. 8, Geneva, Switzerland.

11. Annex

11.1. Reference data

11.1.1. In situ surface albedo

Data set	Domain	Parameter	Spatial cov.	Spatial res.	Temporal cov.	Temporal res.	Terms	Comment	Utility	
Baseline Surface Radiation Network (BSRN)	In situ	Up- and downwelling SW flux; surface albedo	Global, most stations situated in Europe and the US	~100 m²	Station dependent, can be long-term, can be multi-year	Minutes	Free access for non-commercial users	Only two BSRN stations (Toravere, Payerne) provide routine albedo within Meteosat disk. Albedo data maybe also available for Cabauw.	High for con analysis due time series. Limited for validation (footprint, ta heterogeneou surfaces).	Low. Data available and processing metho established.
Free University Berlin - Sudan	In situ	Spectral albedo (0.5-1.6 µm)	Sudan, 15N-17N, 32E-33E	~100 m², some profiles (4 and 1989 5 sites within 2-3 km)	Individual dates in 1988	Individual measurements, diurnal courses	Free access for ALBEDOVAL	Ca. 50 measurements at ca. 40 sites, some taken in homogeneous areas covering several MSA pixels.	High. Among sparsly avai EOS in situ Partly cover homogeneou surfaces.	Low to high. Limited amount o processed data available. Processing of raw data needs to be re-established.
Free University Berlin - Various	In situ	Spectral albedo (0.5-1.6 µm, broadband albedo	Germany, Spain, Italy, Niger, France	~100 m²	Individual dates and short periods from 1987 to 1992	Individual measurements, diurnal courses	Free access for ALBEDOVAL	Data and related tools not easily accessible since relevant staff has retired.	Medium. Amo sparsly avai EOS in situ Often taken heterogeneou surfaces.	Medium to high. Some data just need to be digitized from paper, other require full reprocessing.
Safari 2000	In situ	Broadband albedo	South Africa, Zambia	~100 m²	03/00-12/02	15 minutes	Free access for non-commercial users	Only two stations to provide albedo data.	High. Time s covering alm years for ra homogeneou in Africa.	Medium. Automate processing still to be developed.
FLUXNET	In situ	Broadband albedo	Global, most stations in Europe and the US, some in Africa	Depending on obs. height, up to 50,000 m²	1996-2006	11:00-13:00 local time	Certain stations adhering to "fair use" policy	Albedo taken at heights between 5 and 50 m concomitantly with CO2-flux rate masurements.	High. Long t partly taken towers above homogeneou	Low. Data available and processing metho established.

11.1.2. Satellite derived surface albedo

Data set	Domain	Parameter	Spatial cov.	Spatial res.	Temporal cov.	Temporal res.	Terms	Comment	Utility	Effort
LSA-SAF Albedo	Sat	Albedo retrieval from MSG/SEVIRI based on Roujean lon BRDF model	Meteosat disk, centered at 0°	3 km at nadir	From 09/05	Daily	Free access for non-commercial users	Daily values based on 15 min. observations of 0.6, 0.8 and 1.6 µm channels. Atmospheric correction based on forecasts of TCWV and aerosol climatology (replaced by MACC forecasts in 2012).	Medium. Five months overlap with MSA.	Low. Data available and processing methods established.
AVHRR	Sat	Spectral reflectance; Broadband albedo	Europe, 27N-72N, 10W-42E	0.01°	01/89-12/09 can be extended up to now. Above 55N only summer season (04-10)	Daily	Free access for ALBEDOVAL	Data and related tools not easily accessible since relevant staff has retired.	High. Full spatial coverage since 1989, instruments well intercalibrated and navigated.	Medium to High. Data need to be retrieved from old archives and pre-processed according to study needs.
MODIS	Sat	Broadband albedo	Global	500 m and 0.05°	From 03/00	Every 8 days, represent. 16 days	Free access for non-commercial users	Collection 5 to be used, only use first two quality grades.	High. Global coverage, high spatial resolution.	Low. Automated processing methods established.
MISR	Sat	Broadband albedo	Global	1.1 km	From 03/00	Overpass every 16 days near equator, every 3 days near poles	Free access for non-commercial users	Near instantaneous measurements under nine angles.	High. Simultaneous multi-angle retrieval providing uncertainty estimate for actual sky condition.	High. Data processing laborious, data access complicated.
GlobAlbedo	Sat	Broadband albedo	Global	1 km, 0.05° as well as 0.5°	06/98-06(12)/11	Every 8 days, repres. a "halfwidth" of a few days	Free access for GlobAlbedo users	Albedo values derived using optimal estimation approach with input from MERIS, Vegetation, MODIS.	High. Provides uncertainly estimate	Low. Data available and processing methods established.

11.1.3. Ancillary data

Data set	Domain	Parameter	Spatial cov.	Spatial res.	Temporal cov.	Temporal res.	Terms	Comment	Utility	Effort
GLCC-IGBP	Ancillary	Land cover map derived from AVHRR imagery, 17 LC classes	Global	1 km	1992-1993	does not apply	Free access for non-commercial users	Well established and tested LC map based on almost 20 years old data	High. Allows stratification of MSA data for various analyses.	Low. Data readily available in GIS-compatible formats.
MACC-II	Ancillary	Re-analysis of AOD at 550 nm for sea salt, dust, organic matter, black carbon, sulphate	Global	1.125°	2003-2010	Daily	Free access for EU-27 non-commercial users.	Most relevant input is MODIS AOD.	High. Allows to investagate aerosol related quality aspects.	Low. Data available and processing methods established.
AERONET	Ancillary	Spectral AOD	Global, most stations in Europe and the US	Does not apply	Depending on actual station, earliest data from 1996	Minutes	Free access for non-commercial users	About 15 stations located within 0° coverage and IODC.	High. Allows to investagate aerosol related quality aspects.	Medium. Automated processing still to be developed

12. Reference surface targets

Table 17: Selection of reference surface targets used for ALBEDOVAL quality assessment purposes. Only targets explicitly mentioned in this report are listed below. The homogeneity definition can be found in section 5.4.2. The full list of surface targets considered for this study is available in a separate Excel spreadsheet.

Name	Country	Lat	Lon	IGBP Land Cover	Homogeneity	Program
DE_Hai	Germany	51.080	10.450	Decidouous broadleaf forest	low	FLUXNET
Egypt_One	Egypt	27.120	26.100	Barren or sparsely vegetated	high	SATCAL
H_NAV_1	Morocco	15.970	52.139	Barren or sparsely vegetated	low	ALBEDOVAL
H_NAV_2	Egypt	20.094	37.206	Barren or sparsely vegetated	average	ALBEDOVAL
H_NAV_3	Egypt	18.030	-16.011	Barren or sparsely vegetated	low	ALBEDOVAL
HU_Bug	Hungary	46.690	19.600	Croplands	low	FLUXNET
Libya	Libya	21.500	28.500	Barren or sparsely vegetated	high	SATCAL
Moldova	Moldova	47.000	28.816	Cropland/natural vegetation	average	AERONET
Mongu	Sambia	-15.438	23.253	Evergreen broadleaf forest	low	SAFARI-2000, AERONET
Murzuq_Desert	Libya	24.750	12.500	Barren or sparsely vegetated	high	SATCAL
Omani_Desert	Oman	19.000	55.500	Barren or sparsely vegetated	high	SATCAL
Skukuza	South Africa	-25.020	31.483	Croplands	high	SAFARI-2000
Solar_Village	Saudi Arabia	24.907	46.397	Open shrublands	low	AERONET
Toravere	Estonia	58.254	26.462	Evergreen needleleaf forest	low	BSRN, AERONET
V_NAV_1	Mauretania	31.354	27.206	Barren or sparsely vegetated	average	ALBEDOVAL
V_NAV_2	Sudan	31.111	33.611	Water bodies	low	ALBEDOVAL
V_NAV_3	Yemen	27.976	-12.646	Barren or sparsely vegetated	average	ALBEDOVAL

12.3. GCOS Climate Monitoring Principles

The GCOS Climate Monitoring Principles (GCMPs) to ensure the effectiveness of climate monitoring systems are listed in Panel 4 below [GCOS-143, 2010].

1. The impact of new systems or changes to existing systems should be assessed prior to implementation.

2. A suitable period of overlap for new and old observing systems is required.

3. The details and history of local conditions, instruments, operating procedures, data processing algorithms and other factors pertinent to interpreting data (i.e., metadata) should be documented and treated with the same care as the data themselves.

4. The quality and homogeneity of data should be regularly assessed as a part of routine operations.

5. Consideration of the needs for environmental and climate-monitoring products and assessments, such as IPCC assessments, should be integrated into national, regional and global observing priorities.

6. Operation of historically-uninterrupted stations and observing systems should be maintained.

7. High priority for additional observations should be focused on data-poor regions, poorly-observed parameters, regions sensitive to change, and key measurements with inadequate temporal resolution.

8. Long-term requirements, including appropriate sampling frequencies, should be specified to network designers, operators and instrument engineers at the outset of system design and implementation.

9. The conversion of research observing systems to long-term operations in a carefully-planned manner should be promoted.

10. Data management systems that facilitate access, use and interpretation of data and products should be included as essential elements of climate monitoring systems.

Panel 4: GCOS Climate Monitoring Principles (GCMPs) to ensure effective climate monitoring systems.

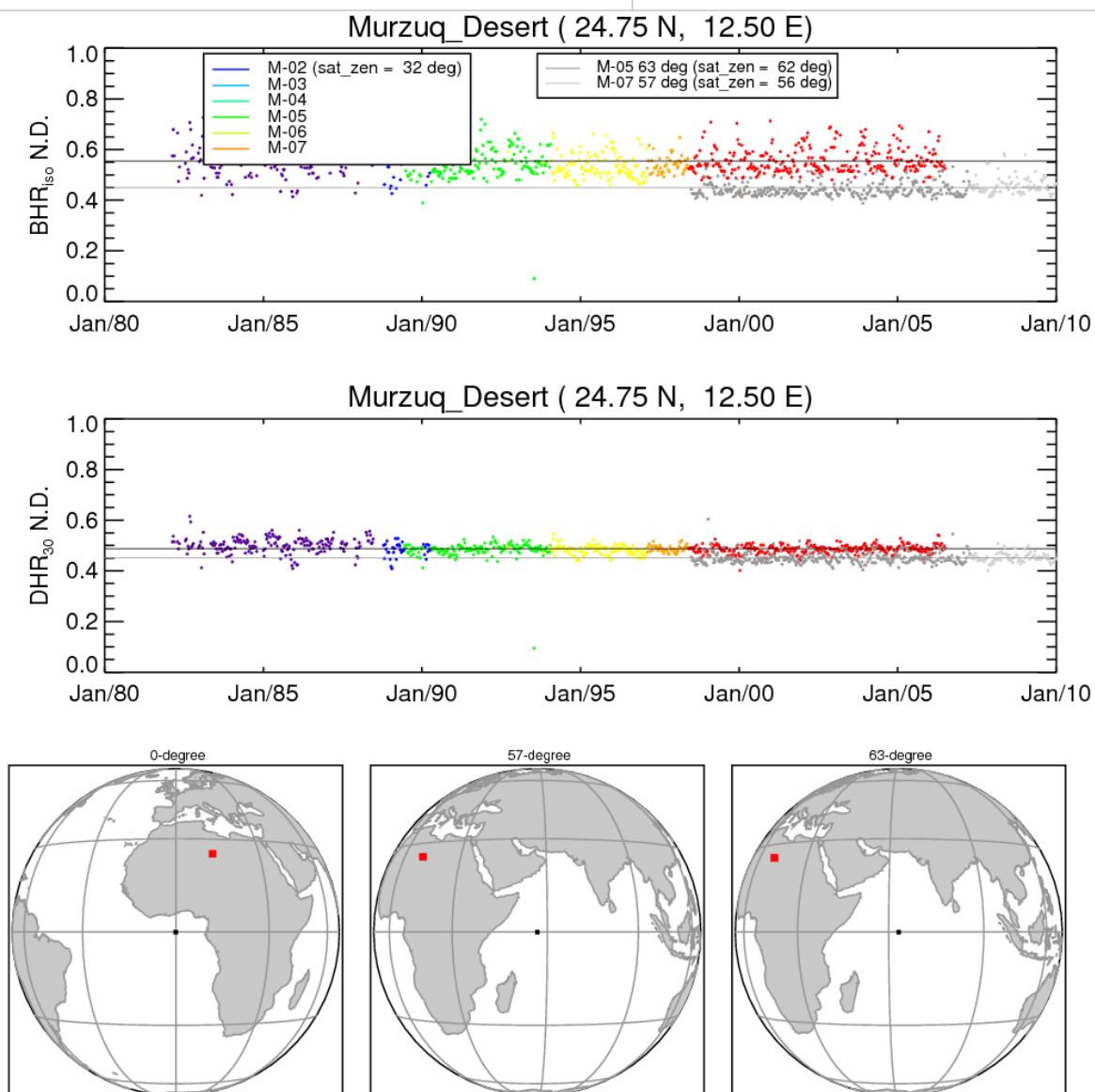## 12.4. MSA time series at selected sites

Figure 40: Long-term time series of BHR
three plots show the position of the target site on the respective 0-degree and IODC disks. The coloured dots show pentad averages for 0-degree coverage, the grey dots for IODC coverage. The dark and light-grey lines show the long-term averages for the two coverage areas.
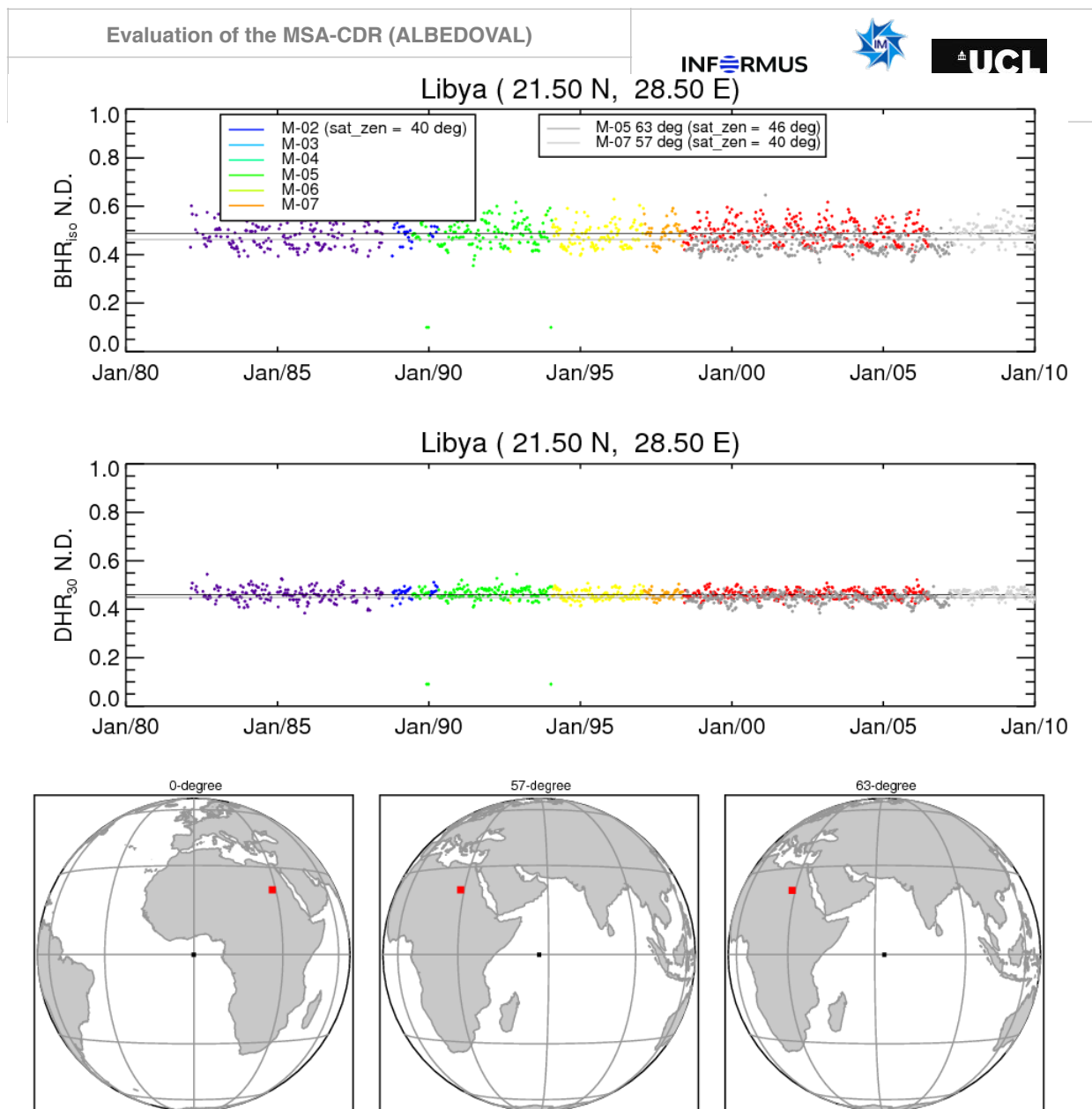
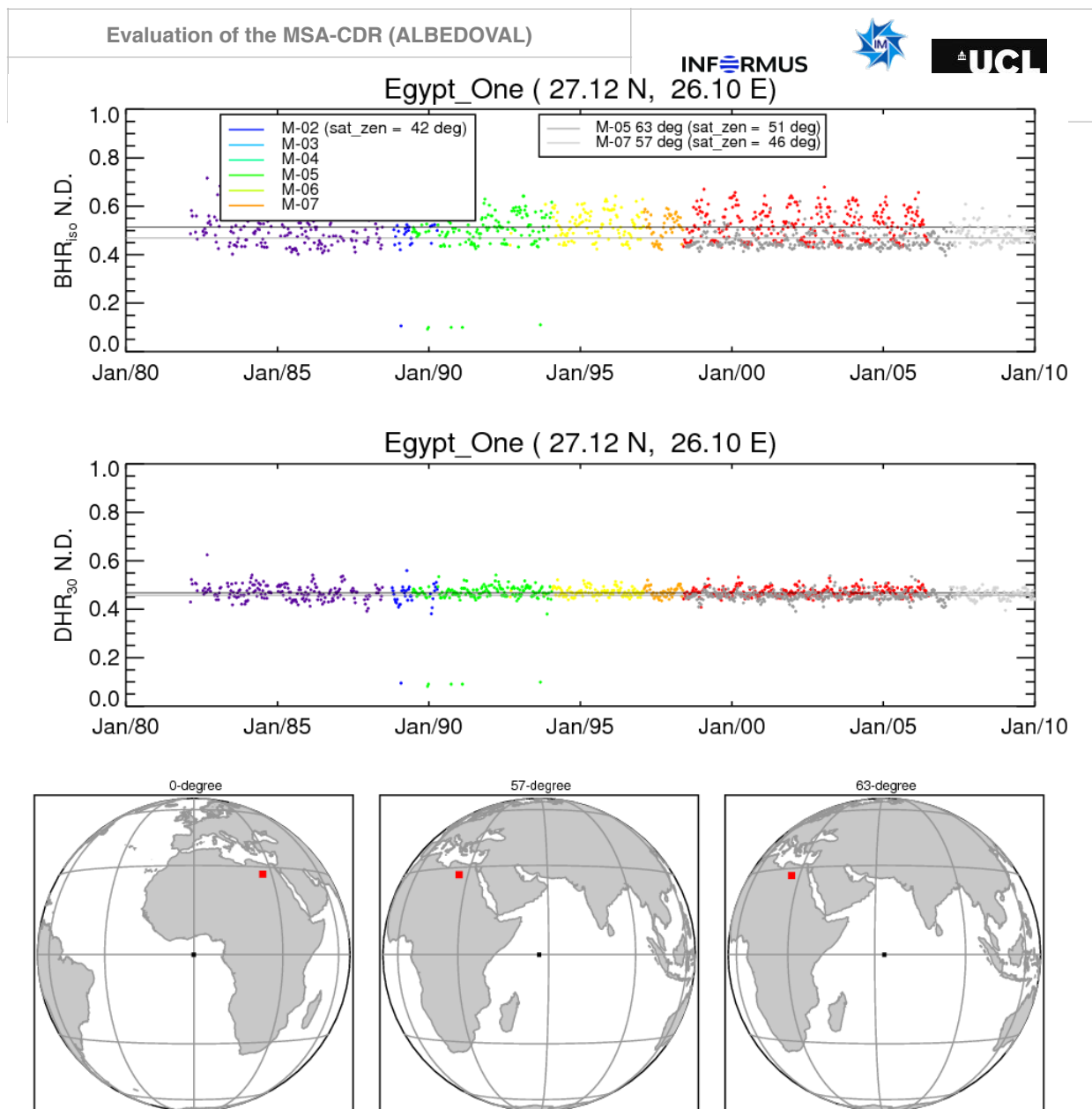Figure 41: Same as Figure 40 but for site "Libyan Desert".

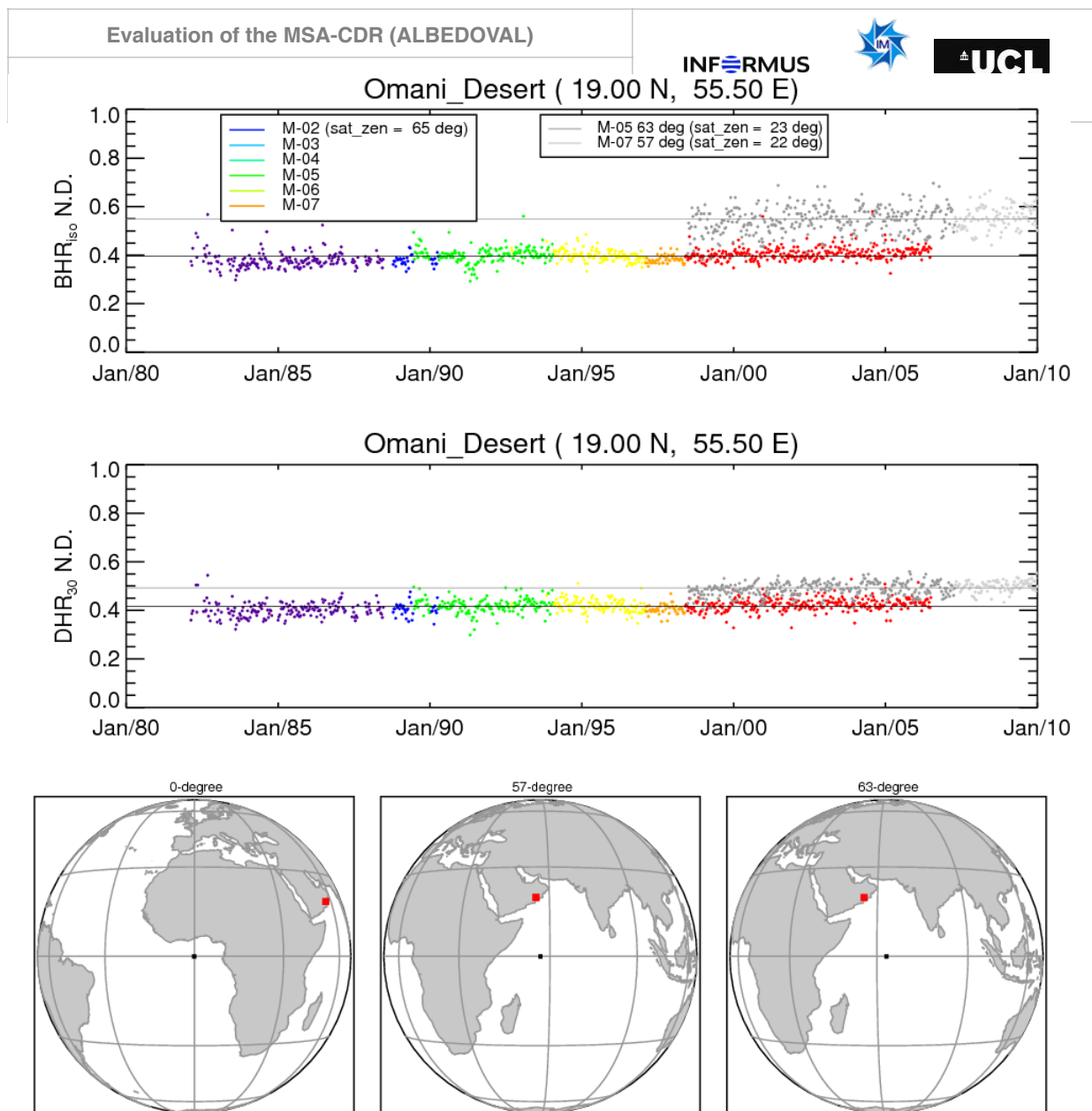Figure 42: Same as Figure 40 but for site "Egypt One".

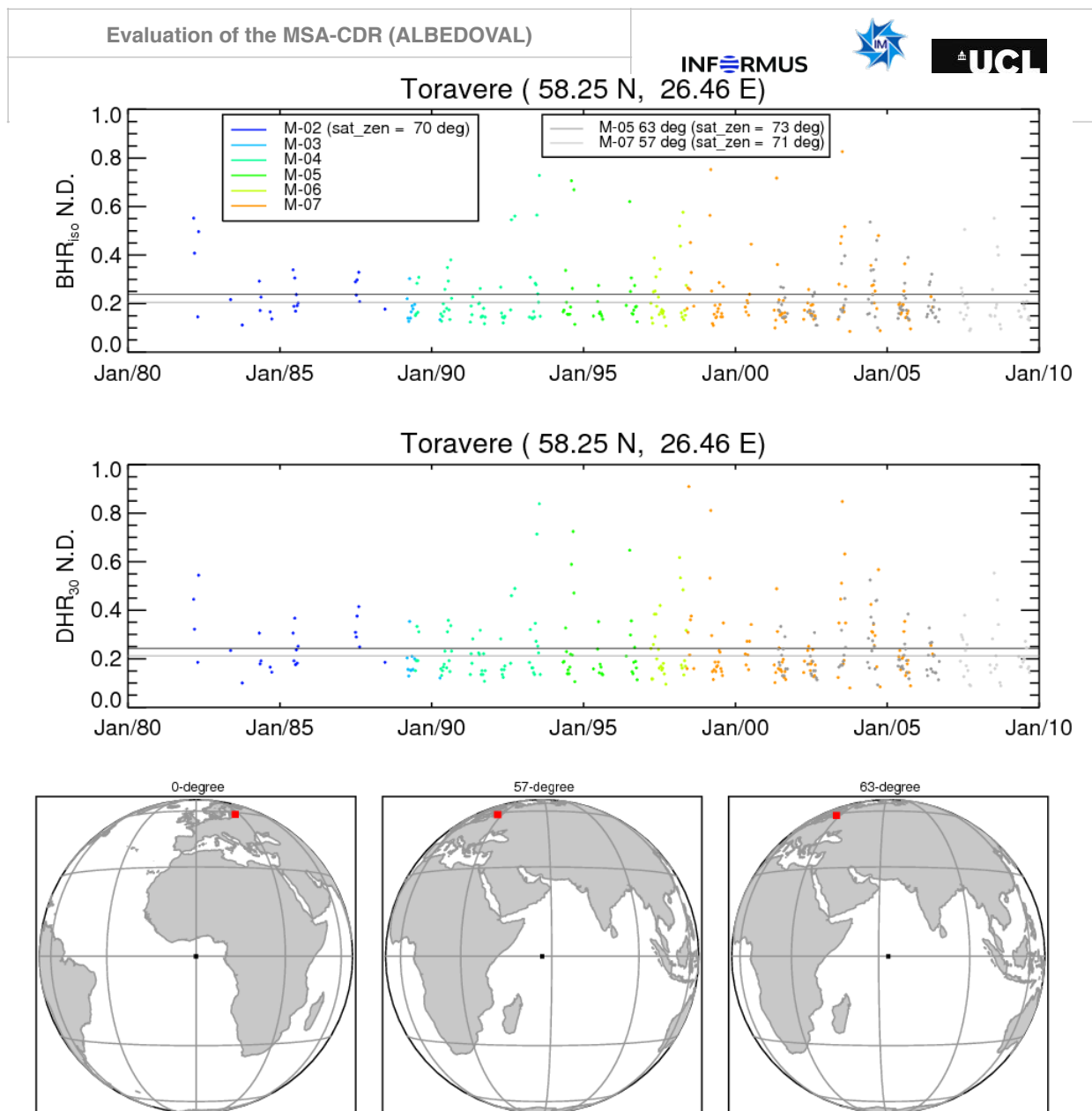**Figure 43: Same as Figure 40 but for site "Omani Desert".**

Figure 44: Same as Figure 40 but for site "Toravere" (Estonia). Note the observation gaps in winter and residual cloud contamination.
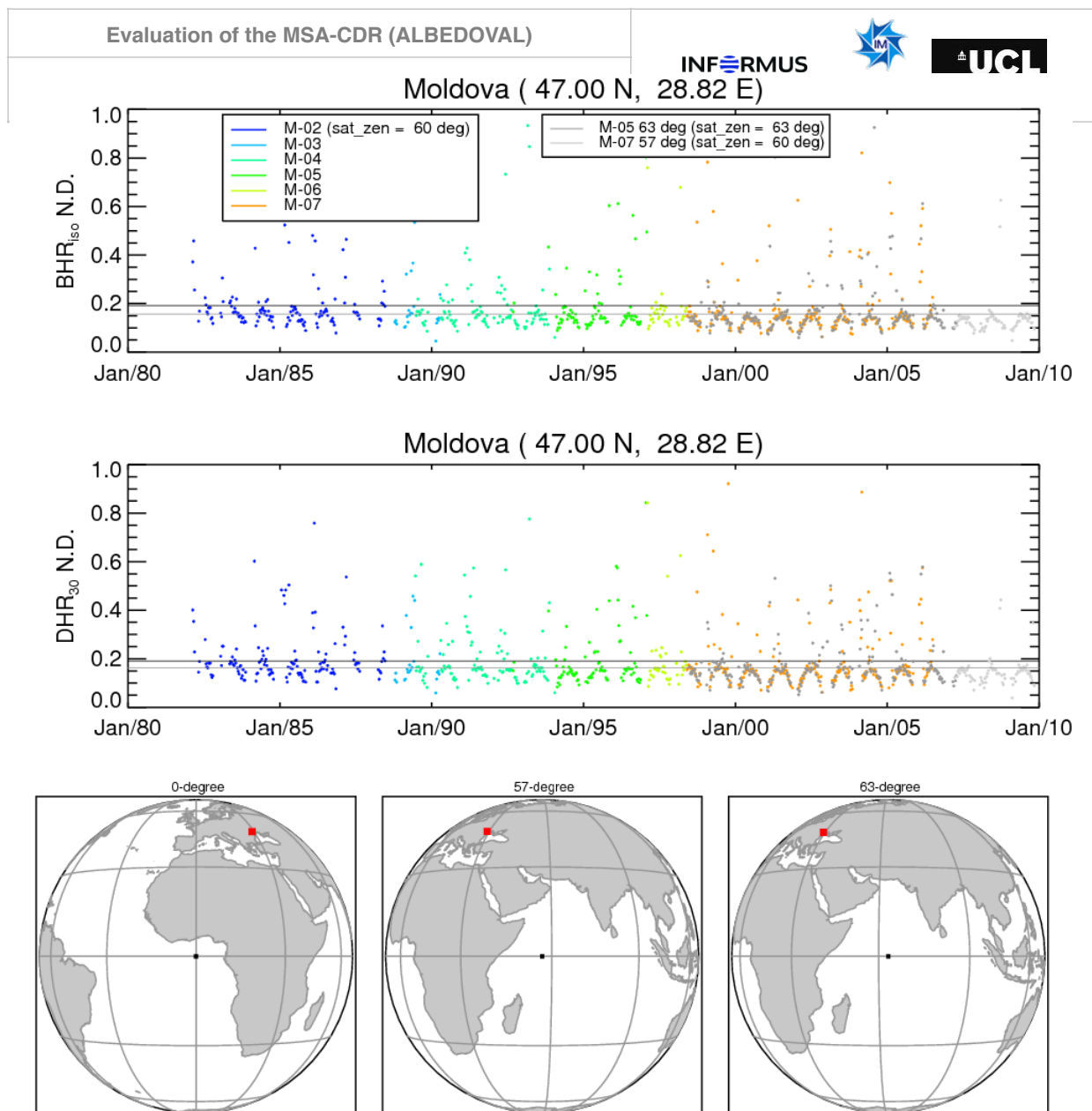
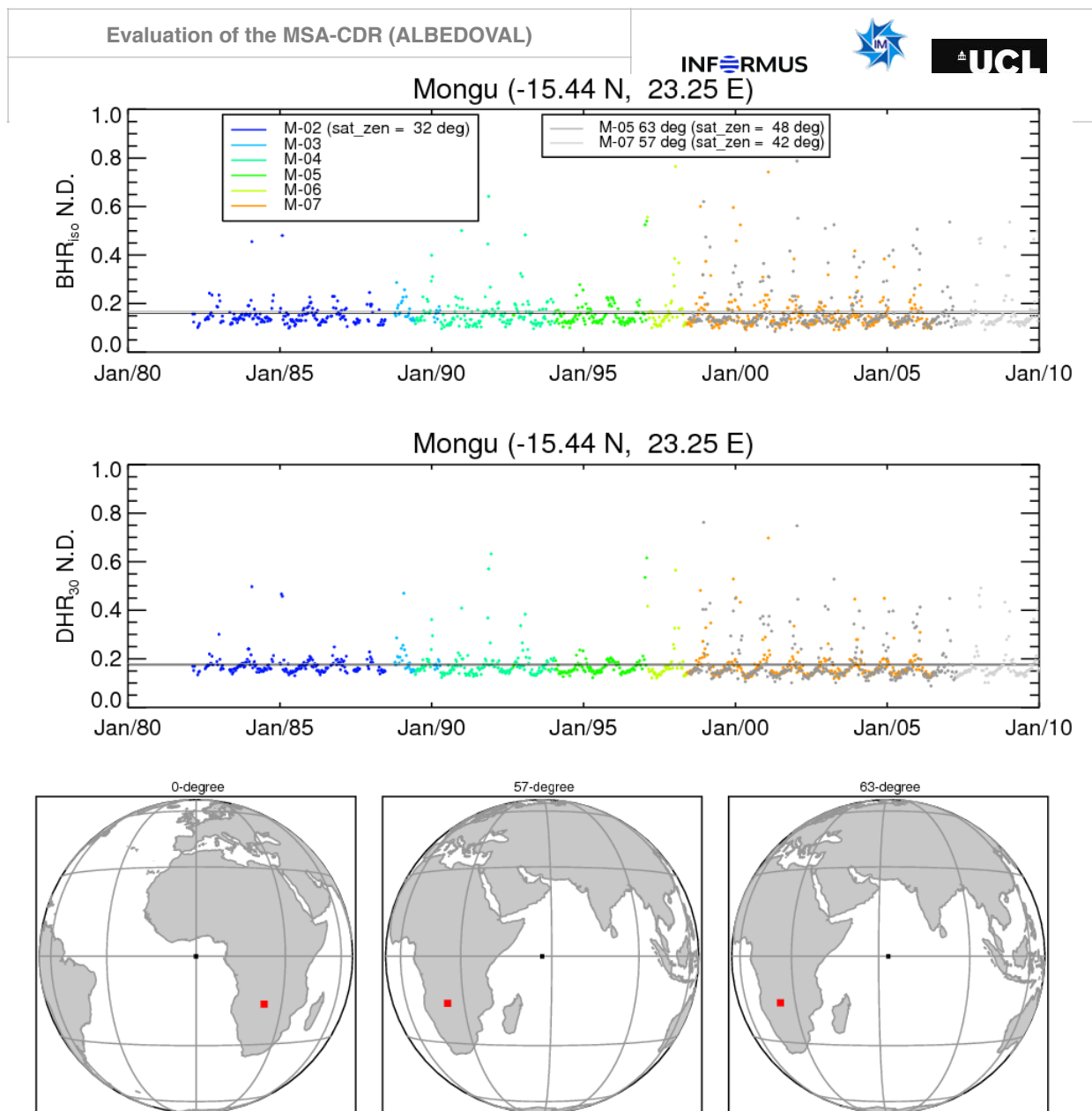**Figure 45: Same as Figure 40 but for site "Moldova".**

Mongu (-15.44 N, 23.25 E)

Mongu (-15.44 N, 23.25 E)

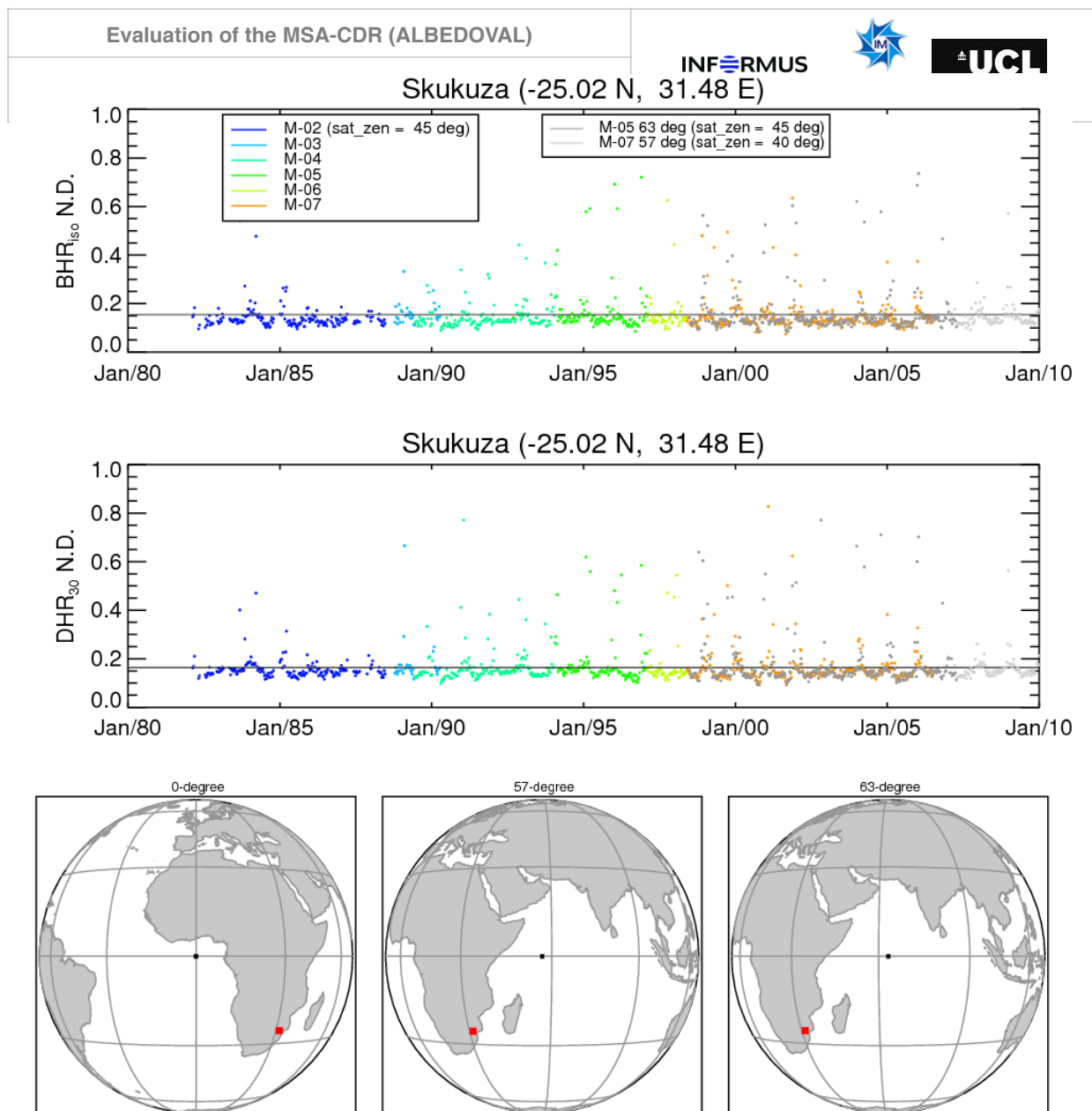**Figure 46: Same as Figure 40 but for site "Mongu" (Zambia).**

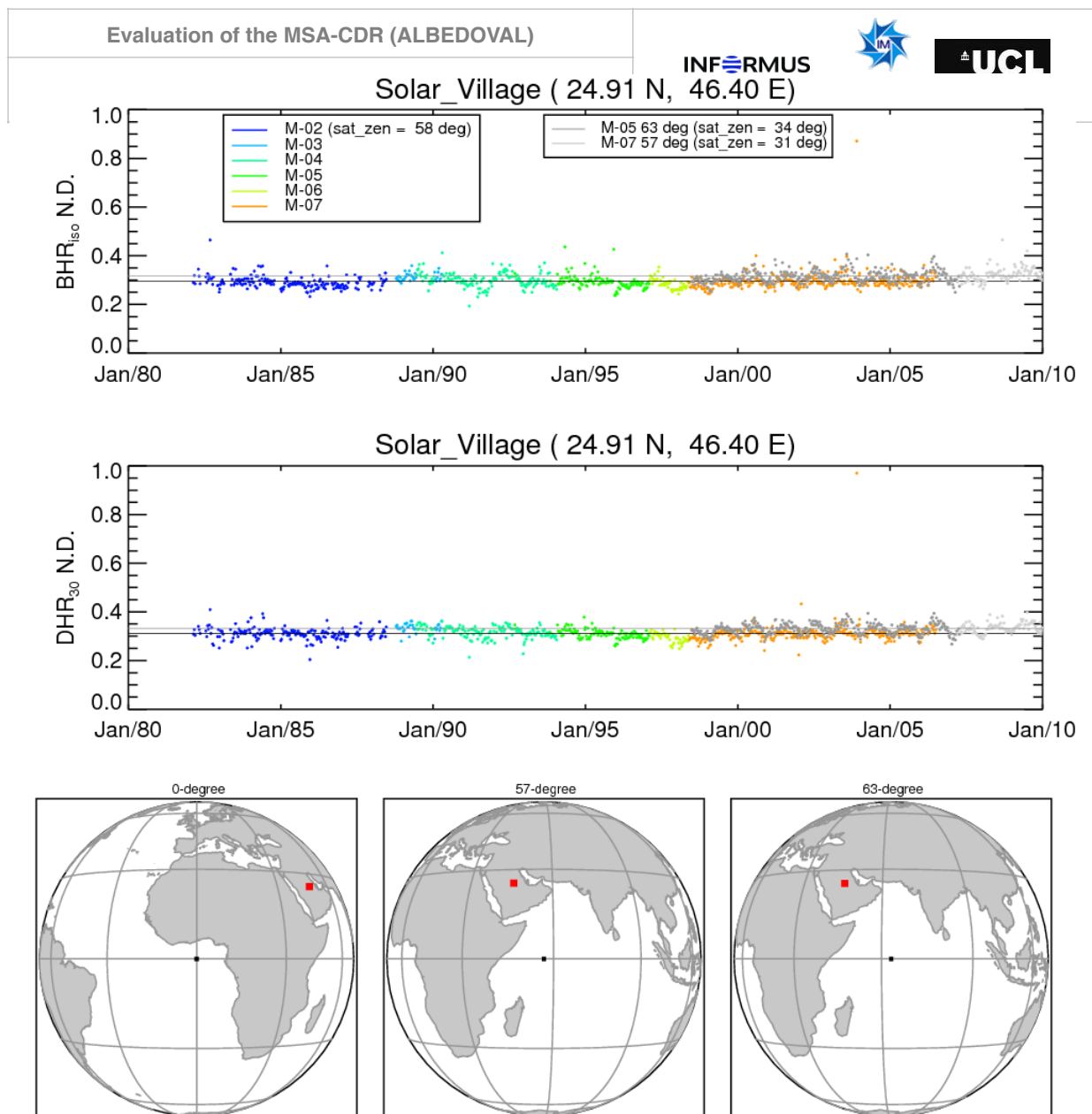**Figure 47: Same as Figure 40 but for site "Skukuza" (South Africa).**

Figure 48: Same as Figure 40 but for site "Solar Village" (Saudi Arabia).

12.5. Georeferencing software

12.5.1. MPEF_georef.pro: latitude/longitude to column/row

Mapping latitude/longitude to column/row is performed using the routine MPEF_georef.pro using the following calling sequence:

IDL> flag = MPEF_georef (lat,lon,column,row,/vis)

Output flag =0 indicates no error has occurred.

In order to access the correct pixels in the MSA data file corresponding to the chosen latitude/longitude, the column and row values for the MVIRI full disk resulting from MPEF_georef.pro need to be converted as follows:

$$\text{Column\_MSA} = \text{column\_MVIRI} - \text{startpixel}$$

$$\text{Row\_MSA} = \text{row\_MVIRI} - \text{startline}$$

where the values of startline and startpixel are given in Table 15.

There are three optional keywords controlling the behaviour of the MPEF_georef.pro:

➢ /VIS: force the "visible" resolution (default: IR)

➢ /SATLON: set longitude of satellite (default: 0˚)

➢ /MSG: set parameters to match MSG (default: MFG)

12.5.2. MPEF_refgeo.pro: column/row to latitude/longitude

In order to convert a given row/column location on the MSA 3261 x 3842 (0DEG) data field into latitude/longitude, the routine MPEF_refgeo.pro is invoked with the following calling sequence:

IDL> flag = MPEF_refgeo (column + startpixel,row + startline,lat,lon,/vis)

Output flag =0 indicates no error in conversion. Note that "startpixel" and "startline" need to be added as the routine requires the position in the MVIRI 5000 x 5000 full disk.

Keywords to MPEF_refgeo.pro are identical to those to MPEF_georef.pro.

12.5.3. Georeferencing example

In order to illustrate some issues related to geo-location and to address some apparent inconsistencies between the IDL geo-location routines and the static geo-location files, the following test was run at the example of the BSRN Toravere site (Figure 49): A 20x20 km^2 neighbourhood was subdivided in into a grid of 800x800 points, equivalent to a spacing of 25 meters. For each of those grid points, the corresponding MVIRI pixel was determined using the IDL routines provided by EUMETSAT. At the same time, the pixel location of Toravere was calculated using

1. The IDL geo-location routines provided by EUMETSAT, and

2. A nearest neighbour search in the static files associated with the MSA product.

Outcome:

➢ If a nearest neighbour search for Toravere is performed on the MSA Static files, the pixel corresponding to the yellow dot will be obtained.

➢ If the location of Toravere is calculated using the IDL routines, the pixel corresponding to the blue dot will be obtained.

➢ These results are consistent. The discrepancy is caused by the slanted observation geometry of MFG and the actual location of Toravere (red dot) in the far corner of the pixel corresponding to the blue dot.

➢ This study also suggests that the geo-location routines map to the centre of a pixel and not the lower left corner. (See the location of the yellow and blue dot in the centre of their respective pixel).
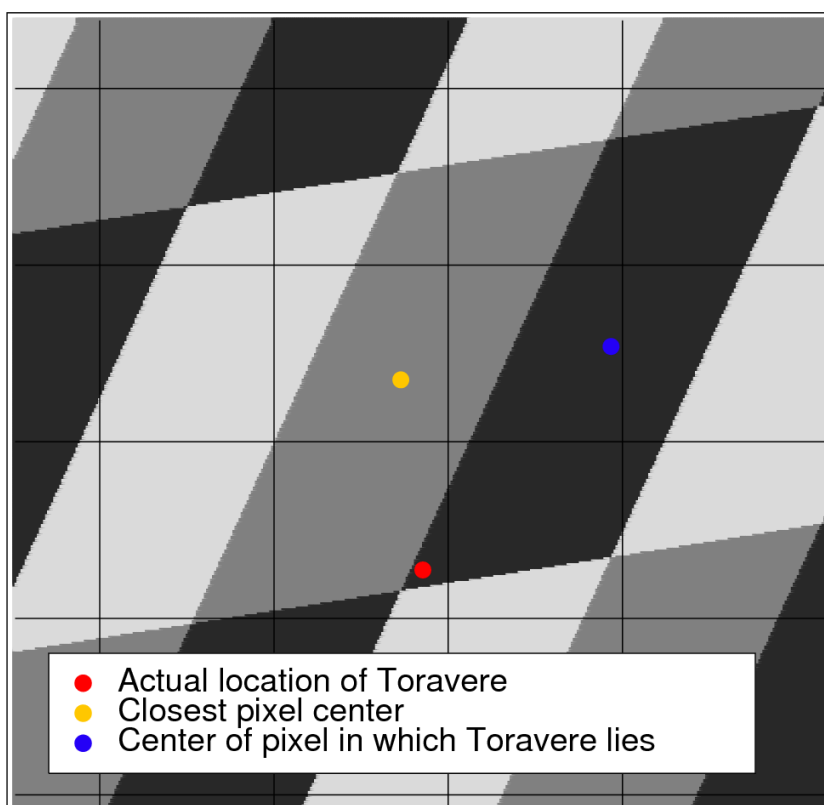
Figure 49: Location and orientation of the MVIRI pixels around the Toravere reference site (Estonia) at 58.254 N/ 26.462 E. The different grey-shaded boxes represent the different MVIRI pixels. The horizontal and vertical lines are spaced at 2.5 km distance in the meridional and zonal directions. The yellow dot represents the pixel centre closest to Toravere and the blue dot indicates the centre of the pixel which contains Toravere.